ENERGY ABSORPTION AND VIBRATIONAL HEATING IN MOLECULES FOLLOWING INTENSE LASER EXCITATION

by

RONALD ERWIN MCNAIR

B.S., North Carolina Agricultural and Technical State University
(1971)

SUBMITTED IN PARTIAL FULFILLMENT

OF THE REQUIREMENTS FOR THE

DEGREE OF DOCTOR OF

PHILOSOPHY

at the

MASSACHUSETTS INSTITUTE OF TECHNOLOGY

November, 1976
(i.e. February 1977)

Signature of Author .. Signature redacted
Department of Physics

Certified by.. Signature redacted .....
Thesis Supervisor

Accepted by..... Signature redacted .....
Chairman, Departmental Committee on Graduate Students

ENERGY ABSORPTION AND VIBRATIONAL HEATING IN MOLECULES FOLLOWING INTENSE LASER EXCITATION

by

Ronald Erwin McNair

Submitted to the Department of Physics in partial fulfillment of the requirements for the degree of Doctor of Philosophy.

ABSTRACT

Studies are made of the energy flow into and among the vibrational degrees of freedom of polyatomic molecules due to vibration-vibration (V-V) collisions following intense laser excitation. These studies have been made theoretically, by computer analysis, and experimentally.

Simple closed form expressions are derived for predicting the energy absorbed by an oscillator from an intense saturating laser pulse. This analysis treats the regime where high vibrational excitation is accomplished via V-V exchange collisions. The fundamental results obtained employ the novel assumption of a time dependent quasi-equilibrium distribution existing among the upper vibrational states. This assumption is verified by detailed computer simulations.

A similiar formalism is applied to a simple polyatomic molecule with one mode under laser irradiaiton. Theoretical, computer, and experimental evidence are presented supporting the remarkable finding that: the energy absorbed by a polyatomic can be predicted by the simple expressions derived for a diatomic molecule.

Energy absorption of CO_2 laser radiation by CH_3F gas have shown that at 5.0 Torr CH_3F pressure, $\sim$2.5 quanta per molecule is absorbed by the gas. For a known laser pulse duration (3.0μsec) the simple theoretical expressions yield a V-V up-

the-ladder rate for the ν_3(C-F stretch) mode of $0.8\pm.2\mu sec^{-1}$-$torr^{-1}$ which agrees well with measurements by laser fluorescence techniques. This shows that an energy absorption experiment is now a method for determining V-V rates.

A new method for measuring the energy stored in the vibrational degrees of freedom is introduced. Using this technique--the "cold gas filter" method--approximately 50% of the total energy absorbed is found to reside in the C-F stretch mode of CH_3F at about 9.6μm. Vibrational temperatures of $\sim 3000^{\circ}K$ are observed after all the modes reach a vibrational steady state while the translational temperature remains a constant.

The re-distribution of energy by intra-mode V-V collisional coupling is observed and presented in the transient and steady state regimes. The energy stored in the modes of CH_3F that are collisionally coupled to the laser pumped mode is measured, again, by laser induced fluorescence. By calibrating the spontaneous emission intensity of the n^{th} mode by that of ν_3, which is measured by the cold gas filter, the intensity ratios I_n/I_3 are used to obtain the energy storage. I_n is the intensity of any mode in CH_3F and I_3 is the ν_3 intensity.

A model for predicting the steady state partitioning of energy in polyatomics is presented and applied to CH_3F. The good agreement between the model predicted partitioning of energy and the measured energies prove that the modes equilibrate at different vibrational temperatures and that the energy flow path used is the dominant and most probable one.

These findings manifest some of the heretofore unobserved behavior of polyatomics and their interaction with strong resonant laser pulses. In addition, new possibilities are opened in the areas of laser induced photochemistry and intra-mode and inter-molecular energy transfer lasers.

Thesis Supervisor: Michael S. Feld
Title: Associate Professor of Physics

I DEDICATE THIS THESIS TO:

My Mother, Mrs. Pearl M. McNair

My Father, Mr. Carl C. McNair

My Grandmother, Mrs. Mable Montgomery

My Grandfather, Mr. James L. Montgomery

.....whose love and guidance shaped my will, desire, and stamina.

ACKNOWLEDGEMENTS

To Prof. Michael Feld, I thank you for your contact during the course of my thesis research and your concern, many hours, and support over the years. Through your teachings and enthusiam I have reached new heights in my enjoyment, appreciation, and understanding of physics.

To Prof. Ali Javan, thank you for your encouragement during my early years, and I am grateful for your support and confidence throughout my stay at M.I.T.

To Prof. Ron Mickens and Dr. Shirly Jackson, thank you for your help, guidance, and models as sucessful Black physicists.

To Dean John Turner and Dr. Clarence Williams, thank you for helping to make M.I.T. a more livable and enjoyable envirement.

To Prof. George Flynn and Dr. Barry Feldman, thank you for your many discussions, contributions, and enthusiasm towards this work.

To Steve Fulghum, thank you for your many contributions to this work, for your friendship and for your struggling with me through those hard times of NH_3, probing, N_2O, etc.

To Rick Forber, thank you for your fresh insights which have aided in solving some difficult problems.

To Julius Goldhar and Irving Herman, thank you for your

many lively discussions, willing assistance, and close friendship over the years.

To Bill Ryan, thank you for sharing your tremendous expertise and being able to joke about a laboratory disaster.

To Ellen Gurwitz and Mary Donoghue, thank you for being excited on my behalf on appropriate occassions.

To Antonio Sanchez, Mike Kelly, and Mike Guerra, thank you for your experimental advice and many discussions.

To Jose, Krikor, Richard, Michael B., Bert, John, Pete, Bob, Charley, and all the members of the laser group, thank you.

To Marion Neville and Lorraine Powell, thank you for your help in typing this thesis.

To members of St. Paul A.M.E. Church and the St. Paul A.M.E. Karate-Do, thank you for providing me with my greatest source of strength .

" To my very loving wife, Cheryl, your warmth and understanding has made pleasant a very painful endeavor. I thank you for your frequent role as lab assistant, for your drafting my figures, for your help in preparing this thesis, and for sharing your many talents. Thank you for caring and being a source of my happiness and motivation. "

TABLE OF CONTENTS

LIST OF FIGURES

I. INTRODUCTION

STATEMENT OF PROBLEMS ADDRESSED AND SOLVED

The interaction of intense electromagnetic fields with molecular systems and the subsequent inter-molecular processes is an area of great interest among physicists and chemists. The very broad range of potential applications and the rich physical content makes the study of such phenomena very exciting. The laser has provided an excellent tool for probing the flow of energy within the internal degrees of freedom of molecules, and it has become a major source of energy for obtaining high levels of excitation. Conversely, the increased knowledge of energy absorption, energy transfer, and relaxation processes in molecules has led to new and improved lasers with many more possibilities ahead as the cycle continues.

Very little has been understood about the detailed kinetics involved in the energy absorption process in molecules, nor has the redistribution of absorbed energy among the vibrational degrees of freedom of polyatomics been fully understood. Because of the lack of information on interaction potentials, collisional rate constants, and energy flow mechanisms, and spectroscopic complexities, polyatomic molecules have not been investigated as thoroughly as some diatomics.

This thesis presents a detailed study of the energy absorption of molecules from an intense resonant laser pulse in the V-V collisional regime and subsequent intra-mode and inter-molecular energy transfer. Simple closed form expressions for predicting the number of laser quanta absorbed by the molecule are presented. The model from which the equations are derived employ two new features, namely: (1) the addition of a laser pumping term to previously solved rate equations[17] for collisionally coupled oscillators, and (2) the assumption of a time dependent equilibrium distribution established among the $V \geq 1$ vibrational levels of the pumped oscillator during the laser pulse.

An extension of the theoretical analysis to a two mode polyatomic has revealed the new result that the energy absorbed by a polyatomic molecule can be predicted by the diatomic results. This remarkable finding is fundamental and basic to the understanding of the intra-mode kinetics of polyatomics in the presence of an intense field. Computer simulations are presented that verify these findings and all of the assumptions employed. In addition to the theoretical and computer findings, experiments are presented which prove that the simple relations derived from the diatomic theory do predict the polyatomic energy absorption.

A measurement of absolute energy stored in the vibrational modes of a polyatomic is presented here for the first time. It is shown that during the energy absorption

process all the modes of a polyatomic are collisionally excited. A new technique for measuring the energy storage -- the "cold gas filter" technique -- is described in detail. This method utilizes the intensity of the spontaneous emission from the mode under observation after the lowest component has been removed by an absorbing room temperature gas (cold gas filter). The cold gas filter technique was very successfully used for measuring the energy storage in CH_3F following CO_2 laser excitation. The analysis and results of these experiments are given.

A simple model for predicting the partitioning of energy among the tightly coupled modes of CH_3F is also given. This model makes use of the experimentally observed vibrational steady state which exists among the modes and it utilizes detailed balancing arguments. Given a specific known energy flow path, the model is shown to give good agreement with the experimental findings.

MOTIVATION

This work was motivated by the demands of the recent interest in new laser development, in laser induced chemical reactions, and chemical lasers.[1] It is the rates and paths

of energy flow during and after excitation that determines gain, power outputs, reaction rates, mode specific excitation, etc. Because of the long lived vibrational levels of some molecules, the vibrational degrees of freedom can be utilized as energy storage media for subsequent transfer of energy to other molecules which cannot be efficiently optically pumped, or they can be used for intra-mode stimulated emission and laser oscillation. Once the transient mechanisms of energy absorption are understood and how, how long, why, and where the energy flows, a very vast set of applications are waiting. Several new features of energy absorption and transfer in molecules are presented.

There has been a great deal of experimental work on the rates and kinetics of molecules under very weak excitation (<10 Kilowatts) by Weitz and Flynn[2], Moore[3,4], Chen[5-7], Osgood et.al.[8-9], Rockwood[10], and many others using laser induced fluorescence techniques. However, as the laser energies are increased and the vibrational equilibrium distribution begins to depart from ambient, many anomalies and complexities begin to show up. Investigations by Osgood et.al.[9] and by Weitz and Flynn[2] have shown that the relaxation rates of vibrational states involving multiquantum exchanges become non-linear as the pump energies get larger. Hence, because of this behavior of highly excited polyatomics, it is necessary to further investigate them in detail in order to fully enjoy the potential they

offer.

In 1975 and 1976, it was discovered that the overall energy absorption process in molecules is totally different when the source of excitation is an extremely intense laser (>10^2 Megawatts) instead of a laser with moderate intensity (<.5 Mwatts).[1, 14] Letokhov and Ambartzumian of the Soviet Union [11] and Rockwood[12] and others in the United States have found that under extremely high-power pumping, molecules can absorb several hundred laser quanta before dissociating. These absorption processes take place on time scales before any vibration-vibration exchange collisions occur. Consequently, this regime has become known as the "collisionless" absorption regime where the absorption process is totally radiative rather than collisional. It has been postulated that the V-V energy transfer observed in these experiments is also a collisionless phenomenon.[13] Although the study of this regime is of great interest for isotope separation, the collisionless absorption process is not always amenable to applications to such areas as laser chemistry, selective energy transfer, and other studies where collisions play a crucial role. Therefore, in this work, the attention will be placed entirely on the "collision" regime of absorption where the laser pump energy is sufficient to saturate the interacting transitions but too weak for the collisionless processes to be important.

SUMMARY

In Chapter II a theoretical model for determining the energy absorbed by diatomics and polyatomics is given. This mode assumes oscillators with neglibible anharmonicities for lower levels and a laser pulse of sufficient intensity to equalize the populations of the V=0 and V=1 vibrational levels of the interacting oscillator. Assuming the establishment of a time dependent equilibrium distribution among the $V \geq 1$ vibrational states, closed form expressions are presented which gives the energy absorption in terms of the laser pulse duration (τ_p) and the V-V collision rate (γ_{V-V}).

The analysis of energy absorption from a saturating laser pulse for a two mode molecular system is given in Chapter III. Careful computer analysis of the rate equations governing this process have indicated that the simple closed form results for a diatomic molecule are applicable to polyatomics under the prescribed conditions. Detailed compute calculations of these processes are given in Chapter IV.

The methyl halides, which are symmetric top molecules, form a class of molecules, which are susceptible to the processes studied here because of their rapid intra-mode equilibration times, long vibration-translations times, very fast rotation-rotation collision times, and relatively small anharmonicities in their C-X stretches. Appendix D describes some properties of the rotational and vibrational spectra of

symmetric tops. The symmetric top, methyl fluoride (CH_3F) was used in many of the experiments to be described because the rates and energy flow paths have been well studied by Flynn and co-workers.

A description of the basic experimental apparatus is given in Chapter V. Vibration-translation relaxation measurements in CH_3F in the low and high energy excitation regimes are presented in Chapter VI.

The absorption of CO_2 laser radiation by CH_3F gas is the topic of Chapter VII. Experiments show that several CO_2 quanta are absorbed and stored in CH_3F. Measurements of the rise-time of spontaneous emission from the mode being pumped indicate that the energy is being stored as vibrational energy. In addition, evidence is presented indicating that all modes of CH_3F reach a steady state very rapidly at sufficiently high pressures. Since there is a rapid collisional coupling among the modes, the total energy absorbed by the molecule is distributed among the vibrational degrees of freedom. Three techniques for measuring the energy stored in each vibration during the steady state is presented.

The first technique, described in Chapter VIII. uses infrared double resonance for determining the energy stored in the pumped mode. (This method did not prove useful for high excitation). In this technique the population difference between the two interacting states is monitored after

excitation by observing the change of absorption. The amplitude of this change is then calibrated to give the equilibrium temperature and, thus, the energy stored assuming a Boltzmann distribution. Because of the sensitivity of the rotational-vibrational transition intensities to small changes of the rotational temperature, the analysis of this method was distorted by thermal heating and other transport phenomena.

The second and a very successful technique involve the observation of laser induced fluorescence and is presented in Chapter IX. Assuming that a Boltzmann equilibrium exists at a high vibrational temperature, CH_3F gas at room temperature is used to filter out the V=1→0 component of the total spontaneous emission intensity. The ratio of the V=1→0 component to the total intensity defines the vibrational temperature and the number of quanta stored.

The third technique, which is given in Chapter X, again utilizes laser induced fluorescence for determining the energy storage. Using the appropriate optical filters, the emitted wavelengths from each mode are isolated and observed. The energy stored in any mode is obtained by comparing the spontaneous emission intensity of the mode to the spontaneous emission intensity of a mode whose temperature is known. A knowledge of the transition moments leads to a simple relationship between the vibrational temperatures

of the two modes in terms of the spontaneous emission amplitude ratios and the ratio of absorption coefficients.

A model for predicting the partitioning of energy among the vibrational degrees of freedom of a polyatomic is presented in Chapter XI. A knowledge of the energy flow path is necessary (or a good guess and a comparison with experiment will suffice). The rate equations for the V-V collision processes are solved in the steady state to give a very simple relationship between the vibrational temperatures where detailed balancing is employed. This relationship is applied to each step of the intra-mode coupling to relate the energy storage of all the modes. The predicted energy storage is found to agree very well with the measured partitioning of energy. These findings also reconfirm previously measured energy flow paths in CH_3F.

II. ENERGY ABSORPTION FROM AN INTENSE LASER PULSE BY DIATOMIC MOLECULES

TYPES OF COLLISION PROCESSES

The absorption of radiation from an intense laser pulse depends on the efficiency and time scales of collisional couplings of all the internal degrees of freedom (i.e. rotational, vibrational, and translational). The times for each degree of freedom to reach equilibrium are several orders of magnitude apart. For the very large cross section (10^{-13}-10^{-14} cm^2)[58] rotational collisions, the rotational-rotational (or R-R) thermalization occurs in ~1 gas kinetic collision. For the smaller cross-section vibration-vibration coupling (~10^{-15}-10^{-17} cm^2)[16], the vibration-vibration (or V-V) thermalization occurs in ~10 gas kinetic collisions. The slowest process in most molecules is the vibration-translation collisional transfer which has a cross section of (~10^{-18}-10^{-20} cm^2)[16,5] and thermalizes typically in approximately 10^3-10^4 gas kinetic collisions.[16,25,6]

These large difference in equilibration rates can be accounted for by noting the amount of energy exchanged during the various processes and the kinematics involved. R-R, R-T, and T-T collisions are very efficient because of the small amount of energy being exchanged ($E << kT_R$), where T_R is room temperature. These small energies can easily be compensated for by the translation degrees of freedom at room temperature.

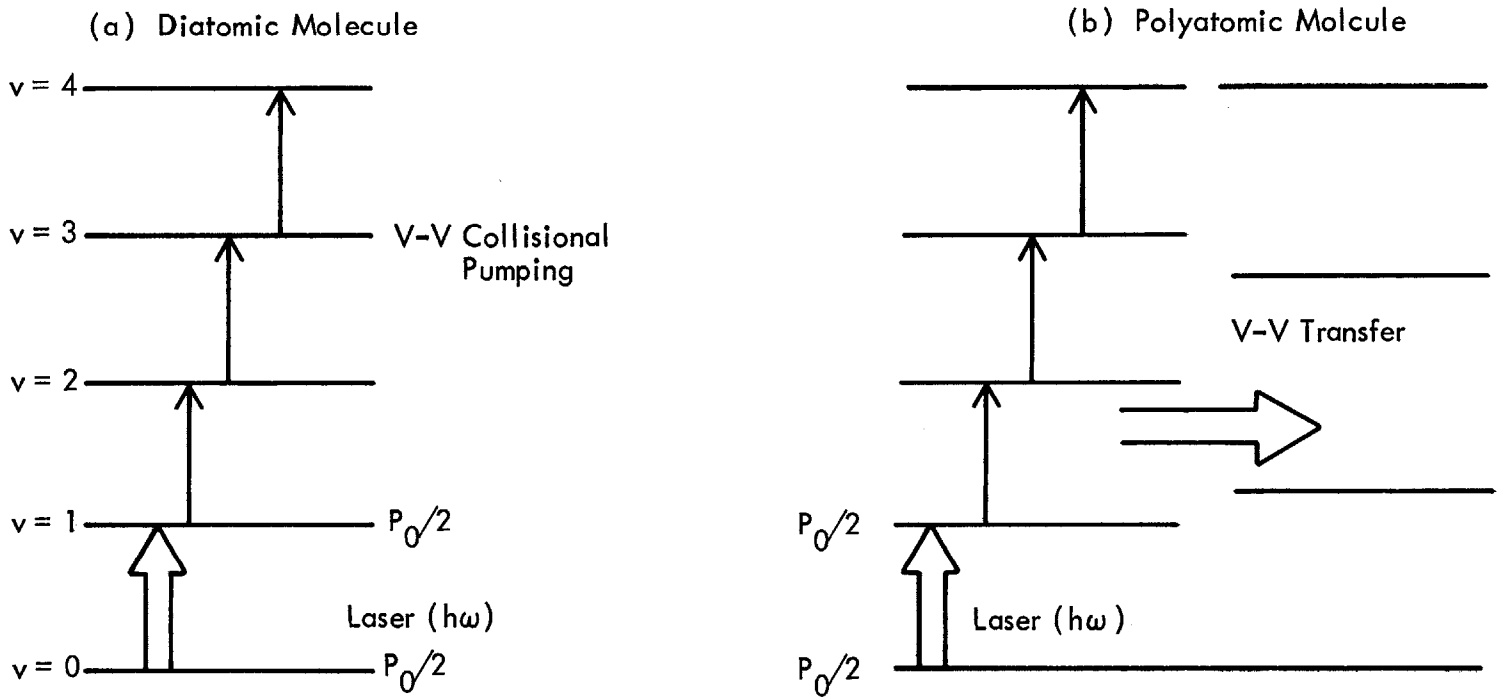

$$\tau_{R-T} \ll \tau_{v-v} \ll \tau_p \ll \tau_{v-T}$$

τ_{R-T} Rotational-Translational equilibration time

τ_{v-v} Vibrational-Vibrational equilibration time

τ_p Laser pulse duration

τ_{v-T} Vibrational-Translational equilibration time

P_0 Probability of finding molecule in ground state

Fig. 1. Laser saturation and V-V pumping of a (a) diatomic (b) polyatomic

The efficiency of V-V collisional transfer is determined in part by the oscillation frequency differences of the vibrators and the masses of the collision partners.[39] (These oscillators may be viewed as classical spring-mass systems). In V-T relaxation, a very large amount of energy is being deposited into the translational degrees of freedom requiring many collisoins to complete the process.

ABSORPTION OF ENERGY FROM A SATURATING LASER PULSE--DISCUSSION

The long lived vibrational states of molecules make them excellent energy storage media if these states can be efficiently excited. It is the fast V-V up-the-ladder and R-R collisions which determine how efficiently the vibrational levels are pumped by an interacting laser pulse.

How energy is absorbed by V-V pumping can be seen by considering an oscillator with an intense laser pulse interacting with the oscillator's v=0→1 rotational-vibrational transition (Fig. 1a). Let us neglect rotational structure for now. If the laser pulse is long compared to the V-V thermalization time, then, many V-V collisions will occur before the pulse terminates. The presence of the intense laser pulse disturbs the room temperature Boltzmann distribution by creating "excess" population in the v=1 level. V-V collisions immediately begin an attempt to bring the distribution back to equili-

brium at an elevated vibrational temperature by pumping population to higher vibrational states. This pumping occurs by processes of the type[15]

$$(V=1) + (V=1) \longrightarrow (V=2) + (V=0)$$

In the meantime, the intense laser pulse continues to transfer from v=0 excess population to the v=1 state for its entire duration while the V-V collisions continue to pump this population higher. The net effect of these two competing processes is the removal of energy from the laser pulse and susequent heating of the molecules's vibrational states.[16] This entire process occurs on time scales short compared to the V-T time, thus, significant thermal heating does not occur. Therefore, the energy is essentially stored as vibrational energy until V-T becomes appreciable.

If we now examine the role of rotational collisions, we find that a finite time is required for the laser to interact with all of the v=0 rotational states, J. This time is determined by the fraction of population in the lower J state being directly pumped, z_J, and the rotational thermalization time, τ_{R-R}. If the time for all the levels to interact with the laser is much less than the time for V-V equilibration, τ_{V-V}, and the laser pulse time, τ_p, then efficient pumping of the v=0 state can occur. If the converse is true, a "bottleneck" will occur at the v=0 rotational states, thus, prohibiting

efficient pumping. This phenomenon is commonly called the "rotational bottleneck" effect.[34] The bottleneck time $\tau_B = \tau_{R-R}/Z_J$, must satify the condition (from Appendix A)

$$\tau_B = \frac{\tau_{R-R}}{Z_J} << \tau_{V-V}$$

and in summation, the conditions for efficient pumping on all the various collision times involved and the laser pulse time are

$$\tau_B << \tau_{V-V} << \tau_P << \tau_{V-T} .$$

The above types of collisions form the basis of energy absorption via V-V pumping and it is the foundation around which the following model is built to describe and predict the energy absorption. The problem of the relaxation of a system of oscillators has been solved by Shuler and Weiss[60], Treanor[18], and others; Letokhov has solved the problem in the presence of inefficient laser pumping[34], that is saturation of the entire band was not obtained. Although Letokhov's studies utilized intense pump pulses, the ability to saturate was limited by the duration of the laser pulse and the rotational bottleneck effect.(See Appendix A) The new features of the analysis presented here are: 1) the presence of a saturating laser term in the coupled V-V rate equations in the limit of no bottleneck, and 2)the susequent establishment of a quasi-equilibrium among the upper states. Closed form expressions for the number of laser quanta absorbed by a diatomic

are derived in the following section, and a similiar analysis for polyatomics is derived in Chapter III.

ABSORPTION FROM A SATURATING LASER PULSE--THEORY

Consider the interaction of an intense laser pulse with the v=0→1 vibrational transition of a "near harmonic" oscillator, anharmonic to the extent that the laser interacts with the v=0→1 levels only. It is assumed that that the rotational thermalization time, τ_{R-R}, is on a time scale shorter than the vibration-vibration thermalization time, τ_{V-V}, to prevent rotational bottlenecking. These fast rotational collisions permit all of the rotational levels in the v=0 state to be pumped to the v=1 state by filling in the hole created by the laser in the equilibrium distribution of the rotational levels. By the same token, the fast collisions remove population from the upper J states, therefore, permitting further pumping by the laser. If the rotational bottlenecking is removed, each vibrational band of levels can be treated as a single state. The laser can, thus, promote half of the ground state population to the v=1 state for sufficiently long pulse durations or at sufficiently high pressures.[22]

If we denote P_v as the probability of a molecule being in state v, where the number in state v is given by

$$N_v = P_v N_{tot}$$

the rate equations describing the interaction of the laser with the oscillator system may be written as

$$\frac{dP_0}{dt} = \left(\frac{dP_0}{dt}\right)_{collision} - (P_0 - P_1)\sigma I \qquad (II\text{-}1)$$

$$\frac{dP_1}{dt} = \left(\frac{dP_1}{dt}\right)_{collision} + (P_0 - P_1)\sigma I \qquad (II\text{-}2)$$

$$\frac{dP_v}{dt} = \left(\frac{dP_v}{dt}\right)_{Collision} \quad V \geq 2 \qquad (II\text{-}3)$$

where σ is the absorption cross section and I is defined as the laser pulse intensity in photons/cm^2-sec. represents the change in the population of level v due to collisions. If we assume binary collisions in the energy transfer process which are governed by the Landau-Teller model[23] and a dipole-dipole dominanted interaction, then, the collision part of the coupled rate equations can be written (see derivation in Appendix B)

$$\left(\frac{dP_v}{dt}\right)_{\text{Collision}} = \left(\frac{\gamma_{vv}}{2}\right) \sum_{v'=0}^{\infty} \Big[(v+1)v' + v(v'+1) \Big] P_v P_{v'} + vv' P_{v-1} P_{v'}$$

$$+ \Big[(v+1)(v'+1) \Big] P_{v+1} P_{v'} \quad . \qquad \text{(II-4)}$$

γ_{v-v} is defined such that for an isolated three level system (v=0,1,2),

$$\frac{dP_1}{dt} = \frac{\gamma_{vv}}{2} \left(2P_2 P_0 - 2P_1^2 \right)$$

and $$\gamma_{v-v} = \tau_{v-v}^{-1} \quad ,$$

where γ_{V-V} is characteristic up-the-ladder V-V collision rate.[24] Equation (II-4) may be further simplified by utilizing the statement of particle conservation, namely,

$$\sum_{v=0}^{\infty} P_v = 1 \quad , \qquad \text{(II-5)}$$

and noting that the mean energy of an oscillator is given by

$$\mathcal{E} = \sum_{v=0}^{\infty} v P_v \quad , \qquad \text{(II-6)}$$

where $\mathcal{E} = \frac{\text{Total Energy}}{\text{Molecule}} \frac{1}{\hbar\omega}$.

Summing over v' in eq. (II-4) gives

$$\left(\frac{dP_v}{dt}\right)_{\text{collision}} = \frac{\gamma_{vv}}{2} \Big\{ -(v+1) P_v \sum_{v'} v' P_{v'} + v P_v \sum_{v'} v' P_{v'} + v P_v \sum_{v'} v' P_{v'}$$

$$+ v P_{v-1} \sum_{v'} v' P_{v'} + v P_{v+1} \sum_{v'} v' P_{v'} + P_{v+1} \sum_{v'} v' P_{v'} + v P_{v+1} \sum_{v'} P_{v'} + P_{v+1} \sum_{v'} P_{v'} \Big\} .$$

Using eqs. (II-5) and (II-6) and simplifying, we get

$$\left(\frac{dP_v}{dt}\right)_{collision} = \frac{\gamma_{vv}}{2}\left\{\left[(-2v-1)\mathcal{E}-v\right]P_v + v\mathcal{E}P_{v-1} + (v+1)(\mathcal{E}+1)P_{v+1}\right\} . \qquad (II-7)$$

We now wish to examine the problem in the limit in which the laser heavily saturates the v=0→1 transition such that

$$\frac{dP_0}{dt} \approx \frac{dP_1}{dt} . \qquad (II-8)$$

The laser is sufficiently intense such that the time rate of change of levels one and zero are locked together, but sufficiently weak so that collisionless or hot band absorptions are avoided.

Using eq. (II-8) in eqs. (II-1) and (II-2), we find

$$P_0 - P_1 \approx \frac{1}{2\sigma I}\left[\left(\frac{dP_0}{dt}\right)_{collision} - \left(\frac{dP_1}{dt}\right)_{collision}\right] . \qquad (II-9)$$

If the laser pumping rate $2\sigma I$ is sufficiently greater than the characteristic V-V rate γ_{V-V}, then,

$$P_0 \approx P_1 . \qquad (II-10)$$

Thus, $2\sigma I > \gamma_{V-V}$ is a statement of what is meant by sufficiently intense to saturate the v=0→1 transition.

Let us now find an expression for time rate of change of energy flow. From eqs. (II-1) and (II-9),

$$\frac{dP_0}{dt} = \left(\frac{dP_0}{dt}\right)_{collision} - \frac{1}{2}\left[\left(\frac{dP_0}{dt}\right)_{collision} - \left(\frac{dP_1}{dt}\right)_{collision}\right]$$

$$= \frac{1}{2}\left[\left(\frac{dP_0}{dt}\right)_{collision} + \left(\frac{dP_1}{dt}\right)_{collision}\right] \qquad \text{(II-11)}$$

Equations (II-1), (II-2), and (II-3) are added, then, multiplied through by v and summed over v to give

$$\sum_v v\left(\frac{dP_0}{dt} + \frac{dP_1}{dt} + \frac{dP_v}{dt}\right) = \sum_v v\left[\left(\frac{dP_0}{dt}\right)_{collision} + \left(\frac{dP_1}{dt}\right)_{collision} + \left(\frac{dP_v}{dt}\right)_{collision}\right] \qquad \text{(II-12)}$$

If we now differentiate eq. (II-6), we find

$$\dot{\mathcal{E}} = \sum_v v \dot{P}_v \qquad \text{(II-13)}$$

Using eqs. (II-13) and (II-11) in (II-12) gives

$$\dot{\mathcal{E}} = \frac{1}{2}\left[\left(\frac{dP_0}{dt}\right)_{collision} - \left(\frac{dP_1}{dt}\right)_{collision}\right] + \sum_{v=2}^{\infty} v\left(dP_v/dt\right)_{collision} \qquad \text{(II-14)}$$

where $\sum_{v=2}^{\infty} v(dP_v/dt) = 0$ since collisions by these molecules ($v > 1$) can only transfer energy and not absorb. From eq. (II-1), (II-9), and (II-14) we obtain

$$\frac{dP_0}{dt} = \left(\frac{dP_0}{dt}\right)_{Collision} - \frac{1}{2}\left[\left(\frac{dP_0}{dt}\right)_{Collision} - \left(\frac{dP_1}{dt}\right)_{Collision}\right]$$

$$= \left(\frac{dP_0}{dt}\right)_{Collision} - \dot{\mathcal{E}} \quad . \qquad \text{(II-15a)}$$

Similiarly, for eq. (II-2) , we have

$$\frac{dP_1}{dt} = \left(\frac{dP_1}{dt}\right)_{collision} + \dot{\mathcal{E}} \qquad \text{(II-15b)}$$

and

$$\frac{dP_v}{dt} = \left(\frac{dP_v}{dt}\right)_{Collision} \quad v \geq 2 \quad . \quad \text{(II-15c)}$$

The terms for the energy absorption, $\dot{\mathcal{E}}$ may be considered perturbations (not necessarily small) on the harmonic oscillator rate equations.

We now invoke the following boundary condition: at t=0 the laser instantaneously equalizes the population of the v=0 and v=1 levels such that half the ground state population is promoted to the v=1 level giving

$$P_0(t=0) = P_1(t=0) = \frac{1}{2} \qquad \text{(II-16)}$$

and from eq. (II-6) $\mathcal{E}(t=0) = \frac{1}{2}$

We further stipulate from eq. (II-9) that $P_0(t) \approx P_1(t)$.

Once the above initial distributions are established, V-V processes begin an attempt to return the oscillator to

an equilibrium distribution. Thus, V-V collisions of the type described on p.23 begin to pump molecules to higher vibrational levels. The presence of the laser pumping term in eqs. (II-15a) and (II-15b) tend to retard this equilibration process by keeping the v=0 and v=1 populations equal (see Fig. 2a) The net effect is the removal of energy from the laser pulse and its deposition into higher vibrational states.

The most outstanding feature and the most fundamental hypothesis of this analysis is the existence of an equilibrium distribution of the upper vibrational states with respect to the two lowest states of the oscillator system during the laser pulse.

Due to the rapid V-V processes occuring, we can assume that the vibrational levels $v \geq 2$ rapidly come into equilibrium with the v=1 level. Thus, the probability distribution (shown in Figure 2b) takes the form of [27]

$$P_0 = P_1$$
$$P_v = P_1 e^{-(v-1)\Theta} \quad , \qquad (II-17)$$

where $\Theta = \hbar\omega/kT_{eff.}$ with $T_{eff.}(t)$ being the effective vibrational temperature of the $v=1 \rightarrow \infty$ vibrational levels. This assumption was verified by computer simulations of the laser driven rate equations and will be discussed in more detail in the next chapter.

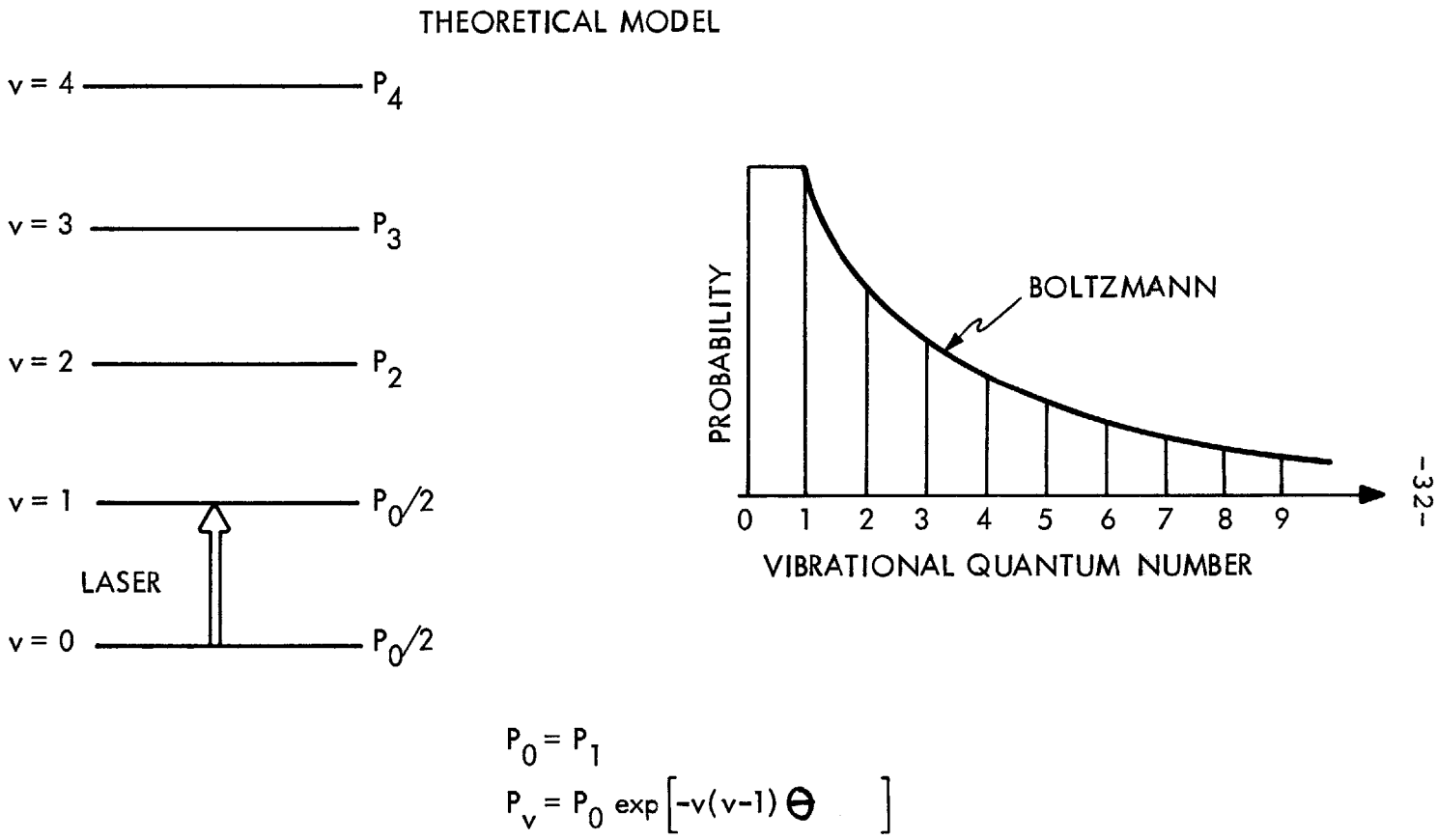

Fig.2. V-V pumping by a saturating laser pulse and the time dependent probability distribution.

From number consversation,

$$\sum_{v} P_v = 1$$

and from eq. (II-17), we find

$$2P_1 + \sum_{v=2}^{\infty} P_1 e^{-(v-1)\Theta} = 1$$

and

$$P_1 = \left(\frac{1-e^{-\Theta}}{2-e^{-\Theta}}\right) \qquad \text{(II-18)}$$

From the energy relation, $\mathcal{E} = \sum_v v P_v$ we find

$$\mathcal{E} = \sum_{v=0}^{\infty} v e^{-(v-1)\Theta}$$

$$= P_1 \left[e^{-\Theta} \frac{\partial}{\partial \Theta} \left(\sum_{v=0}^{\infty} e^{-v\Theta} \right) \right] = \frac{1}{(1-e^{-\Theta})^2} \qquad \text{(II-19)}$$

From eqs. (II-18) and (II-19), we get

$$\mathcal{E} = \frac{1}{(1-e^{-\Theta})(2-e^{-\Theta})} \qquad \text{(II-20)}$$

Solving eq. (II-18) for $e^{-\Theta}$ gives

$$e^{-\Theta} = (1-2P_1)/(1-P_1) \quad , \text{ and}$$

substituting into eq. (II-20) we find

$$\mathcal{E} = (1-P_1)^2/P_1 \qquad \text{(II-21)}$$

or

$$\dot{\mathcal{E}} = -(1-P_1^2)\dot{P}_1/P_1^2 \qquad \text{(II-22)}$$

Returning to eq. (II-7) and noting that $\dot{P}_0 \approx \dot{P}_1$ and $P_0 \approx P_1$,

we obtain,

$$\left(\frac{dP_o}{dt}\right)_{Collision} \approx \frac{\gamma_{VV}}{2} P_1 \quad .$$

Using this expression in eq. (II-15a) gives

$$\dot{\mathcal{E}} = \frac{\gamma_{VV}}{2} P_1 - \dot{P}_1 \qquad (II-23)$$

Equations (II-22) and (II-23) are expressions for $\dot{\mathcal{E}}$ which cam be equated to give the differential equation

$$\frac{dP_1}{P_1}\left(\frac{1-P_1^2}{P_1}\right) = \frac{\gamma_{VV}}{2} + \frac{dP_1}{P_1}$$

Using the integration limits, $P_1 = 0 \rightarrow P_1(\tau_p)$ and $t = 0 \rightarrow \tau_p$, and the initial conditions (eq.(II-16)), a closed form expression for the probability, P_1, is derived given by

$$\frac{1}{P_1^2} + 4\ln(2P_1) = \gamma_{VV}\,\tau_p + 4 \qquad (II-24)$$

Therefore, eqs. (II-21) and (II-24) together specify the number of quanta per molecule absorbed by a diatomic molecule for a given V-V rate (γ_{V-V}) and laser pulse duration, τ_p.

These findings make it possible to predict the energy flow into a diatomic molecule from a saturating laser pulse. Thus, the parameters (γ_{V-V} & τ_p) can be tailored to maximize energy flow for susequent use as vibrational energy.

This theory gives a good approximation to the energy absorption process in molecules with relatively small anharmonicities such that Treanor pumping and other anharmonic effects are small.[18] In Chapters III, IV, and VII, it will be shown that the simple expressions calculated here, eqs. (II-21) and (II-24), also predict the energy abso predict the energy absorbed by polyatomics.

III. LASER HEATING OF A TWO MODE VIBRATIONAL SYSTEM

THEORY

The energy absorbed by a diatomic under intense irradiation has been solved and analyzed in detail in the previous chapter. The energy absorption process has been analyzed for the case of a closely coupled non-resonant mode of a polyatomic. It is found that the energy absorbed by a two mode system is the same as the energy absorbed by a single mode system. The details of this analysis shall be given.

In this problem, the energy has the freedom to flow up the vibrational ladder of the mode being pumped via V-V processes or it can flow over to the other mode and up its vibrational ladder via V-V cross over collisions.[25] In addition to the fundamentals, combination states must be included in the analysis.

Consider a two mode, non-resonant, vibrational system with modes of energies, E_A and E_B $(E_B > E_A)$[54] and having vibrational quantum numbers m and n, respectively. We represent a state of the system by[26] $|m,n\rangle$ where m and n are the vibrational quantum numbers of A and B.

Let us examine the relaxation of these modes in the absence of laser pumping. For binary collisions of the type where A exchanges energy with A(A:A), B exchanges with B(B:B) and A exchanges with B(A:B and B:A), we assume that only single quantum transfers can occur through dipole-dipole

coupling where energy is conserved. For two colliding molecules, we denote the levels of molecules 1 as $|j,k\rangle$ and molecule 2 as $|m,n\rangle$. The processes to be considered in the interactions are: (III-1)

MOLECULE 1		MOLECULE 2	
Initial State	Final State	Initial State	Final State
$\|j\pm1,K\rangle$	$\|j,K\rangle$	$\|m\mp1,n\rangle$	$\|m,n\rangle$
$\|j\mp1,K\rangle$	$\|j,K\rangle$	$\|m,n\mp1\rangle$	$\|m,n\rangle$
$\|j,K\pm1\rangle$	$\|j,k\rangle$	$\|m,n\mp1\rangle$	$\|m,n\rangle$
$\|j,K\pm1\rangle$	$\|j,k\rangle$	$\|m\mp1,n\rangle$	$\|m,n\rangle$

Analyzing the transition probabilites in the manner done in Appendix B, the time rate of change of probability, $\dot{P}_{jk}$, can be written in four parts:

$$\dot{P}_{jK}^{(1)} = C' \sum_{m,n}^{\infty} |\mu_o^A|^2 |\mu_o^A|^2 (j+1)m \left[P_{j+1,K} P_{m-1,n} - P_{jK} P_{mn}\right] + |\mu_o^A|^2 |\mu_o^A|^2 (m+1)j \left[P_{j-1,K} P_{m+1,n} - P_{jK} P_{mn}\right]$$

$$\dot{P}_{jk}^{(2)} = C \sum_{m,n} |\mu_o^A|^2 |\mu_o^B|^2 (j+1)n \left[\alpha P_{j+1,K} P_{m,n-1} - P_{jK} P_{mn}\right] + |\mu_o^A|^2 |\mu_o^B|^2 (n+1)j \left[P_{j-1,K} P_{m,n+1} - \alpha P_{jK} P_{mn}\right]$$

$$\dot{P}_{jK}^{(3)} = C'' \sum_{m,n} |\mu_o^B|^2 |\mu_o^B|^2 (K+1)n \left[P_{j,K+1} P_{m,n-1} - P_{j,K} P_{mn}\right] + |\mu_o^B|^2 |\mu_o^B|^2 (n+1)K \left[P_{j,K-1} P_{m,n+1} - P_{jK} P_{mn}\right]$$

$$\dot{P}_{jK}^{(4)} = C \sum_{m,n} |\mu_o^B|^2 |\mu_o^A|^2 (K+1)m \left[P_{j,K+1} P_{m-1,n} - \alpha P_{jK} P_{mn}\right] + |\mu_o^B|^2 |\mu_o| (m+1)K \left[\alpha P_{j,K+1} P_{m+1,n} - P_{jK} P_{mn}\right].$$

(III-2)

μ_o^A and μ_o^B are the transition dipole moments for modes A and B and C, C', and C'' are constants such that the V-V exchange rates for A:A, B:B, and A:B(B:A) are given by

$$\gamma_A \equiv C' |\mu_o^A|^2 |\mu_o^A|^2$$
$$\gamma_B \equiv C'' |\mu_o^B|^2 |\mu_o^B|^2$$
$$\gamma_{AB} \equiv \gamma_{BA} = C |\mu_o^A|^2 |\mu_o^B|^2 \quad .$$

Conservation of number requires that

$$\sum_m \sum_n P_{mn} = 1 \quad . \qquad \text{(III-2)}$$

The mean energies per molecule in modes A and B are given by

$$\epsilon_A = \sum_{m,o} m P_{mn} \qquad \text{and} \qquad \epsilon_B = \sum_{o,n} n P_{mn} \quad , \qquad \text{(III-3)}$$

and the total energy per molecule in the system is given by

$$\epsilon_{tot} = \epsilon_A + \epsilon_B \quad . \qquad \text{(III-4)}$$

The condition of detailed balancing requires that

$$\gamma_A / \gamma_B = e^{-\Delta E/kT_R} = e^{-\theta_R} = \alpha$$

where $\Delta E = E_B - E_A$ and T_R is room temperature. Using the above definitions of γ_A, γ_B, and γ_{AB} along with eq.(III-3), the $\dot{P}_{jk}$ terms may be combined and written as

$$\begin{aligned}\dot{P}_{jk} = {} & P_{j+1,k}\left[\gamma_A(1+\epsilon_A)+\alpha\gamma_{AB}(1+\epsilon_B)\right](j+1) \\ & + P_{j,k+1}\left[\gamma_B(1+\epsilon_B)+\gamma_{AB}(1+\epsilon_A)\right](k+1) \\ & + P_{j-1,k}\left[\gamma_A\epsilon_A+\gamma_{AB}\epsilon_B\right](j) \\ & + P_{j,k-1}\left[\gamma_B\epsilon_B+\alpha\gamma_{AB}\epsilon_A\right](k) \\ & - P_{j,k}\left[\gamma_A(1+\epsilon_A)+\alpha\gamma_{AB}(1+\epsilon_B)\right](j) \\ & - P_{jk}\left[\gamma_A\epsilon_A+\gamma_{AB}\epsilon_B\right](j+1) \\ & - P_{jk}\left[\gamma_B(1+\epsilon_B)+\gamma_{AB}(1+\epsilon_A)\right](k) \\ & - P_{jk}\left[\gamma_B\epsilon_B+\alpha\gamma_{AB}\epsilon_A\right](k+1)\end{aligned} \qquad \text{(III-5)}$$

γ_A and γ_B are the up-the-ladder V-V rates in A and B, and γ_{AB} is the V-V cross-over rate for the intra-mode processes.

If the ϵ_A and ϵ_B terms of equation (III-5) are factored and regrouped, $\dot{P}_{jk}$ can then be written as

$$\begin{aligned}\dot{P}_{jk} = {} & \epsilon_A\left\{\gamma_A\left[(j+1)P_{j+1,k}-(2j+1)P_{jk}+jP_{j-1,k}\right.\right. \\ & \left.\left.+\gamma_{AB}\left[(k+1)P_{j,k+1}-(k+\alpha k+\alpha)P_{jk}+\alpha kP_{j,k-1}\right]\right\}\right. \\ & + \epsilon_B\left\{\gamma_B\left[(k+1)P_{j,k+1}-(2k+1)P_{jk}+kP_{j-1,k}\right]\right\} \qquad \text{(III-6)} \\ & + \gamma_{AB}\left[\alpha(j+1)P_{j+1,k}-(j+\alpha j+1)P_{jk}+jP_{j-1,k}\right]\} \\ & + (\gamma_A+\alpha\gamma_{AB})\left[(j+1)P_{j+1,k}-jP_{jk}\right]+(\gamma_B+\gamma_{AB})\left[(k+1)P_{j,k+1}-kP_{jk}\right].\end{aligned}$$

Multiplying both sides by k and summing over (j,k), we find

$$\dot{\epsilon}_A = -\gamma_{AB}(\alpha\epsilon_A - \epsilon_B) - (1-\alpha)\gamma_{AB}\epsilon_A\epsilon_B . \qquad (III-7a)$$

Similiarly, multiplying j and summing over (j,k) we obtain

$$\dot{\epsilon}_B = \gamma_{AB}(\alpha\epsilon_A - \epsilon_B) + (1-\alpha)\gamma_{AB}\epsilon_A\epsilon_B . \qquad (III-7b)$$

We now assume that modes A and B are at vibrational temperatures T_A and T_B, then, the probability distribution can be written as

$$P_{mn} = P_{oo}\exp[m\theta_A - n\theta_B)]$$

where $\theta_A = \frac{E_A}{kT_A}$ and $\theta_B = \frac{E_B}{kT_B}$

and P_{00} is the ground state probability. This representation includes all combination states of the system. Eq.(III-3) now becomes

$$\epsilon_A = (e^{\theta_A} - 1)^{-1} \quad \text{and} \quad \epsilon_B = (e^{\theta_B} - 1)^{-1} \qquad (III-8X)$$

The vibrational steady state solution for (III-7) may be obtained by setting $\dot{\epsilon}_A = \dot{\epsilon}_B = 0$ and substituting eq.(III-8X). Simplifying this result yields the well-know result for vibrational equilibrium[18]

$$\theta_B - \theta_A = \theta_R$$

Let us now examine the processes in the presence of the laser pulse. To include the interaction of the laser in the energy equations, a pump term must be added to the collision part of the rate equations. As before, we assume a laser pulse that interacts with only the P_{00} and P_{10} states of the system,

the rate equations can be written as

$$\frac{dP_{00}}{dt} = \left(\frac{dP_{00}}{dt}\right)_{\text{Collision}} - \sigma I (P_{00} - P_{10}) \qquad \text{(III-8a)}$$

$$\frac{dP_{10}}{dt} = \left(\frac{dP_{10}}{dt}\right)_{\text{Collision}} + \sigma I (P_{00} - P_{10}) \qquad \text{(III-8b)}$$

$$\frac{dP_{jk}}{dt} = \left(\frac{dP_{jk}}{dt}\right)_{\text{Collision}} \quad \text{for } (j,k) \neq (0,0), (1,0),$$

where $(dP/dt)_{\text{collision}}$ is given by eq. (III-6), σ is the absorption cross section, and I is the laser pulse intensity in photons/cm^2-sec.

The number of molecules pumped per unit time is then given by $\dot{\epsilon}_L = \sigma I (P_{00} - P_{10})$. (III-9)

Therefore, the energy equations (eq. (III-7)) become,

$$\dot{\epsilon}_A = -\gamma_{AB}\left[(\alpha\epsilon_A - \epsilon_B) - (1-\alpha)\epsilon_A\epsilon_B\right] + \dot{\epsilon}_L \qquad \text{(III-10a)}$$

$$\dot{\epsilon}_B = \gamma_{AB}\left[(\alpha\epsilon_A - \epsilon_B) - (1-\alpha)\epsilon_A\epsilon_B\right]. \qquad \text{(III-10b)}$$

Substituting eq. (III-9) into eq. (III-8a), we get

$$\dot{P}_{00} = \left(\frac{dP_{00}}{dt}\right)_{\text{Collision}} - \dot{\epsilon}_L . \qquad \text{(III-11)}$$

Using eq. (III-5), we find that

$$\begin{aligned}\left(\frac{dP_{00}}{dt}\right)_{\text{Collision}} = {} & P_{10}(\gamma_A + \gamma_A\epsilon_A + \alpha\gamma_{AB} + \alpha\gamma_{AB}\epsilon_B) \\ & + P_{01}(\gamma_B + \gamma_B\epsilon_B + \gamma_{AB} + \gamma_{AB}\epsilon_A) \qquad \text{(III-12)} \\ & + P_{00}(\gamma_A\epsilon_A + \gamma_{AB}\epsilon_B + \gamma_B\epsilon_B + \alpha\gamma_{AB}\epsilon_A).\end{aligned}$$

We now assume for the mode system connected by a common ground state a probability distribution where the P_{00} and P_{10} states are connected by the laser to get

$$P_{00} = P$$
$$P_{10} = P \qquad \text{(III-13)}$$
$$P_{mn} = P \exp(-m\Theta_A - n\Theta_B).$$

This assumption is analogous to the one of (II-17) which again is of fundamental importance. Equation (III-11) becomes

$$\dot{P} = \left(\frac{dP}{dt}\right)_{\text{Collision}} - \dot{\epsilon}_L \,, \qquad \text{(III-14)}$$

and using eq.(III-13) in eq.(III-12), we have

$$\left(\frac{dP}{dt}\right)_{\text{Collision}} = \gamma_A P + \left[\gamma_{AB}(\alpha + \alpha\epsilon_B - \epsilon_B - \alpha\epsilon_A) - \gamma_B \epsilon_B\right] P$$
$$+ \left[\gamma_{AB}(1+\epsilon_A) + \gamma_B(1+\epsilon_B)\right] P e^{-\Theta_B}. \qquad \text{(III-15)}$$

To find ϵ_A and ϵ_B, we now utilize number conservation

$$1 = \sum_{m=0}^{\infty}\sum_{n=0}^{\infty} P_{mn} = \sum_{m=2}^{\infty} P e^{-m\Theta_A} + 2P + \sum_{m=0}^{\infty}\sum_{n=1}^{\infty} P e^{-m\Theta_A - n\Theta_B} e$$
$$= P\left\{2 + \frac{e^{-2\Theta_A}}{1-e^{-\Theta_A}} + \frac{1}{1-e^{-\Theta_A}} \frac{1}{1-e^{-\Theta_B}}\right\}$$

$$= P\left\{\frac{(1+1-2e^{-\theta_A}+e^{-2\theta_A})(1-e^{-\theta_B})+e^{-\theta_B}}{(1-e^{-\theta_A})(1-e^{-\theta_B})}\right\},$$

or

$$\frac{1}{P} = \frac{1}{(1-e^{-\theta_A})(1-e^{-\theta_B})} \qquad \text{(III-16)}$$

$$+\left[\frac{1-2e^{-\theta_A}+e^{-2\theta_A}+2e^{-(\theta_A+\theta_B)}-e^{-2(\theta_A+\theta_B)}}{(1-e^{-\theta_A})(1-e^{-\theta_B})}\right].$$

It is now assumed that the intermode coupling exhibits a time dependent steady state according to detailed balancing such that $\theta_B = \theta_A + \theta_R$.

As the laser quickly excited A, θ_A gets small because of the rapidly and largely increased T_A. θ_B remains of order one. Then, an examination of eq.(III-16) shows

$$(1-e^{-\theta_A})^2(1-e^{-\theta_B})+e^{-\theta_B} \ll 1, \qquad \text{(III-17)}$$

therefore, in eq.(III-10)

$$P \approx (1-e^{-\theta_A})(1-e^{-\theta_B}). \qquad \text{(III-18)}$$

We can write ϵ_B as

$$\epsilon_B = \sum_m \sum_n n P_{m\,n} = P \sum_m e^{-m\theta_A} \sum_n n e^{-n\theta_B}$$

$$= P \frac{1}{(1-e^{-\theta_A})}\left[\frac{e^{-\theta_B}}{(1-e^{-\theta_B})^2}\right].$$

Using eq. (III_18) gives

$$\epsilon_B = \frac{1}{e^{\theta_B}-1}. \qquad \text{(III-19)}$$

Similiarly,

$$\epsilon_A = \sum_m \sum_n m P_{mn} = \frac{e^{-\theta_A}}{1-e^{-\theta_A}} + P(1-e^{-\theta_A}). \qquad \text{(III-20)}$$

Note that from eq. (III-17)

$$(1-e^{-\theta_A})^2 (1-e^{-\theta_B}) << 1$$

or $(1-e^{-\theta_A})^2 << 1$,

then, the expression for ϵ_A becomes

$$\epsilon_A \simeq \frac{1}{e^{\theta_A}-1} \qquad \text{(III-21)}$$

and we find that

$$P \simeq \frac{1}{1+\epsilon_A} \frac{1}{1+\epsilon_B} \simeq \frac{1}{1+\epsilon_T+\epsilon_A\epsilon_B} .$$

If we now return to eq. (III-5), we find

$$\left(\frac{dP}{dt}\right)_{\text{Collision}} = \gamma_A P + \left\{\gamma_{AB}\left[\alpha(1+\epsilon_B-\epsilon_A) + e^{-\theta_B}(1+\epsilon_A) - \epsilon_B\right]\right.$$

$$\left. + \gamma_B\left[-\epsilon_B(1-e^{-\theta_B}) + e^{-\theta_B}\right]\right\} P \qquad \text{(III-22)}$$

Collecting terms in γ_B and using (III-19), we get

$$-\epsilon_B(1-e^{-\theta_B}) + e^{-\theta_B} = \frac{-e^{-\theta_B}}{1-e^{-\theta_B}}(1-e^{-\theta_B}) + e^{-\theta_B} = 0 .$$

Collecting γ_{AB} terms gives (using eqs. (III-19) and (III-21)

$$\left[e^{-(\Theta_B-\Theta_A)}\left(1+\frac{e^{-\Theta_B}}{1-e^{-\Theta_B}}-\frac{e^{-\Theta_A}}{1-e^{-\Theta_A}}+e^{-\Theta_B}\left(1+\frac{e^{-\Theta_A}}{1-e^{\Theta_A}}\right)\right.\right.$$

$$\left.\left.\frac{-e^{-\Theta_B}}{1-e^{-\Theta_B}}\right]=e^{-(\Theta_B-\Theta_A)}\left[(1-e^{-\Theta_A})(1-e^{-\Theta_B})\right.\right.$$

$$\left.\left.+e^{-\Theta_B}(1-e^{-\Theta_A})-e^{-\Theta_A}(1-e^{-\Theta_B})\right]-e^{-\Theta_B}(1-e^{-\Theta_A})\right.$$

$$=e^{-\Theta_B}e^{-\Theta_A}(1-e^{-\Theta_A}-e^{-\Theta_B}+e^{-(\Theta_A+\Theta_B)}-e^{-\Theta_A}+e^{-(\Theta_A+\Theta_B)}$$

$$-e^{-2\Theta_B}(1-e^{-\Theta_A})+e^{-(\Theta_A+\Theta_B)}(1-e^{-\Theta_B})$$

$$=e^{-\Theta_B}(e^{\Theta_A}-2+e^{-\Theta_A})$$

$$=\frac{e^{-\Theta_B}}{1-e^{-\Theta_B}}\left(\frac{e^{\Theta_A}-1-1+e^{\Theta_A}}{1-e^{-\Theta_A}}\right)P$$

$$=\frac{\epsilon_B}{\epsilon_A}\left[\frac{1}{1-e^{-\Theta_A}}-\frac{1}{e^{\Theta_A}-1}\right]P=\frac{\epsilon_B}{\epsilon_A}P.$$

If we now substitute this result into eq.(III-22), it is found that

$$\dot{P}=\left(\gamma_A+\frac{\epsilon_B}{\epsilon_A}\gamma_{AB}\right)P-\dot{\epsilon}_L \qquad \text{(III-23)}$$

Using $\epsilon_L=\epsilon_A+\epsilon_B$ with eqs.(III-18), (III-19) and (III-21), we obtain

$$\epsilon_L=\frac{e^{-\Theta_A}(1-e^{-\Theta_B})+e^{-\Theta_B}(1-e^{-\Theta_A})}{P}$$

$$= \frac{1 - P - e^{-(\Theta_A + \Theta_B)}}{P} \qquad \text{(III-24)}$$

For large vibrational temperatures, P becomes small, so that

$$\epsilon_L \simeq 1/P \qquad \text{(III-25)}$$

and

$$\dot{\epsilon}_L \simeq \dot{P}/P^2 \qquad \text{(III-26)}$$

If we now assume that $(\epsilon_B/\epsilon_A)\gamma_{AB} << \gamma_A$, that is, the cross over is slower than the up-the-ladder rate,[55] then, eq. (III-23) becomes

$$\dot{P} = \gamma_A P + \dot{P}/P^2 ,$$

Again we note that γ_A is defined such that $\gamma_A = \gamma_{VV}/2$

Separating the variables and integrating gives

$$\int_{P(0)}^{P(\tau_p)} \left(\frac{1}{P} - \frac{1}{P^3}\right) dP = \int_0^{\tau_p} \gamma_A \, dt ,$$

or

$$2 \ln(2P) + \frac{1}{P^2} = \gamma_{VV} \tau_p + 4 , \qquad \text{(III-27)}$$

and

$$\epsilon_{tot} = \epsilon_L = \epsilon_A + \epsilon_B \simeq 1/P , \qquad \text{(III-28)}$$

Thus, these two equations together describe the energy absorbed by the two mode system in terms of γ_{VV} and τ_p, the

laser pulse width.

Now, if we go back to Chapter II and examine the energy absorptions, we find the P_1 equation term by term analogous to corresponding P equation (eq.(III-27)). If we examine the $\dot{\mathcal{E}}$ equation from Chapter II, we find

$$\mathcal{E} = \frac{(1-P_1)^2}{P_1} = \epsilon_{tot} \quad ,$$

which in the small P regime yields

$$\epsilon_{tot} \simeq 1/P_1 \quad ,$$

a result identical to the two mode case[eq. (III-28)].

Thus, it has been shown that with the assumption of a quasi-equilibrium and a temperature relationship between the two modes of the system and high excitation, the energy absorbed by a polyatomic is approximately the same as that for a diatomic. Thus, the simple relationships of Chapter II are valid for polyatomics where the mode structure is similiar to the one described here.

These equations make it possible to obtain a V-V up-the-ladder rate (γ_{V-V}) from a knowledge of the energy absorbed ($\hbar\omega\mathcal{E}$) and the laser pulse time (τ_p). In effect, an energy absorption experiment can now replace the sometimes laborious laser induced fluorescence method for obtaining V-V rates.

Computer simulations of this process have produced similiar results and shall be discussed in the next section. Experimental proof of this phenomenon will be presented in Chapter IV.

IV. COMPUTER ANALYSIS OF SINGLE MODE AND TWO MODE TRANSFER IN THE PRESENCE OF AN INTENSE LASER PULSE

INTRODUCTION

In this chapter the computer results and simulations of all the findings stated in Chapters II and III will be presented. The rate equation analysis were carried out on an IBM 370 computer and the simple expressions were calculated by Hewlett-Packard 25 calculator. The result presented here are as follows:

(1) the time evolution of probability in the vibrational levels of a diatomic molecule in the presence of a saturating laser pulse for fixed V-V rate. The oscillation frequency is considred the same as the ν_3(C-F stretch) vibration of CH_3F (see Appendix D). This result is given for a one mode (ν_3) and a two mode oscillator where the second mode corresponds to the ν_6 bend of CH_3F.

(2) the existence of an effective vibrational temperature for the $V \geq 2$ vibrational levels with $P_o = P_1$. Results for the one and two mode cases are given. This was postulated in eqs. (II-17) and (III-13).

(3) the depletion of probability in the $V=1$ level as a function of increasing total quanta in the mode.

(4) the excellent agreement between the computer generated curves for quanta per molecule vs. VV rate and those generated by the closed form expressions eqs.(II-21) and (II-24) .

(5) the computer verification of the equivalence of the total energy absorbed by a diatomic and polyatomic molecule.

TIME EVOLUTION OF PROBABILITY

To simulate the collision processes for a diatomic during the laser pulse interaction, eqs.(II-1), (II-2), and (II-3) were used, namely,

$$\frac{dP_0}{dt} = \left(\frac{dP_0}{dt}\right)_{collision} - (P_0 - P_1)\sigma I$$

$$\frac{dP_1}{dt} = \left(\frac{dP_1}{dt}\right)_{collision} + (P_0 - P_1)\sigma I$$

$$\frac{dP_v}{dt} = \frac{dP_v}{dt} \quad v \geq 2$$

along with the dP_v/dt equation eq.(II-4),

$$\frac{dP_v}{dt} = (\gamma_{v-v}/2)\sum_{v'=0}^{\infty} -[(v+1)v' + v(v'+1)]P_v P_{v'} + vv' P_{v-1} P_{v'} + [(v+1)(v'+1)]P_{v+1} P_{v'}$$

The laser pump rate was assumed to be much greater than any collisional rate. Only dipole-dipole coupling through single quantum transitions were allowed with γ_{V-V} being an imposed fixed parameter--usually $1.0 \mu sec^{-1}$, consistent with the γ_{V-V} for CH_3F (to be discussed in later chapters). This parameter could be scaled to simulate any desired V-V rate. The laser pumping rate was assumed to be very large and the V-T relaxation was assumed to be negilible on

the time scale of the V-V processes.

For an oscillator of frequency $1048cm^{-1}$ (as is the case for the C-F stretch vibration of CH_3F), the probability distribution among vibrational levels is shown in Fig. 6 for 1.0 μsec and 2.0 μsec laser pulse durations. In each case the probabilities P_1 and P_0 are equal and are decreasing functions of time.

To understand the time build-up of probability in each level, a plot of P_v vs. time is shown in Fig. 3 for v=0,1,2,3,4. As imposed by the initial conditions (eq. (II-16)), P_0 and P_1 are each 1/2 at t-0 and they decrease with time at the same rate while remaining equal for all times $t \leq \tau_p$. These two levels are locked together by the laser pulse, hence, their identical time behavior during the pulse is reasonable. Note also the very rapidly increasing probability of the v=2 level. The filling of the v=2 level is primarily through the process

$$(v=1) + (v=1) \longrightarrow (v=2) + (v=0)$$

where the v=1 level population is initially at a very high value, thereby, making the above reaction a very efficient one. The probabilities of the $v \geq 1$ levels are less rapidly increasing functions of time. This is because of the finite time required for the levels (in the major channels for high v-state activation) to acquire probability through V-V transfer.

To analyze the problem for a two mode system, eq. (III-10) must be solved where eq. (III-5) is employed. The laser pumping term, ε_L, is again considered very large. Both modes share a common ground state and combination states are included in the definition of a state of the system.

If the second, non-resonant oscillator (ν_6 of CH_3F) is added to the problem with an energy defect of $147cm^{-1}$, a V-V crossover rate of 1/10 the ν_3 V-V up-the-ladder rate, and the same up the ladder rate as that of ν_3, the probabilities are given in Fig. 4. The curves show that the probability in levels ν_3 v=1 and v=0 are the same as in Fig. 3 (where ν_6 is absent). Note that the probabilities of the ν_3 (v>1) levels are only slightly perturbed by the presence of ν_6. The probability found in ν_6 is only a small fraction of the total present. The time delay in build-up of probability in ν_6 is seen in the probability vs. time curves of Fig. 5.

THE ESTABLISHMENT OF A TIME DEPENDENT QUASI-EQUILIBRIUM

The existence of a time dependent equilibrium among the $V \geq 2$ levels was postulated by eqs. (II-17) and (III-13). Computer analysis have verified that, indeed, for an oscillator system interacting with a saturating laser pulse and a sufficiently fast up-the-ladder V-V rate, such a distribution does exist for the duration of the laser pulse. Fig. 6 shows a plot of the probability in level V of ν_3 vs. vibrational quantum number for two different laser pulse dura-

tions for a single mode. Note the equality of levels 1 and 0 in each case and the exponential drop-off of the $V \geq 2$ levels.

For the 2.0μsec laser pulse, the effective temperature (2320°K) is greater than that of the 1.0μsec pulse (1570°K) as predicted by eq. (II-21) and (II-22). One may also observe the decrease in probability of the v=0 and v=1 states for the longer pulse widths. The probabilities of the higher V states are observed to increase with time (1→2μsec), thus, forming the higher temperature distribution. Figure 7 shows the distribution in ν_3 in the presence of ν_6 for two different V-V cross-over rates and a constant up-the-ladder rate. For a 3.0μsec laser pulse, Fig. 7a gives a temperature of 2945°K where the cross-over rate, RATEF, is equal 1/10 the up-the-ladder rate and 2926°K for RATEF equal 7/10 the up-the-ladder rate. The small probability changes of the v=0 and v=1 states are now due to the increased flow of energy for the larger RATEF.

These findings have all given credence to a bold assumption which is crucial to the theoretical analysis -- nemely, the time dependent effective temperature of the $V \geq 2$ levels. This assumption was necessary for the solution of the rate equations for the laser excited oscillator system and is valid for any system with rapid V-V up-the-ladder collisions and negligibly small anharmonicity.

QUANTA ABSORBED BY A ONE AND TWO MODE OSCILLATOR SYSTEM

The energy absorbed by a polyatomic has been shown to be equal to the total energy absorbed by a diatomic by theory and now by computer analysis. The probability distribution for one 20-level oscillator and two non-resonant 20-level oscillators was calculated, then,

$$\varepsilon_{tot}=\sum_{v} vP_v$$

was used for the single mode energy and

$$\mathcal{E}_{tot}=\epsilon_A+\epsilon_B=\sum_{m,n} mP_{mn}+\sum_{m,n} nP_{mn}$$

was used for the two mode total energy.

Fig. 8 shows a plot of the energy in one mode vs. V-V rate, two modes vs. V-V rate, and the theoretical prediction for an infinite oscillator. The most impressive feature is that the one and two mode energies absorbed are exactly the same, thus, supporting the theory. Furthermore, at the lower V-V rates, both the one and two mode curves follow the model predicted curve. This agreement would continue for higher V-V rate, but the computer begins to saturate for a finite 20-level system at large ε. Adding more levels to the program would carry the agreement to higher energies and greater rates.

Hence, the theoretical model has been supported by computer simulations and the results have far reaching consequences. The ability to treat a polyatomic with the simple diatomic relations removes some of the complexities of poly-

atomic absorption. It also gives an insight into the transient behavior of the intra-mode kinetics during laser excitation. These findings will be tested experimentally in Chapter VI.

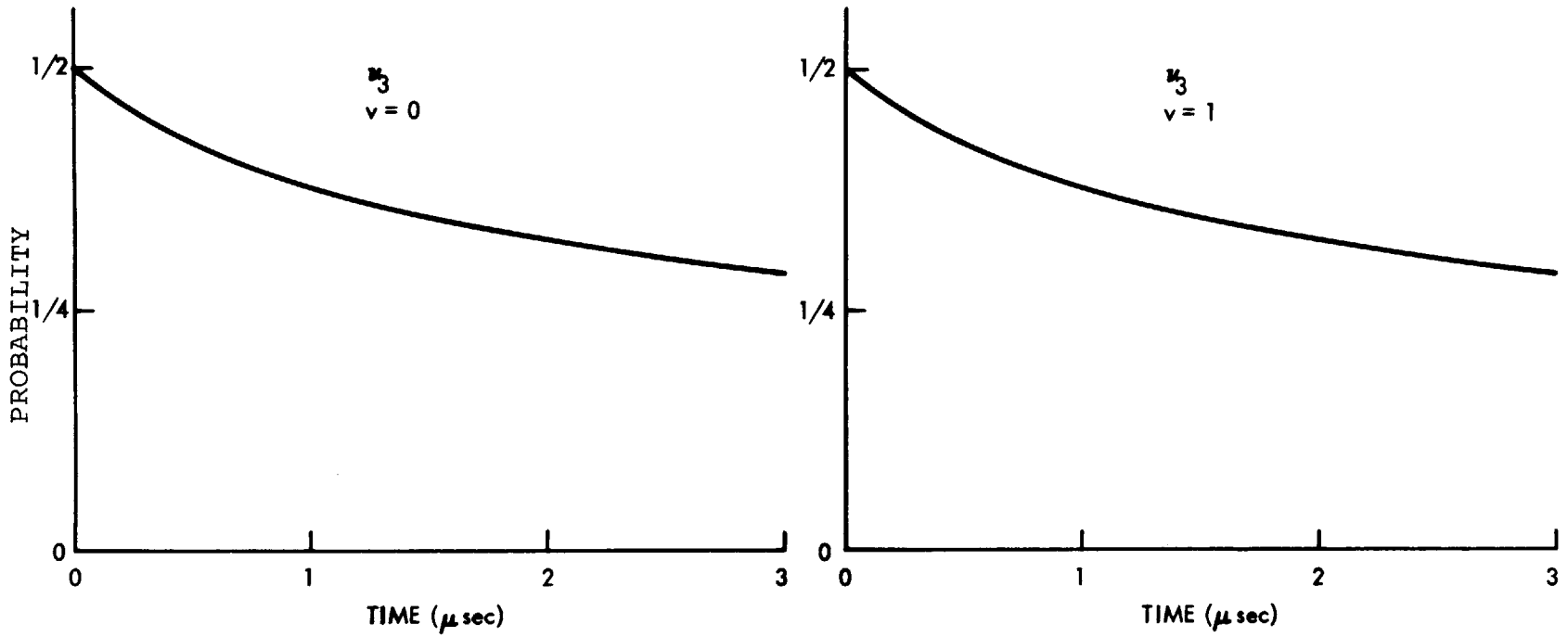

Fig. 3. Time variation of probability for vibrational states of single oscillator with energy levels of 1050cm^{-1}.

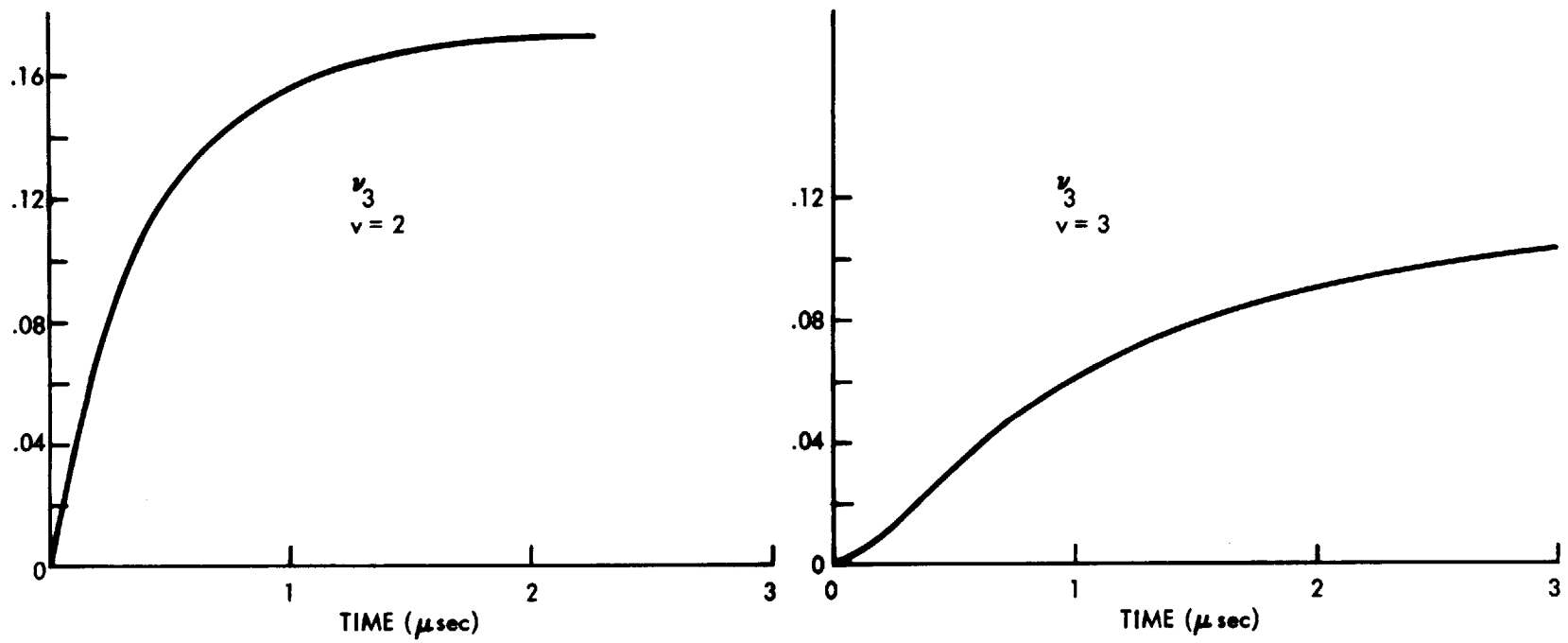

Fig. 3. (Continued)

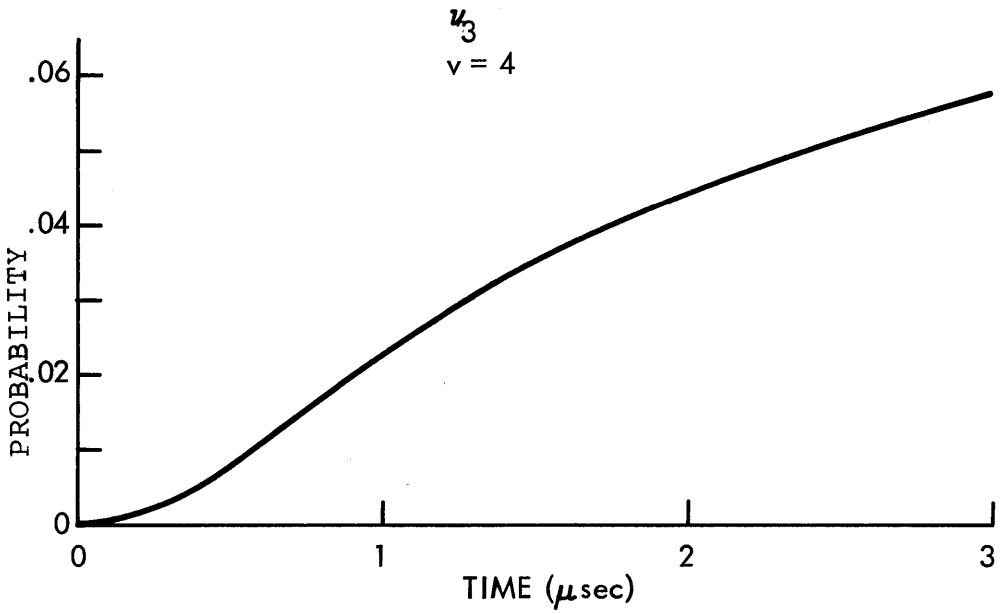

Fig. 3. (Continued)

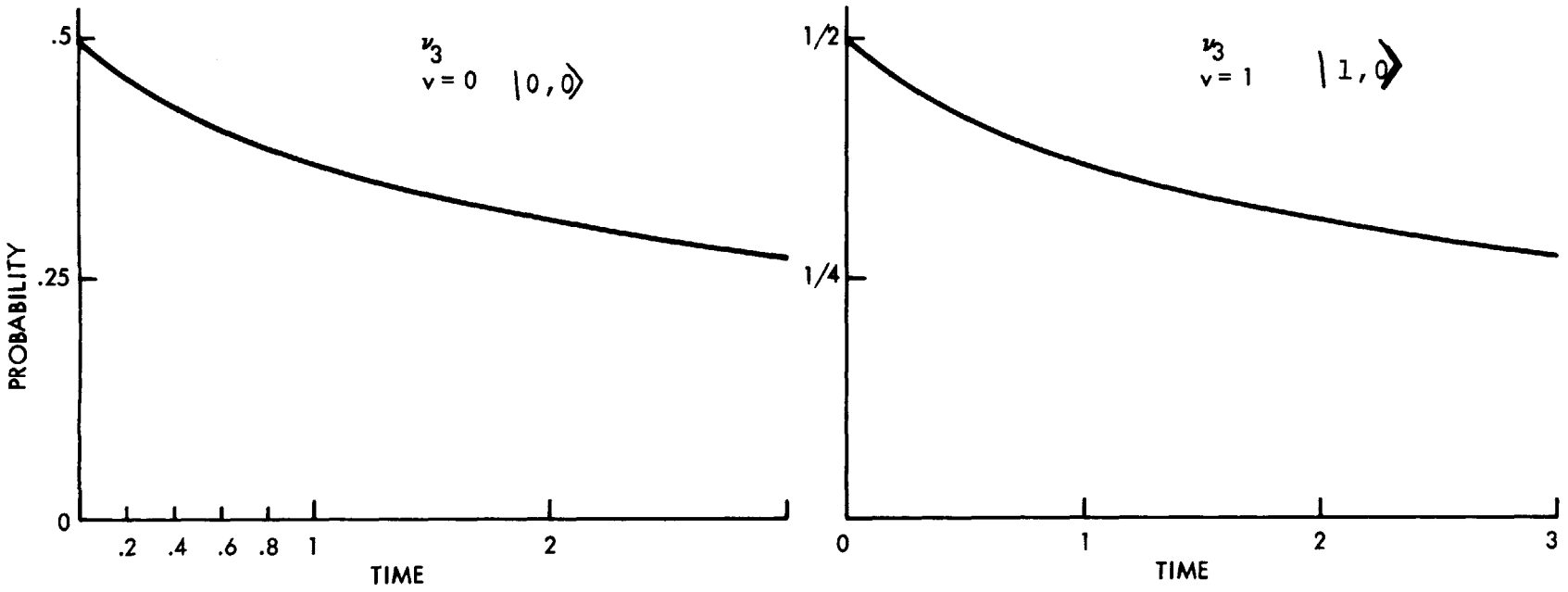

Fig. 4. Time variation of probability of ν_3 in the presence of collisionally coupled ν_6. V-V cross-over rate is 1/10 the up-the-ladder rate.

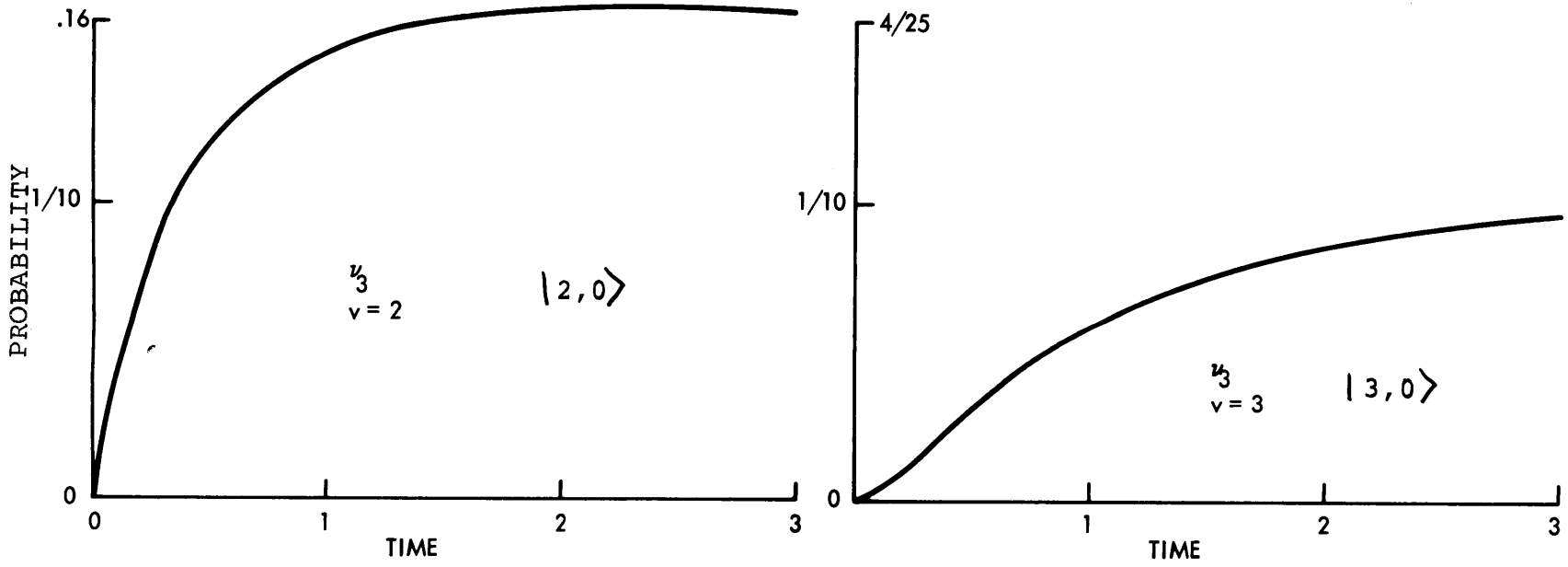

Fig. 4. (Continued)

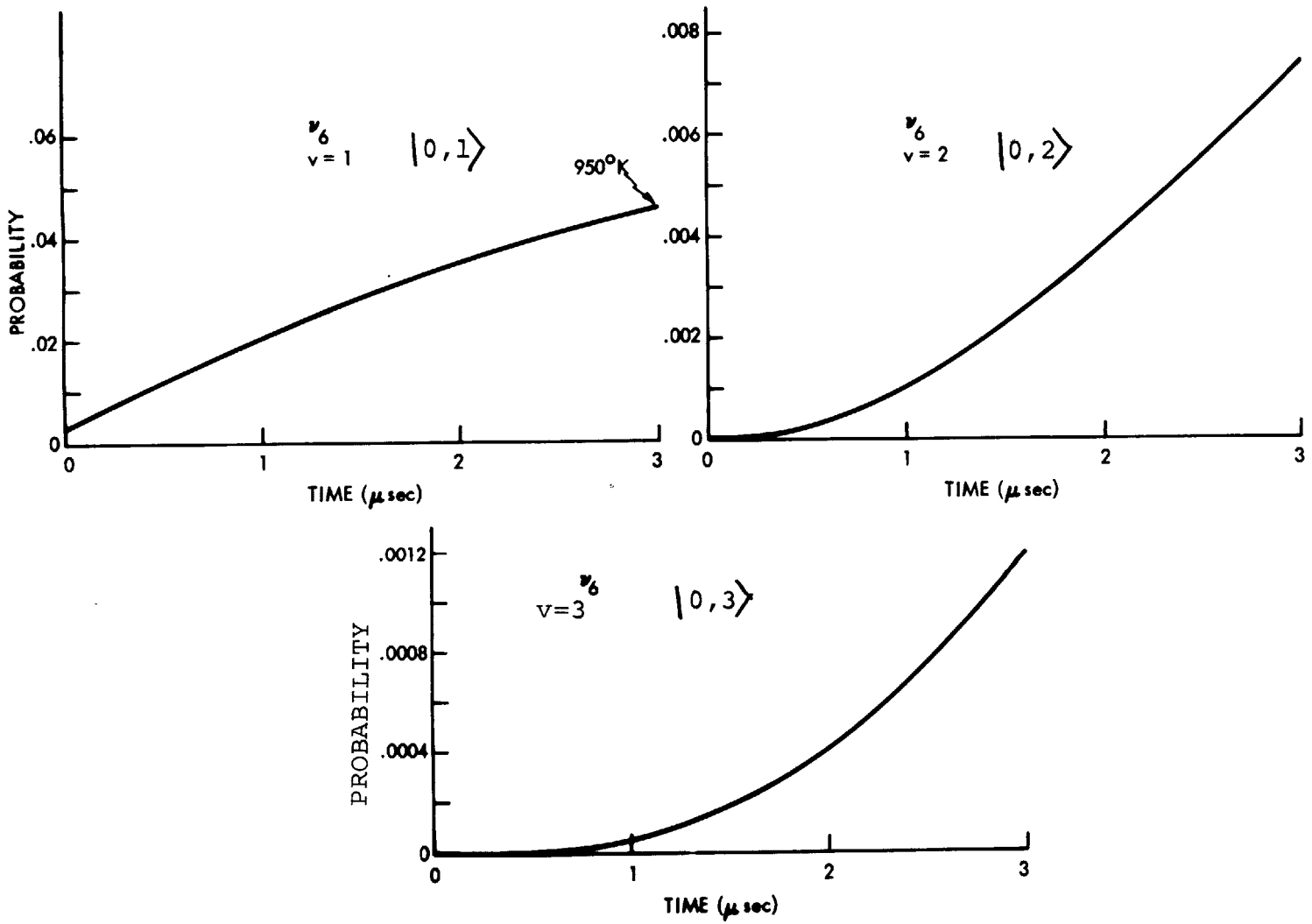

Fig. 5 . Time variation of probability in the ν_6 mode of a two mode oscillator. ν_3 is pumped by the laser.

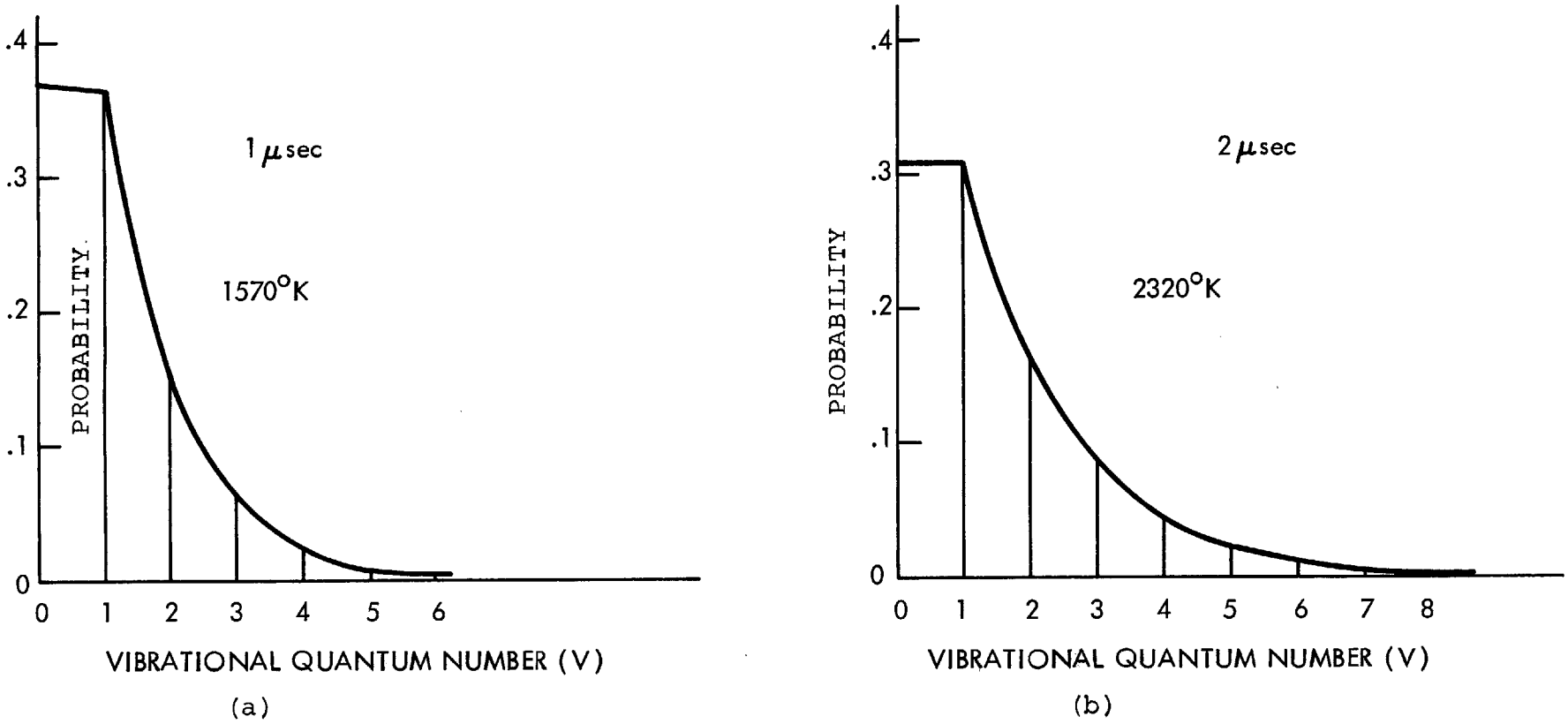

Fig.6. Establishment of a quasi equilibrium distribution for the $v \geq 1$ levels. (a) τ_p=1.0μsec (b) τ_p=2.0μsec.

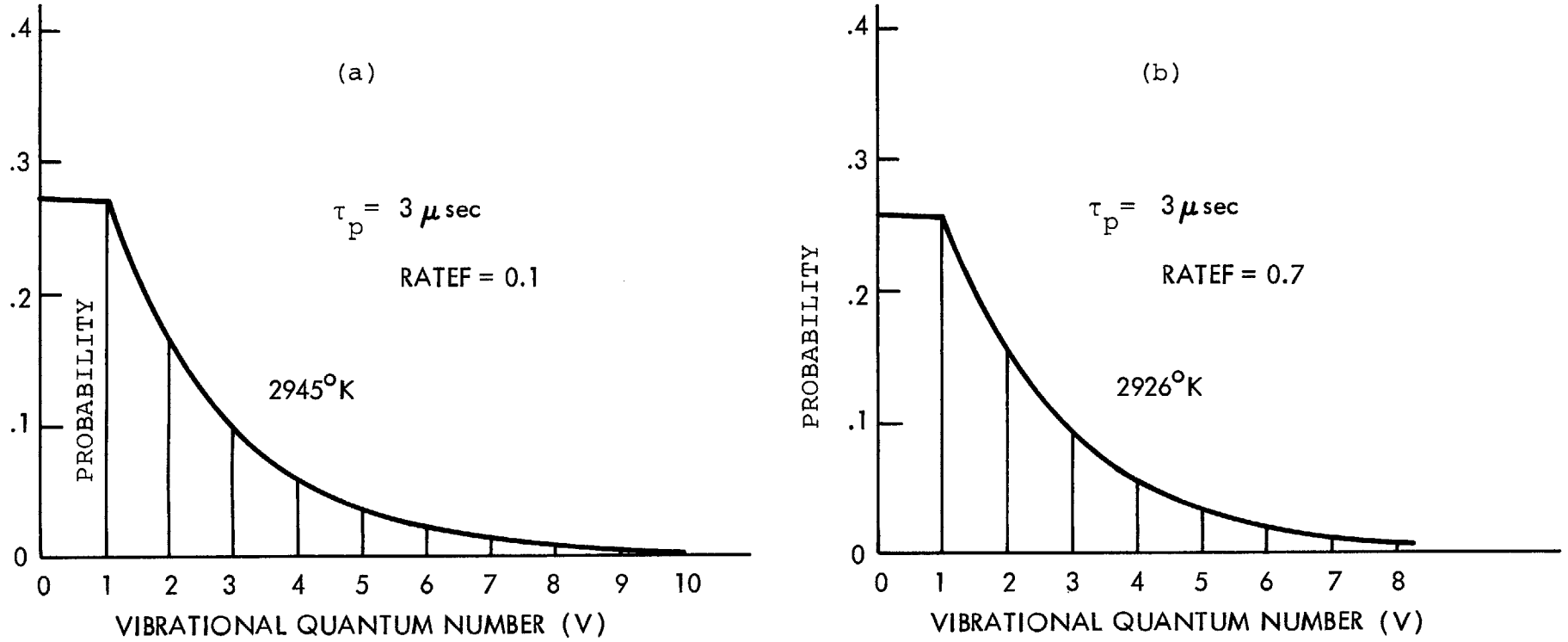

Fig. 7: Establishment of a quasi-equilibrium distribution among the v_1 levels in the presence of a coupled mode.

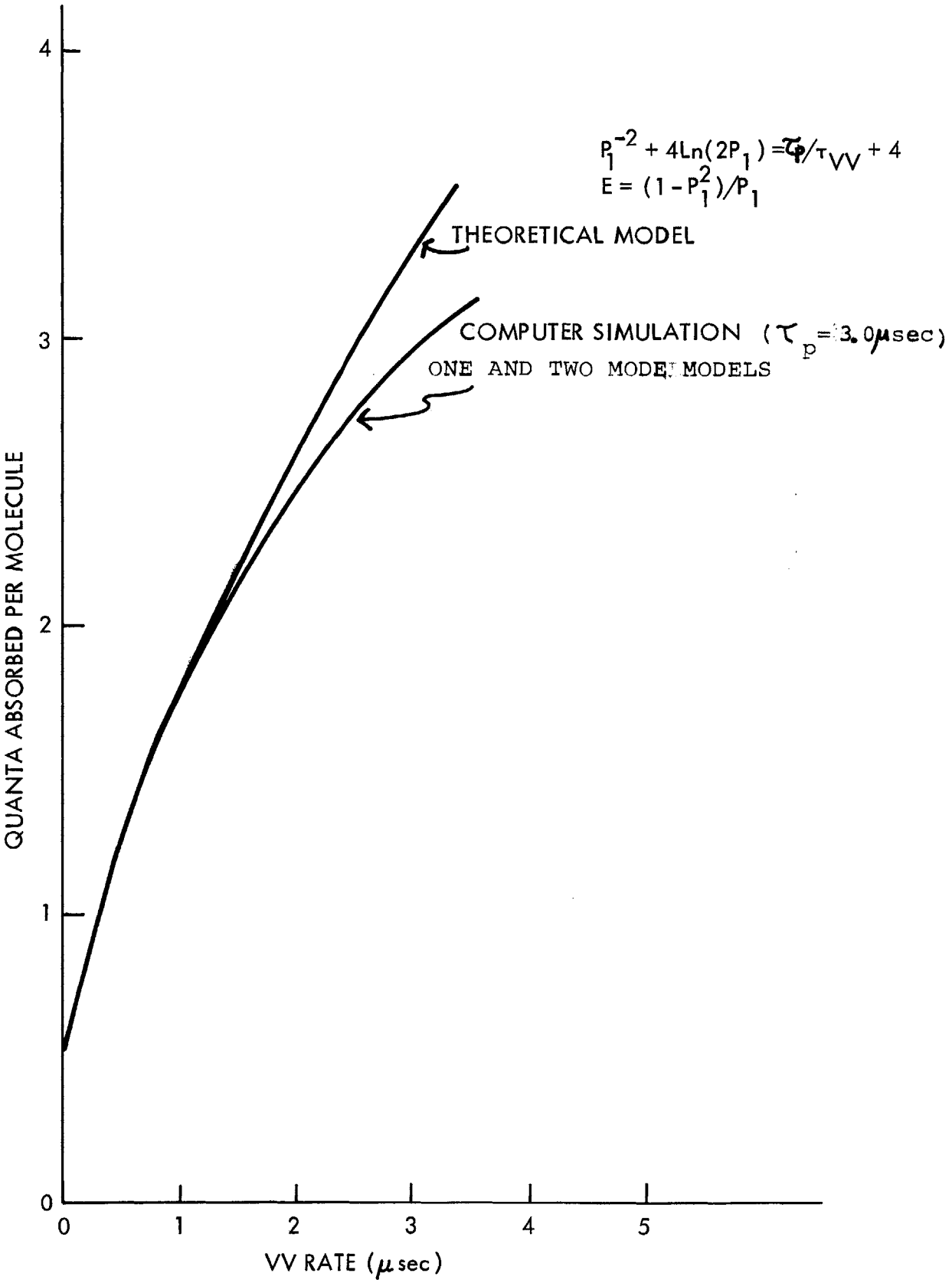

Fig.8. Comparison of theoretical and computer generated quanta absorbed per molecule vs. V-V rate.

V. EXPERIMENTAL APPARATUS

PUMP LASER

The CO_2 laser has many designs and mechanisms for achieving high power oscillation ranging from pulsed discharges and Q-switched cavities to transverse electric discharges and flashtube photoionization methods. In the experiments to be described extremely high powers (>0.5M-watts) were not desirable nor were short pulses (<1.0μsec). Therefore, a simple helical discharge TEA laser proved adequate and extremely reliable.

A 1.93 meter long 5.0 cm diameter plexyglass tube formed the discharge tube. The cathode was formed by 0.5 watt resistors placed in a helical array by first drilling small holes in the plexyglass tube and sealing the resistors in with epoxy-patch. The resistors were all connected to each other by braided copper wire which served as the cathode. A piece of solid 1/2" copper tubing was placed internal to the tube opposite the resistors then connected to ground. Sodium chloride windows were placed at both ends of the tube with Brewster angle polarizations parallel to a vertical axis.

The discharge was pulsed by triggering an EG&G spark-gap with an 800V pulsed power supply. Figures (9) and (10) show the pulsed power supply circuit diagram and the overall electronics circuit diagram, respectively. Upon firing the spark-gap, 30 Kvolts was discharged through a 0.05μf capa-

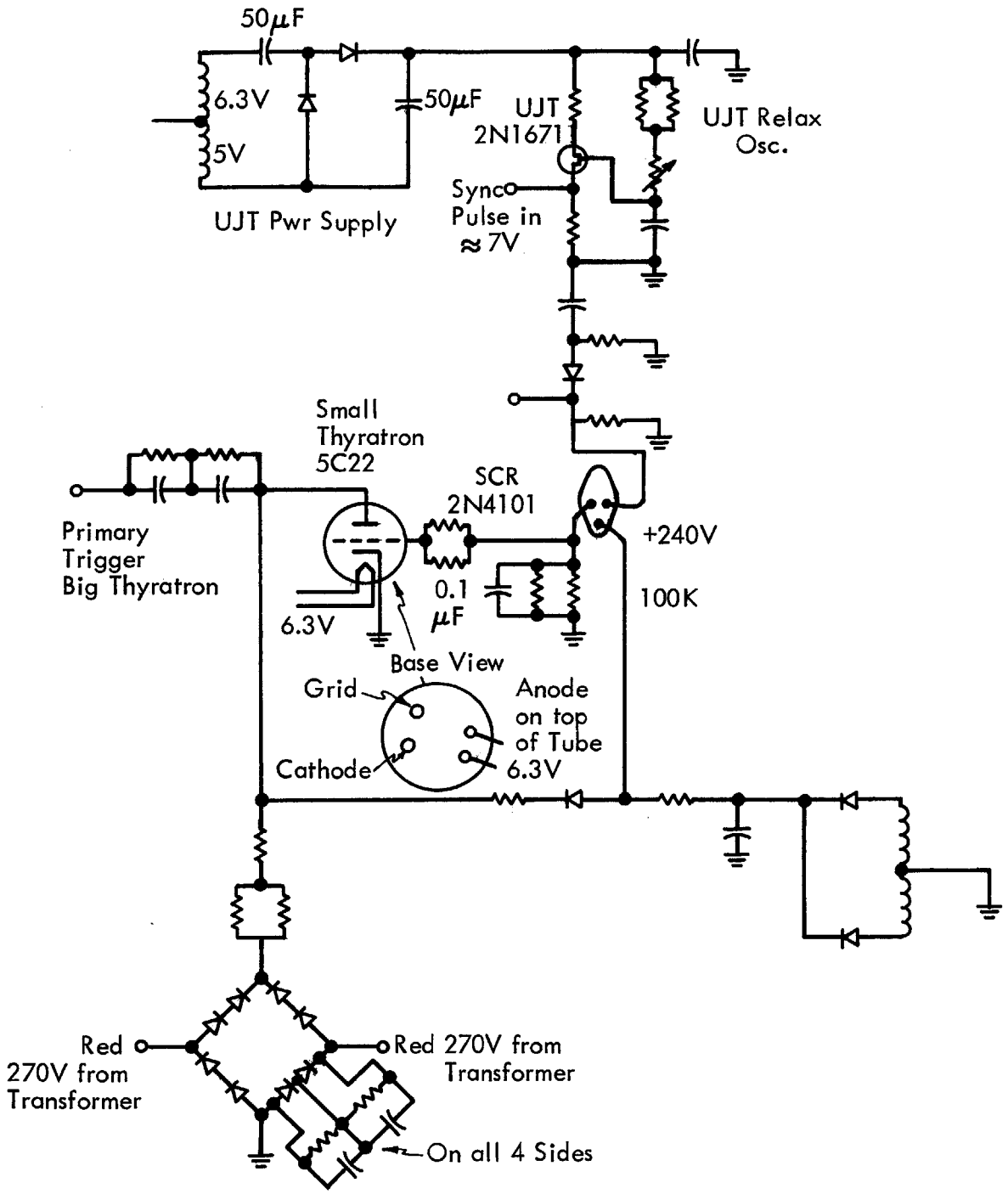

Fig. 9. Schematic of 800 volt pulsed power supply unit.

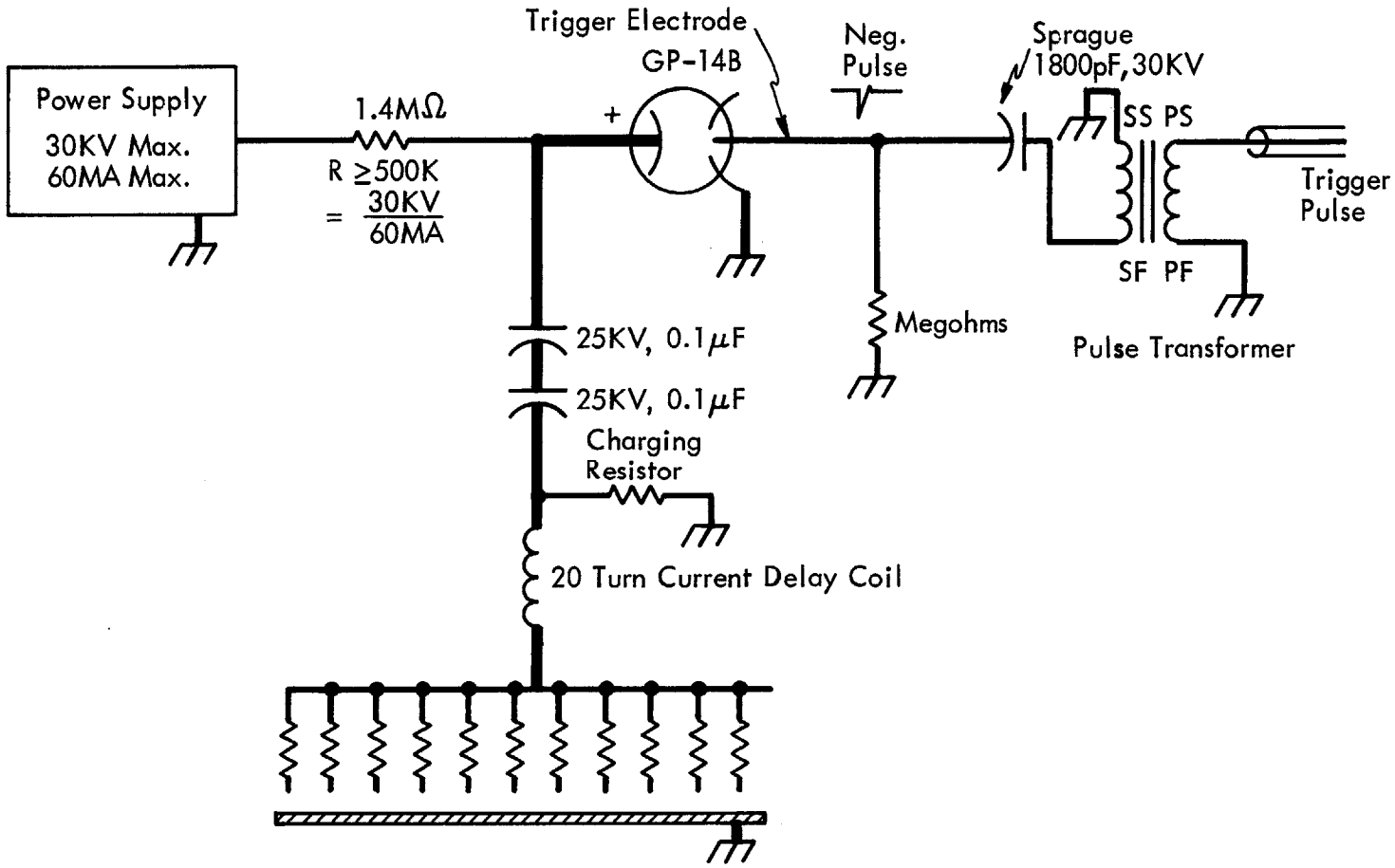

Fig. 10. Circuit diagram for TEA CO_2 laser.

citor, 1.4MΩ resistor bank, and the helical cathode to ground, producing a plasma inside the tube. A 20 turn coil served to lengthen the current pulse so that the power through the resistors was below the critical 0.5 watt level.

A CO_2:N_2:He::1:1:4 gas mixture was found to be optimum for long pulses with maximum energies. Total pressures ranged from 200-600 torr. All of the gases were from Matheson Co. and were flowed through the discharge at a slow rate.

The optical cavity consisted of a gold coated, copper substrate, 8.0 meter radius mirror on one end and a 9.0μm Bausch & Lomb grating at the other. The grating was tuned for single line operation on the 9.0μm band of CO_2 and was oriented with grooves perpendicular to the cavity axis for maximum output coupling. When desired, single mode operation was obtained by closing down two irises inside the cavity, which preferentially biased the gain to the TEM_{oo} mode.

With this laser, single line outputs were typically 500mj in 2.0μsec with pulse rates of 1-5 per second.

PROBE LASER

The probe laser used in the double resonance experiment (Chap.VIII) was a standard three electrode continuous discharge CO_2 laser. The cavity was 1.35 meters long with a 3.0 meter radius gold coated mirror and a 9.0μm grating,

both external to the discharge tube. Sodium chloride windows at Brewster's angle were used to polarize the laser field and seal off the discharge tube. Energy was coupled out off the grating, which was set for 90% reflectivity.

To aid in stabilizing the laser output from power supply ripple, a capacitor filter circuit and two current regulators were employed [Fig. (11) and Fig. (12)]. Figure (13) gives a comparison of the signal to ripple ratio with and without the filters and current regulators. The suspension of the entire apparatus on a floating table eliminated mechanical instabilities. Continuous single line power output was approximately 5.0 watts/cm^2. However, this output was attenuated in the double resonance experiments.

For the low power relaxation measurements, this laser was operated Q-switched by rotating the gold mirror at 60Hz. Outputs of $\sim$1.0mJ in 1.0μsec were obtained at P(20)CO_2 and grating coupling.

GAS HANDLING SYSTEM

The gas handling system was designed for re-cycling the $^{13}CH_3F$ gas and retaining its purity. This was made necessary by the expenses incurred in using large quantities of $^{13}CH_3F$. Also, it was necessary to allow for the mixing of $^{13}CH_3F$, $^{12}CH_3F$, and other gases in two cells through two channels.

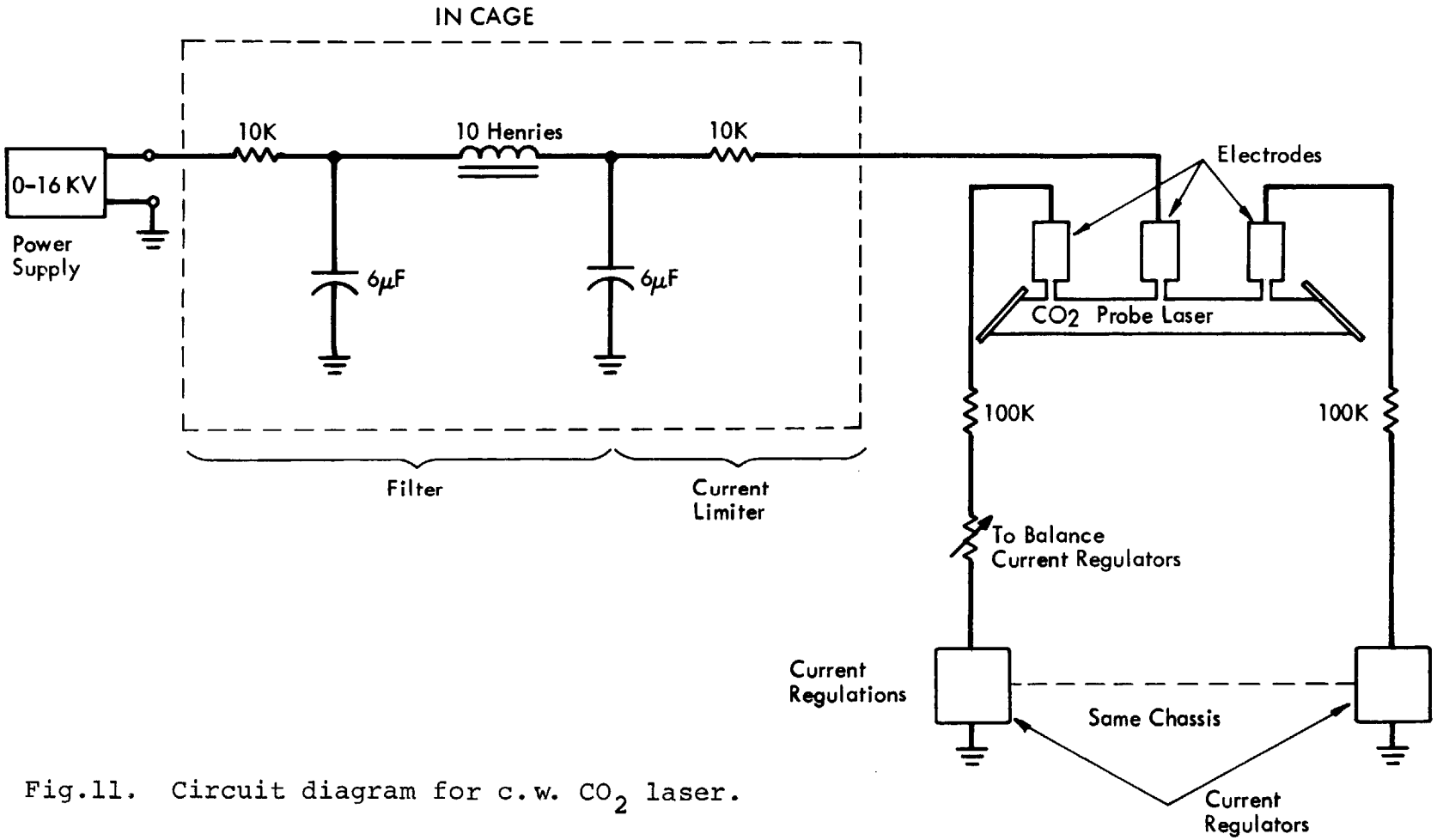

Fig.11. Circuit diagram for c.w. CO_2 laser.

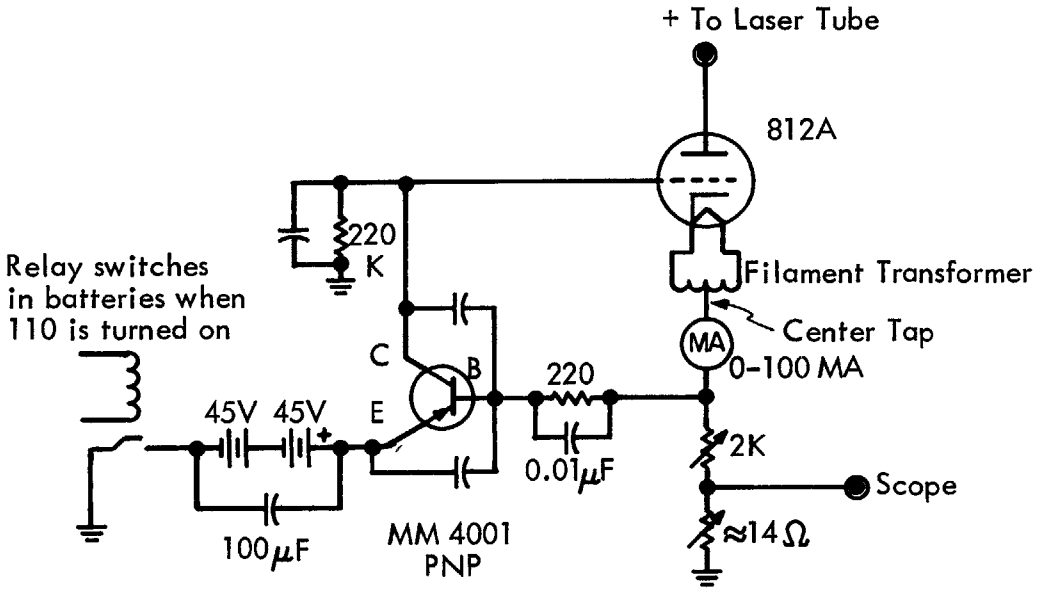

Fig. 12. Schematic of current regulator.

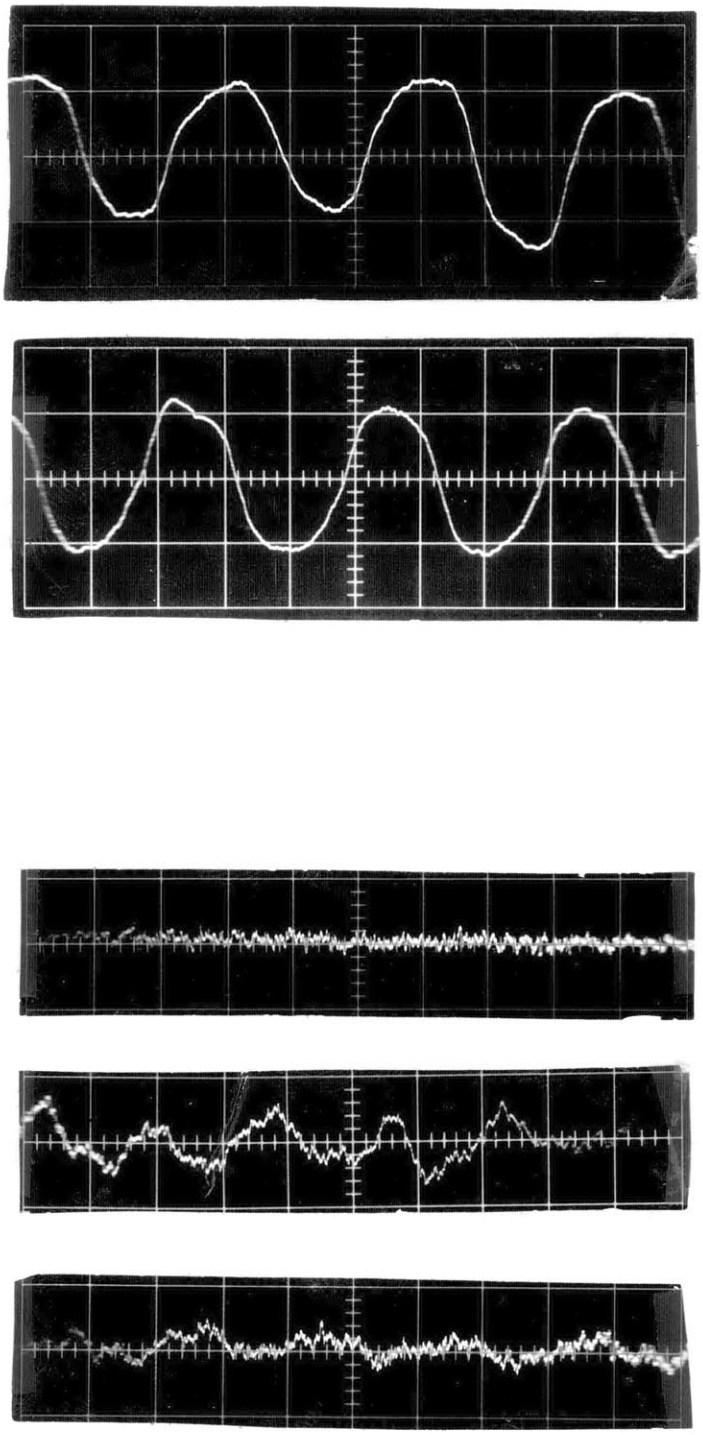

Fig. 13. Filtering of power supply ripple. (a) chopped laser signal without filter circuit (b) with filter circuit (c) detector noise (d) d.c. coupled laser signal with ripple without filter circuit (e) with filter circuit.

Figure (14) shows a diagram of the gas handling system used in all experiments. The $^{13}CH_3F$ used was from Merk & Co. and contained isotopic purities of 90% ^{13}C and 10% ^{12}C. The 100 cm^3 760 torr bottle of gas was divided between bottles A and B in the diagram. This served as a safety precaution in the event of contamination or breakage of either A or B. The entire system was all glass with high vacuum glass stopcock valves. Pressure was expanded into either cell by first filling the volume between the two exit stopcocks of A and B, then expanding this volume at high pressure into the larger low pressure volume. The double stopcocks were, again, a safety feature. Once the gas had been used, it was recollected by opening the stopcocks to bottle C which was brought to 77°K by a liquid nitrogen cold trap. Thus, the $^{13}CH_3F$ was frozen out in C where it remained for future use.

The $^{13}CH_3F$ could be forced to flow to either cell 1 or cell 2 by opening and closing the appropriate stopcocks. In addition, other gases contained in bottles E, F, and G were made accessible to the cells, again by manipulating the appropriate stopcocks. All sections were pumped by first passing through a liquid N_2 cold trap, then, through a three stage diffusion pump.

Pressures in the two cells were monitored by a 0-20.0 torr Wallace & Tiernan gauge and 0-5.0 torr mercury filled McLeod gauge. Pirani gauges were placed throughout the

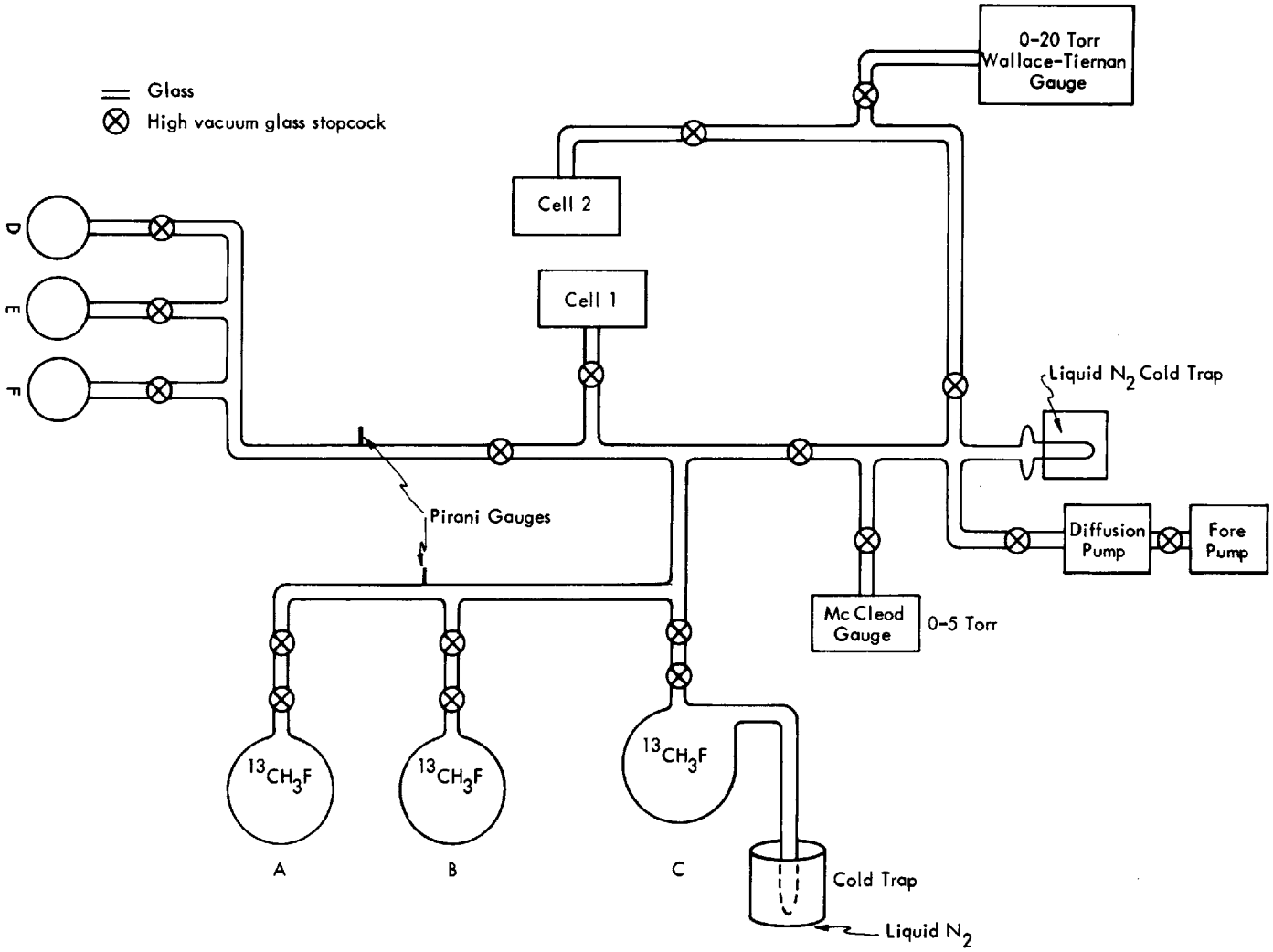

Fig. 14. Gas handling system.

system to monitor the pressures in isolated sections. These pirani gauges were calibrated against the McLeod gauge. Outgas rates of the entire system were typically 20-40 millitorr per 72 hrs.

VI. MEASUREMENT OF V-T RELAXATION TIME IN CH_3F

INTRODUCTION

In this chapter a measurement of the vibration-translation relaxation rates under high and low excitation is presented in order to establish that vibrational degrees of freedom are long lived in both regimes. The observation of fast decaying upper vibrational states and slow decaying lower states have been made by Osgood et al.[8] Here, similar behavior will be shown for levels in CH_3F that are non-linearly coupled to the pump transition.

DISCUSSION: RELAXATION PROCESSES

The relaxation among the degrees of freedom of a molecule is studied primarily to obtain cross sections from which the nature of the interaction potentials can be approximated. These cross sections are often compared with transition probability calculations in order to test the accuracy of the many models and approximations of collision theory.

Most gaseous molecules exchange energy among their rotational, vibrational, and electronic degrees of freedom via collisional low order multipole interactions. One of the major points of interest is how fast and efficient are these exchange processes for vibrational-vibration (V-V) exchange, vibrational-translational (V-T), rotational-Transitional (R-T), etc. What is generally observed experimentally

is the relaxation of internal energy given by

$$\frac{dE}{dt} = \frac{E_{int}(T_R) - E_{int}(t)}{\tau}$$

where τ is the relaxation decay time for the system ($\tau=\tau_{VT}$, τ_{VV}, τ_{RR}, etc.) and T_R is room temperature. The ratio of the relaxation time (τ) to the gas kinetic collision time ($\sim\tau_c=10^{-8}$ sec-torr)[21] gives the number of gas kinetic collisions Z necessary to complete a transfer process ($Z=\tau/\tau_c$).[13]

We shall turn our attention to the collisional relaxation of vibrational energy into translational energy (V-T) for small molecules in gaseous system and the techniques for measuring the rates.

There is no fixed rule governing molecular vibrational-translational relaxation times. The rates can vary greatly between similar molecules. These rates have been measured in many molecules (See Table I.). Many methods have been used to obtain these measurements such as sound absorption in shock tubes, stimulated Raman effect, thermal lensing, visible fluorescence and Raman probes of internal states, vibrational relaxation in liquids and solids, coherent transient effects, saturation spectroscopy, and laser induced fluorescence.

A very widely used method today is laser induced fluorescence, first used by Hocker et. al.[28] Collisional

Table I: V-T Relaxation Rates of Some Molecules

Molecule	V-T Rate (γ_{V-T}) $msec^{-1}torr^{-1}$
CO	1.9×10^{-6}
HF	58
DF	23
HCI	.83
DCI	.28
HBr	.56
DBr	.17
HI	.375
NO	2.7
H_2	4.53×10^{-3}
O_2	9.4×10^{-5}
N_2	3.3×10^{-7}
CO_2	.22
CH_3F	.59
CH_3Cl	6.6

deactivation of excited species is observed by monitoring the spontaneous emission out of the transition's upper levels after laser excitation. Collisional relaxation time in molecules are usually 1sec and the spontaneous emission time in the infrared is generally much longer. Therefore, for infrared and far infrared relaxation studies, the relatively long spontaneous emission time provides a mechanism for monitoring the faster collision processes

A measurement of the vibrational-translational (V-T) relaxation time in $^{12}CH_3F$ was made in both the low power and high power excitation regimes. Because of the rapid vibration to vibration energy exchange,[15] flouresence was observed from the (ν_1, ν_4), (ν_2, ν_5), and the ν_3 vibrational modes at approximately 3.3μm, 6.8μm, and 9.6μm, respectively.

For the low power measurement, excitation was performed by a Q-switched CO_2 laser operating on the P(20) 9.55μm transition.[15] This laser line interacts with the Q(12,2) transition of the ^{12}C species of CH_3F with an absorption coefficient of $0.018 cm^{-1} torr^{-1}$.[29] Pulse times were typically 1.0μsec duration with energies of about 1.0 milliJoule (mJ). The experimental apparatus is shown in Figure 15. A Bausch & Lomb 9.0μm grating is used to select a single rotational-vibrational line and couple energy out of the laser's 1.35 meter cavity. A gold coated 7.0 meter radius rotating mirror was used to Q-switch the gain medium. After coupling off the grating, the laser beam was directed into a stainless

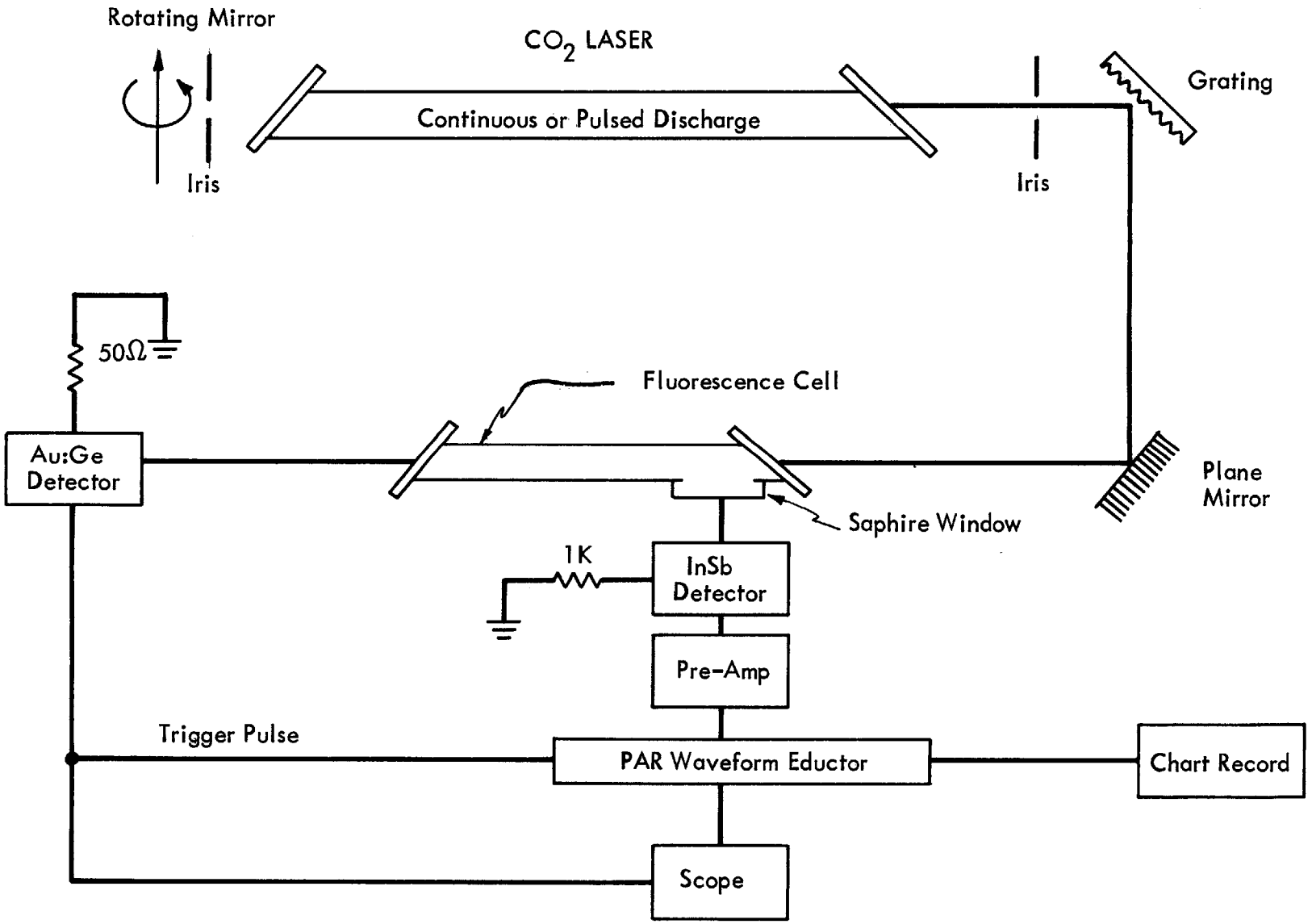

Fig.15. Experimental apparatus for V-T relaxation measurements.

steel cell with NaCl end windows at Brewster's angle. The cell contained a side window made of sapphire for viewing the 3.3μm fluorescence emitted perpendicular to the pump beam. The CH_3F was introduced into the cell through the gas handling system described in Chapter V. When the CO_2 laser excites the CH_3F inside the cell, the infrared emission from the 3.3μm vibration is detected with a liquid nitrogen cooled indium antimonide detector. All other fluorescing wavelengths are eliminated by the sapphire window and the InSb detectivity fall-off around 5.2μm. The InSb output was sent through a textronics 1A7 pre-amplifier then into a PAR waveform eductor for averaging. After passing through the fluorescence cell, the CO_2 signal was detected by an Au:Ge detector and used to trigger the waveform eductor in the external trigger mode. The rotating mirror provided 60 pulses per second for averaging. Averaged signals were viewed on an oscilloscope or a chart recorder [See Fig. 17] from which the amplitudes were fitted to an exponential and the 1/e values were extracted graphically.

For the gas samples used, the low excitation V-T times were measured to be approximately 700μsec-torr. This number is approximately twice as fast as measurements by Flynn[15] but sufficiently slow for the purposes of all experiments presented in this work. This variance is probably due to differences in gas sample purities. The time $\tau_{V-T} \sim 700\mu$sec-torr is the time of relaxation for the process

$$CH_3F(V_1,V_4) + CH_3F(0) \longrightarrow 2CH_3F(0).$$

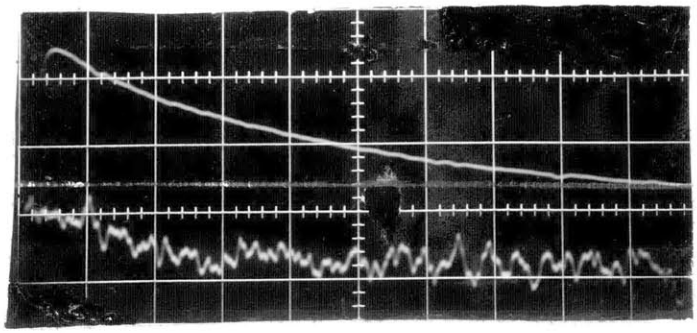

8.0 Torr $^{12}CH_3F$; 20μsec/cm

Fig. 17. Lower trace shows fluorescence signal before averaging. Upper trace shows signal averaging with PAR waveform eductor.

V-T Relaxation at 3.3μm in CH_3F

It has been shown by Weitz and Flynn[25] that at low power excitation, all levels relax to the ground state at the same rate. Thus, τ_{V-T} is the characteristic time constant for the entire CH_3F system at low excitation. Osgood et al[9] have shown that for a system in the high excitation regime, the decay rate goes as $v\gamma_{V-T}$, where v is the quantum number of level from which the relaxation process originates. Thus, the decay rate out of level 1 goes as γ and 2γ and 3γ for levels 2 and 3, etc. This can be seen by considering an ambient population of level 1, $n_1(t)$, and a time dependent deviation from equilibrium $\Delta n_1(t)$, such that

$$n_1(t) = n_1^o + \Delta n_1(t) \quad , \gamma = \gamma_{V-T} \ ,$$

and $\Delta n_1(t) \propto e^{-\gamma t}$. Level 2 is populated by events such as[2]

$$n_1 + n_1 \longrightarrow n_2 + n_0 \ . \qquad (V-1)$$

Hence, the population in n_2 is proportional to

$$[n_1(t)]^2 = (n_1^o)^2 + 2 n_1^o \Delta n_1(t) + [\Delta n_1(t)]^2 .$$

For low excitation $\Delta n(t) << 2n_1$, then,

$$n_2 \propto [n_1(t)]^2 \propto 2 n_1^o \Delta n_1(t) \propto e^{-\gamma t} .$$

For high excitation $\Delta n(t) >> 2n_1^o$, then,

$$n_2 \propto [n_1(t)]^2 \propto [\Delta n_1(t)]^2 \propto e^{-2\gamma t}$$

and

$$n_3(t) \propto n_2(t)\, n_1(t) \propto e^{-3\gamma t} .$$

Therefore, under high excitation, the relaxation rate from level v is

$$n_v \propto e^{-v\gamma t} \ . \qquad (V-2)$$

The investigation of CH_3F relaxation in the high power regime was made by pumping with the P(20) line of a CO_2 TEA laser. The 0.25 Joule 1.0μsec output was focused to a 0.5 cm beam into the fluorescence cell. Single shot pulses were detected with the InSb detector, but the low repetition rate (∿5/sec) of the TEA laser did not permit adequate signal averaging. Also, the signal to noise ratio did not require averaging to extract a decay time.

Because of the large energy absorbed by the molecules the V-T fluorescence signal was eventually distorted by the deposition of energy into translation.[29] This increased kinetic energy caused an enhancement in the kinetic temperature, therefore, an increased thermal population in all the levels. The net effect of the V-T relaxation and thermal repopulation of the upper states was a fast V-T relaxation followed by a long tail due to thermal heating (Figure 16). For higher pressure, fluctuations in the decay signal could be seen due to acoustic waves oscillating across the diameter of the cell. For a cell diameter of 3.0 cm and speed of sound of 3.22×10^4cm, the oscillation frequency was calculated to be ∿6 Hz which is the frequency of oscillation shown in Figure 16.

The decay rates for high powers were observed to be approximately 2-3 times faster than the low power rates. The reasons for the increased rates are numerous and the interpretation of the measured rate is ambiguous, mainly,

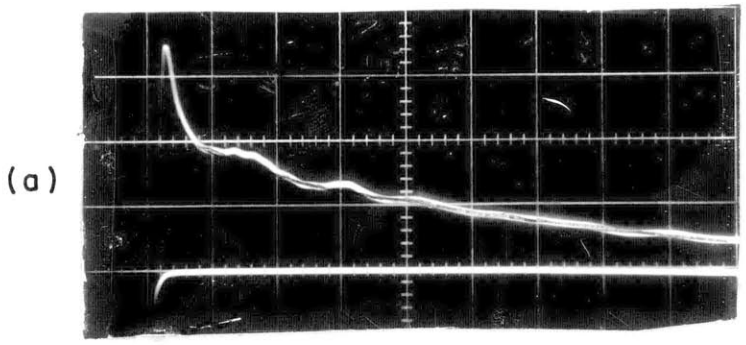

(a)

7.0 Torr $^{12}CH_3F$ 0.1 msec/cm

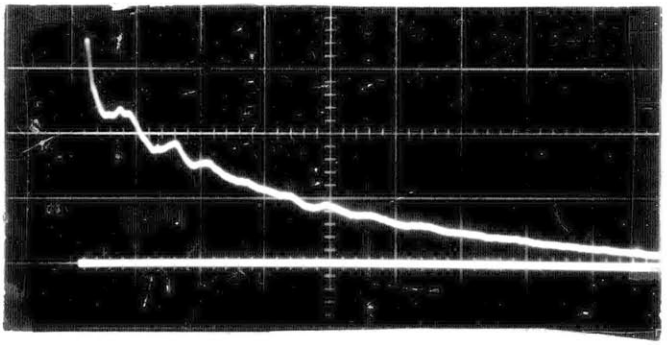

(b)

10.0 Torr $^{12}CH_3F$ 0.2 msec/cm

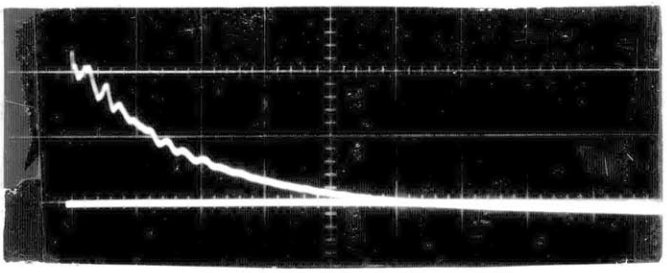

(c)

21.0 Torr $^{12}CH_3F$ 0.5 msec/cm

Fig. 16. V-T relaxation followed by a long heating tail after high power excitation. Oscillations are due to heat transport to the cell walls. 3.3μm emission is shown.

because of the simultaneous detection of the v→v-1 fluorescence components with rates $v\gamma$. The rate is faster because the filling of the (ν_1, ν_4) state can occur through several paths.[15] The two most probable paths are given on p.141 of Chapter XI.

The filling of (ν_1, ν_4) by either path has a non-linear dependence on n_1. Path 1 involves a three quantum process and Path 2 involves a two quantum process. Both paths would, therefore, give rise to relaxations rates different from equation (V-2). However, another contributor to the fast measured rate would be V-T processes of the type

$$CH_3F(0) + CH_3F(n\nu_1, n\nu_4) \rightleftarrows CH_3F(0) + CH_3F$$

These are V-T processes from excited states which occur, again, at $v\gamma$. The 3.3μm detection apparatus does not distinguish between fluorescing transitions from within the mode, hence, the observed rate is the net rate of energy flow out of all levels. Thus, only an upper limit of the decay rate can be obtained in the high excitation regime.

Nevertheless, the "collective" decay rates from the (ν_1, ν_4), ν_3, and (ν_2, ν_5) modes show decay times of several hundred microseconds at a torr, which is still much slower than any V-V processes occuring. This fact will be necessary for later experiments involving V-V coupling.

VII. ENERGY ABSORPTION MEASUREMENT

EXPERIMENT

The methyl fluoride molecule (CH_3F) was chosen for the energy absorption experiment because it has a long V-T[15] relaxation time, a fast V-V time,[2] an even faster R-T time,[21] a strong absorption resonance with CO_2 laser radiation,[29] and well studied rates and energy flow paths.

The long V-T relaxation time asserts that energy is being stored in the molecule a long time before being transferred to the translational degrees of freedom. In addition, the long V-T eliminates the possibility of photons entering through the vibrations, exiting through fast V-T processes, and being subsequently re-absorbed. Thus, an energy absorption experiment would yield valid results.

It is desired to measure the total number of quanta absorbed from the laser pulse per molecule. This quantity is obtained by measuring the total energy absorbed and dividing by the number of molecules present. In order to analyze experimental results in view of the theoretical analysis, it is important that the laser saturates the entire beam volume and that collisionless absorptions[14] are not present.

The TEA laser pulses were typically 3.0μsec duration. This relatively long laser pulse was obtained by using a pressure mixture of 1:1:5::CO_2:N_2:He. Pulse energies were

≈250mJ in a beam diameter of 0.5cm. Single mode operation of the laser was obtained by using two irises in the cavity and a helical discharge. The experimental set-up is shown in Figure (17). The CO_2 laser is focused by a 4.0 meter radius gold coated mirror through a KCl beam splitter, then, through a 16.0cm absorption cell. The beam splitter divides the beam for sampling the intensity before the cell, (I_{in}), and the intensity after the cell, (I_{out}). The laser pulse was found to exhibit a varying duration as one scans from the center to the beam edge (probably due to enhanced quenching rate of the lower laser level by He). To avoid viewing part of the beam, both beams were scattered off ground aluminum to diffuse and mix the wavefront. The aluminum scattering blocks were prepared by grinding on emory paper until the surfaces were coarse. The signals were detected by two Au:Ge detectors viewing small solid angles of the scattered beam. The response times (RC) of the detectors were made long by using large capacitance cables, thus, giving rise to integrated outputs from both detectors.

The detectors were calibrated by first measuring the laser energy with a Scientech 362 energy-power meter. The average amplitude of the detector output was then calibrated to the incident energy. The ratio I_{out}/I_{in} was measured, from which the absorbed energy was calculated using

$$\frac{I_{in}}{I_{out}} = \frac{E_{in}}{E_{in}-\Delta E},$$

where $\Delta E \equiv$ energy absorbed

$E_{in} \equiv$ energy incident

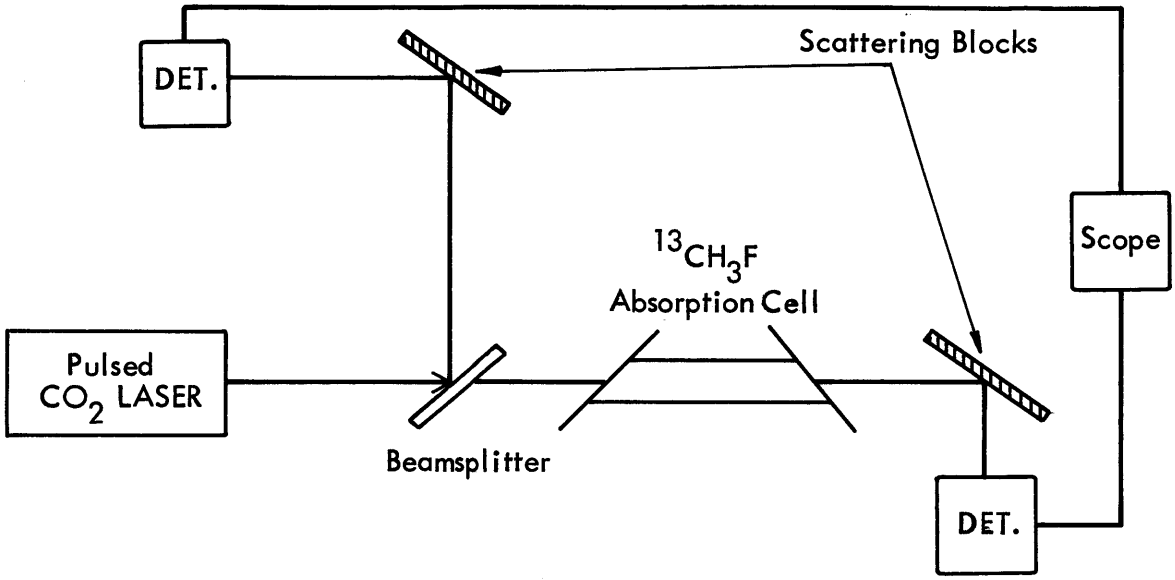

Fig. 17. Apparatus for energy absorption experiment.

($\sim$1.0) Kwatts per square centimeter is required to saturate a rotational transition of $^{13}CH_3F$(21) at 1.0 torr and rapid rotational thermalization and a long laser pulse permits saturation of the entire band as stated earlier. Saturation of the entire Doppler width ($\Delta\nu_D \sim 40$MHz) was insured for powers of order 1 Kwatt ($\mu\varepsilon/\hbar \sim 400$MHz). The total energy measured was then converted into CO_2 quanta (ε) using

$$\varepsilon = \frac{\Delta E}{N_{tot} \hbar\omega_{CO_2}} \quad , \text{ where}$$

$\Delta E \equiv$ Total energy absorbed by volume, V

$h\nu_{CO_2} \equiv$ Energy of CO_2 quantum

N_{tot} = VOL. of beam x 3.2×10^{16} $\frac{\text{molecules}}{\text{cm}^3 - \text{torr}}$

Figure (18) shows the number of CO_2 quanta absorbed as a function of pressure. At 5.0 torr, approximately 2.6 quanta are absorbed before the curve starts to bend downward. This decrease in ε is due to a breakdown in the laser's ability to saturate the entire 18.0cm cell length. Otherwise, ε would continue to rise. At pressures smaller than $\tilde{=}$1.0 torr, the experimental conditions do not satisfy the assumption of a fast V-V equilibration time (i.e. $\tau_{vv} > \tau_p$). Consequently, much of the laser energy is wasted for lack of sufficiently rapid equilibration, resulting in fewer quanta absorbed per molecule.

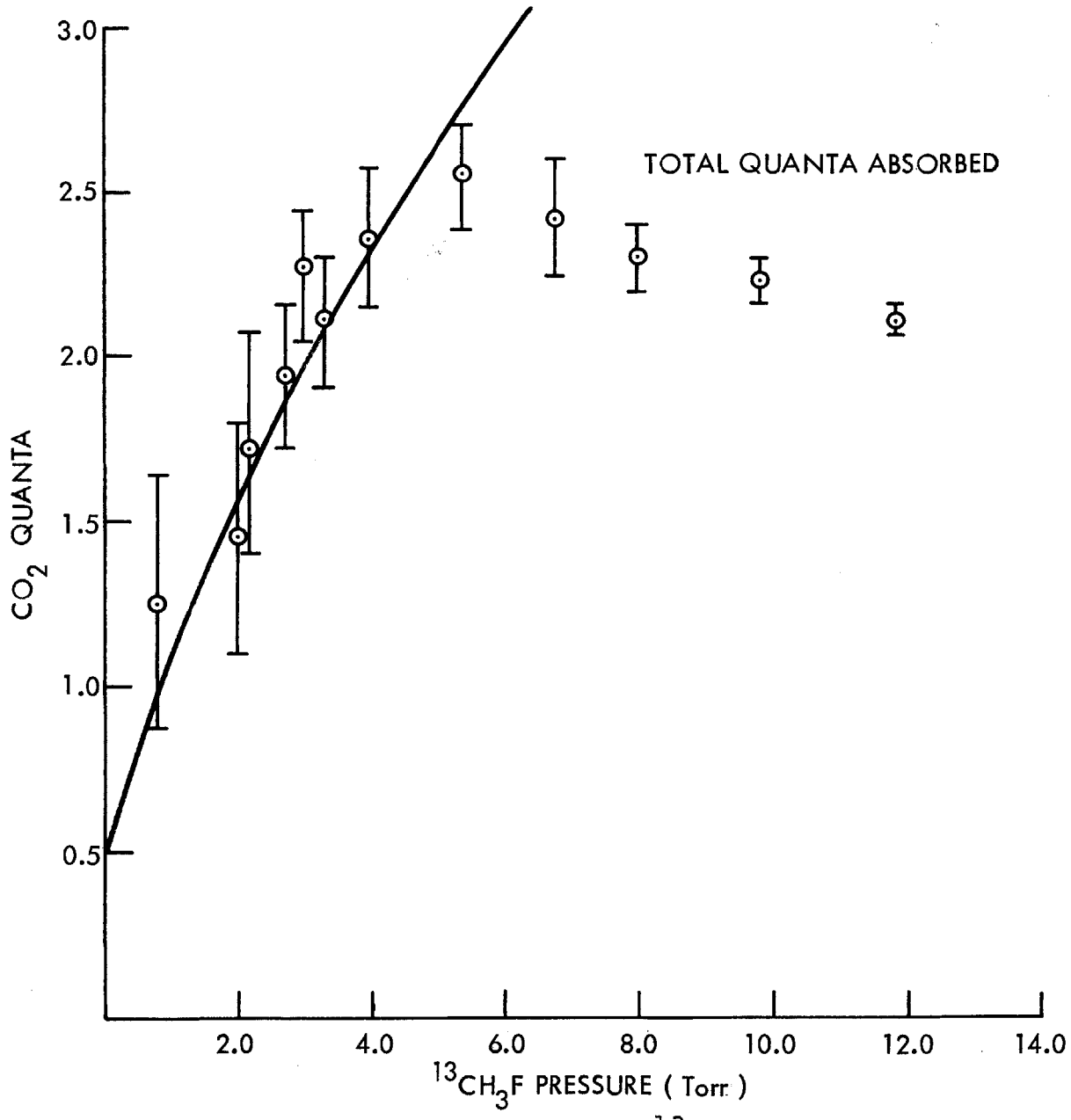

Fig. 18. Absorption of CO_2 quanta vs. $^{13}CH_3F$ pressure.

Experimental error is due primarily to fluctuating laser energies. The detector signals were averaged and calibrated against an averaged laser energy output. Thus, $(\Delta E + \delta)/N_{tot}$ results in larger error when $d(\Delta E)/dP << dN/dP$ and δ is a constant (standard deviation).

Although energy is stored as vibrational energy within the molecule as shown from the absorption and relaxation experiments, precisely how much is stored in a particular mode of a tightly couple set in a polyatomic is yet unknown[2]. To determine the partitioning of energy requires a measurement of the energy in each mode separately. If the vibrational mode has reached a Boltzmann equilibrium on short time scales, then, a knowledge of the vibrational temperature (T_v) would determine the number of quanta stored in the oscillator per molecule.

Several simple techniques for determining the vibrational population distribution in modes have been studied and will be presented in Chapters VIII, IX and X.

COMPARISON WITH THEORY

In Chapter III, it was shown that the number of quanta absorbed by a polyatomic molecule during the time of laser pulse interaction was, to an excellent approximation, the same as that absorbed by a diatomic molecule. Furthermore, Chapter III provided a method for determining the number of quanta absorbed (ε) by the molecule given the laser pulse

time, τ_p, and the V-V rate, γ_{v-v}. Conversely, γ_{v-v} should be easily derived from eq. (II-21) and eq. (II-24) if τ_p and ε are known.

These assertions were tested with the energy absorption data obtained from the $^{13}CH_3F$ experiment. Using the known values of $\tau_p \sim 3.0\mu sec$ and ε from Figure (18) a best fit was made to determine γ_{v-v}. The solid line in Figure (27a) shows this fit which corresponds to a V-V rate of $0.8 \pm 2 \mu sec^{-1} torr^{-1}$. This rate has been previously measured by Earl and Ronn[15] by observing the rise time of $(2\nu_3 \rightarrow 0)$ fluorescence, hence, monitoring the process

$$\nu_3 + \nu_3 \longrightarrow 2\nu_3 + 0$$

These measurements yielded a rate of $1.2 \pm .3$ $sec^{-1} torr^{-1}$ which is within experimental error of the number quoted above.

Thus, the energy absorbed by a polyatomic can be accurately determined by the simple relationships of eqs. (II-21) and (II-24) and the V-V up the ladder rate of polyatomics can be obtained from absorption data.[26] Theory, computer simulations, and experiments all agree that the total energy absorbed by diatomics and polyatomics are the same. Using this knowledge the previously unmeasured V-V rates of other molecules can now be extracted from absorption data. This fundamental result will enhance the understanding of polyatomic behaviour and energy transfer.

Experimental Test for Rotational Bottleneck Effects

To determine if rotational bottleneck effects (Chapter II) were inhibiting the energy absorption process, an inert buffer gas (Argon) was added to the absorption cell of pure CH_3F. The added Argon pressure served to pressure broadened the absorption resonance of CH_3F and, therefore, increase the rotational collision time without significantly influencing V-V or V-T.[49]

The transmitted CO_2 intensity was observed before and after adding 5.0 torr of $^{13}CH_3F$ to the cell. From the known pressure broadening coefficient of $^{13}CH_3F$ (40 MHz/torr FWHM)[21,53], the rotational collision time is given by[21]

$$\tau_{R-R} = \frac{1}{\pi \Delta \nu} = 8 \times 10^{-9} \text{ sec-torr.}$$

Pressure broadening studies of molecules by foreign gases have shown that Argon is approximately one half as efficient in broadening lines as helium.[51,20,52,50] The pressure broadening of methyl fluoride by helium has been measured by Bischel et al [53] to be 6.0 MHz/torr. Thus, the pressure broadening of helium is approximately 3.0 MHz/torr.

To the 5.0 torr of CH_3F, Ar pressure was added up to 400 torr. Fig. 18a shows a plot of transmitted intensity va. Ar pressure. The intensity is observed to be unaltered by Argon pressure up to 400 torr and adding additional pressure had no effect. However, the experimental error is 12% of the change, thus, establishing 12% as the largest possible change in the intensity. For 400 torr of Ar, the CH_3F line of 5.0 torr is broadened 1200 MHz for

a total linewidth of 1.00 MHz— a factor seven larger than before. Thus, τ_{R-R} has decreased by a factor of four from 8 nsec to 1.1 nsec.

Computer calculations of the energy absorbed by ν_3 of CH_3F show that if a bottleneck exists with the stated experimental parameters ($\tau_p = 3\mu sec$, Argon and CH_3F pressure, $\tau_{v-v} \simeq 1\mu sec$), then, a decrease by a factor seven τ_{R-R} would increase the absorbed energy by 50%. No increase in absorption is observed experimentally, thus, giving absolute proof that there is no bottleneck in CH_3F.

From p.24 of Chapter II, the condition for efficient laser pumping (no bottleneck) is

$$\tau_B = \tau_{R-R}/Z_J << \tau_{v-v}$$

or, for symmetric tops

$$\tau_B = \tau_{R-R}/f_{JK} << \tau_{v-v}$$

where f_{JK} is the fraction of population in a (J,K) state (Appendix D). For the R(4,3) transition of CH_3F $f_{JK} = .0073$ and using $\tau_{R-R} = 8 \times 10^{-9}$ sec-torr gives $\tau_B = 1.1\mu sec$. Using the measured value of $\gamma_{v-v} = 0.8\mu sec$-torr, we find $\tau_B \simeq \tau_{v-v}$ and, therefore, a bottleneck existing. This result conflicts with the observed behavior of the system. The Argon experiment suggests that either rotational time is faster than the one used (8 nsec) or f_{JK} is in error. Because of the J dependence of the pressure broadening, there is reason to believe that τ_{R-R} may be affected. In addition, unequal distribution of population among the (J,K) states and the large concentration in

the K = 3, 6, 9... states can shorten the number of collisions necessary to transfer all the molecules through the (J=4, K=3) state for laser pumping.

To resolve the discrepancy, a very careful and detailed inspection of parameters used in the theoretical estimate is required. Nevertheless, experimental observations prove definitively that the rotational bottleneck is not a problem in CH_3F.

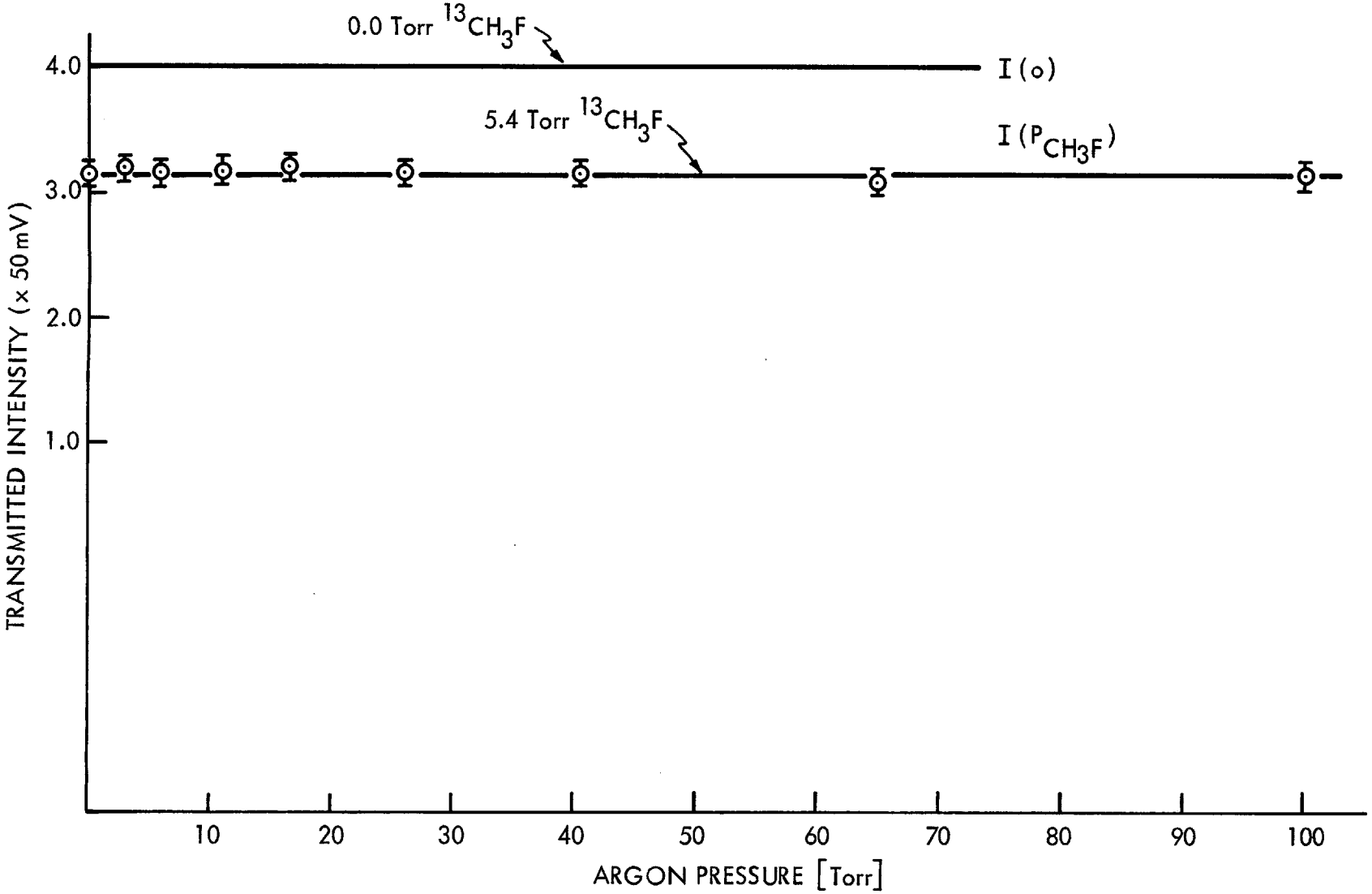

Fig. 18a. Variation of transmitted intensity vs. argon pressure for fixed CH_3F pressure.

VIII. VIBRATIONAL TEMPERATURE MEASUREMENT VIA INFRARED-INFRARED DOUBLE RESONANCE

UNDERLYING PRINCIPLE OF DOUBLE RESONANCE TEMPERATURE MEASUREMENT

The double resonance experiment presented in this chapter did not successfully supply an accurate vibrational temperature. Because of its sensitivity to small changes in the translational temperature and the large energies, the double resonance experiment becomes distorted when large energies are being deposited into the translational degrees of freedom. However, for weak excitation, the analysis is valid and is, thus, elaborated on.

Double resonance techniques have been used in the microwave[30] and infrared regions[2] for monitoring the evolution of level populations by means of absorption changes. Consider a continuous probe laser interacting with one rotational-vibrational transition of a molecule. If a strong pulse resonant with a coupled transition introduces additional population to the transition's upper state, then, absorption of the probe will decrease due to the decreased population differences between the upper and lower states.

For absorption by a symmetric top (such as CH_3F) the Doppler broadened absorption, which is a function of the population difference between the interacting states, de-

pends on the vibrational temperature of the absorbing mode. If the population of the vibrational level is changed, the population of each rotational state within the band is changed.

Since the absorption is a function of the vibrational temperature, monitoring the absorption change would provide a measurement of the temperature and the energy stored.

Consider a weak probe laser incident on a gas cell with intensity I_o. When gas is introduced into the cell of length L, linear absorption reduces the intensity to[33] $I=I_o e^{-\alpha_o PL}$ (VIII-1) where α_o is the Doppler broadened absorption coefficient and P is pressure.

When a laser pulse suddenly removes population from the ground to the upper vibrational state,[43] the absorption will decrease (or the transmitted signal will increase) to I_H at a rate proportional to the pumping rate. This heated intensity, I_H, will relax back to the ambient level, I at the V-T relaxation rate of the system[2]. Thus,

$$I_H = I_o e^{-\alpha_H PL} \quad \text{(VII-2)}$$

where α_H represents the absorption coefficient at an elevated vibrational temperature, T_v.

If equations (VIII-1) and (VIII-2) are solved for α_o and α_H and their ratio is taken, it is found that

$$R = \alpha_o/\alpha_H = \frac{\ln(I_H/I_o)}{\ln(I/I_o)}$$

Using $\Delta=0$, $I=1/2$, $KT_R=210cm^{-1}$, $B=0.85cm^{-1}$, $C=5.13cm^{-1}$ and $(J,K)\rightarrow(12,2)$ it is found that

$$\alpha_H = C\left(\frac{T}{T_V}\right)^{3/2} e^{-(0.68\,T_R/T_V)},$$

where α_H is expressed in terms room temperature.

Then,

$$R = \frac{\alpha_H}{\alpha_0} = \left(\frac{T_R}{T_V}\right)^{3/2} e^{-0.68(T_R/T_V-1)} \qquad \text{(VIII-7)}$$

Equating the expressions for R from eq. (VII-3) and (VIII-7) it is found that

$$\frac{\ln(I_H/I_0)}{\ln(I/I_0)} = \left(\frac{T_R}{T_V}\right)^{3/2} e^{-0.68(T_R/T_V-1)} \qquad \text{(VIII-8)}$$

Figure (20) shows the experimental apparatus used on the double resonance experiment. The probe laser was a continuous CO_2 laser operating on the P(32) line of the 9.0μm band. This laser is described in Chapter (VI). The grating output was reflected off two gold mirrors through two irises and a zinc selemide (ZnSe) window into the 70.0cm absorption cell. The ZnSe window was polarized at Brewster's angle to allow maximum transmission of the probe. ZnSe was used because its relatively large refractive index (4.5) provided maximum reflectivity for 9.6μm radiation polarized perpendicular to the ZnSe Brewster's angle. Power levels of the c.w. laser were kept below 0.5 watts to avoid overheating the gas sample.

This ratio is a function of the vibrational temperature and involves three experimentally measurable parameters, I_H, I and I_o. To directly relate the three measurable quantities to temperature, α_H/α_o must be explicitly evaluated.

Thus, the experimental parameters I_o, I , and I_H are directly related to the vibrational temperature (T_v). Figure (19) shows a plot of R vs. T_v. R is plotted for a model where all the modes are excited. By comparing the measured value of R to the R vs. T_v curve, T_v can be extracted.

For the Q-Branch of a Doppler broadened symmetric top, the absorption is given by[20]

$$\alpha_H = \left[\frac{4\pi}{\hbar u}^{3/2} e^{-(\Delta/ku)}\right]\left[N_o \frac{\mu_o^2}{3} \frac{(2J+1)K^2}{J(J+1)}\right] \frac{f_{JK}}{2J+1}(f_i - f_v) \qquad \text{(VIII-4)}$$

with

$$\frac{f_{JK}}{2J+1} = \frac{S(I,K)}{4\sqrt{\pi}} \sqrt{\frac{B^2 C}{(KT_R)^3}} \exp\left\{-\left[BJ(J+1)+(C-B)K^2\right]/KT_R\right\} \qquad \text{(VIII-5)}$$

and

$$f_v = e^{-E_v/KT_v} \prod_n \left(1 - e^{-\hbar\omega_n/KT_n}\right)^{dn} \qquad \text{(VIII-6)}$$

S(I,K) is the nuclear spin degeneracy factor given (Appendix D) and d_n is the degeneracy of the n^{th} mode, B and C are rotational constants, and f_{JK} and f_v are the fractions of molecules in a rotational and vibrational state, respectively.

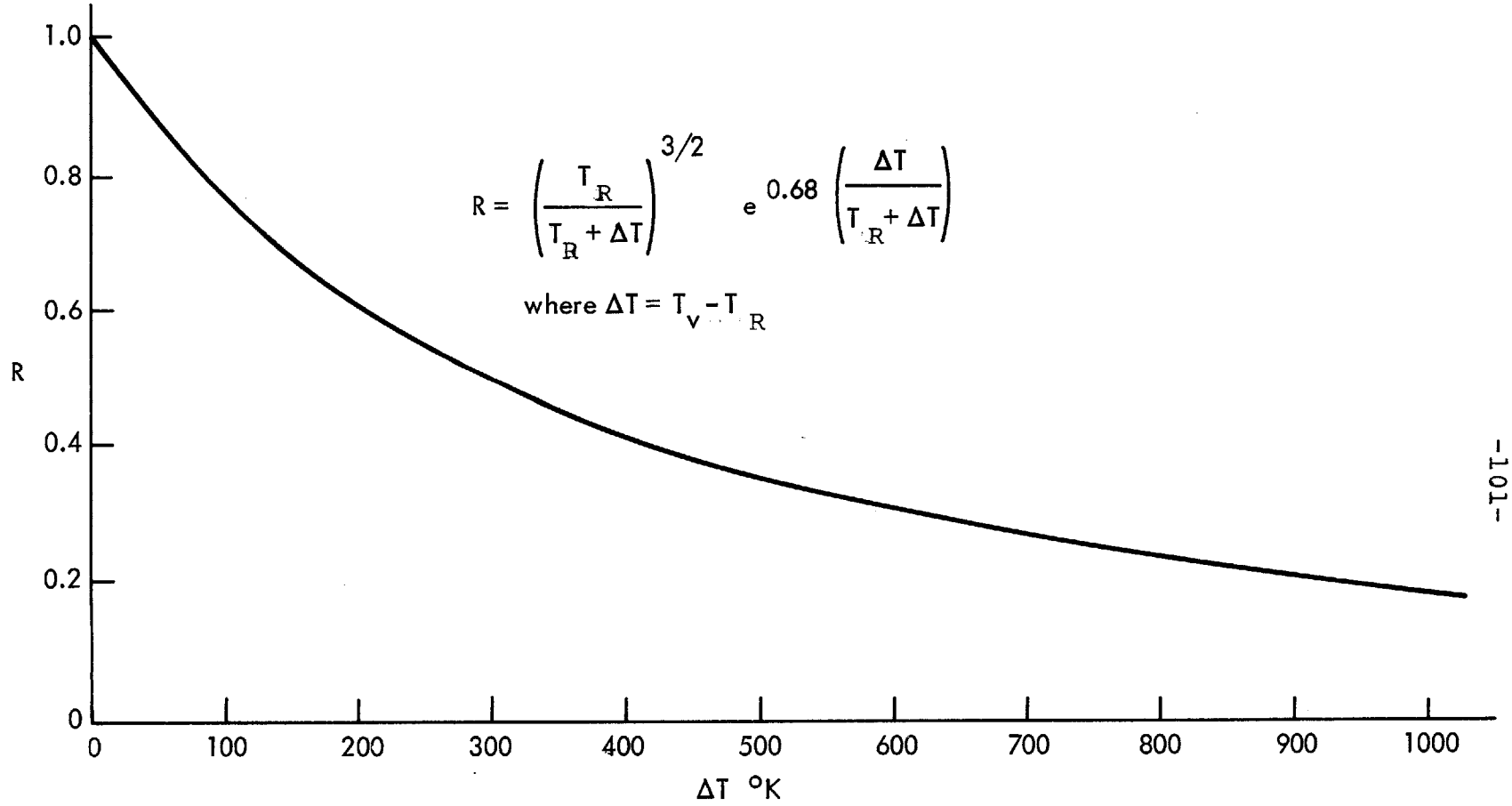

Fig. 19. Ratio of absorption coefficients ($R=\alpha_0/\alpha_H$) vs. change in vibrational temperature (ΔT).

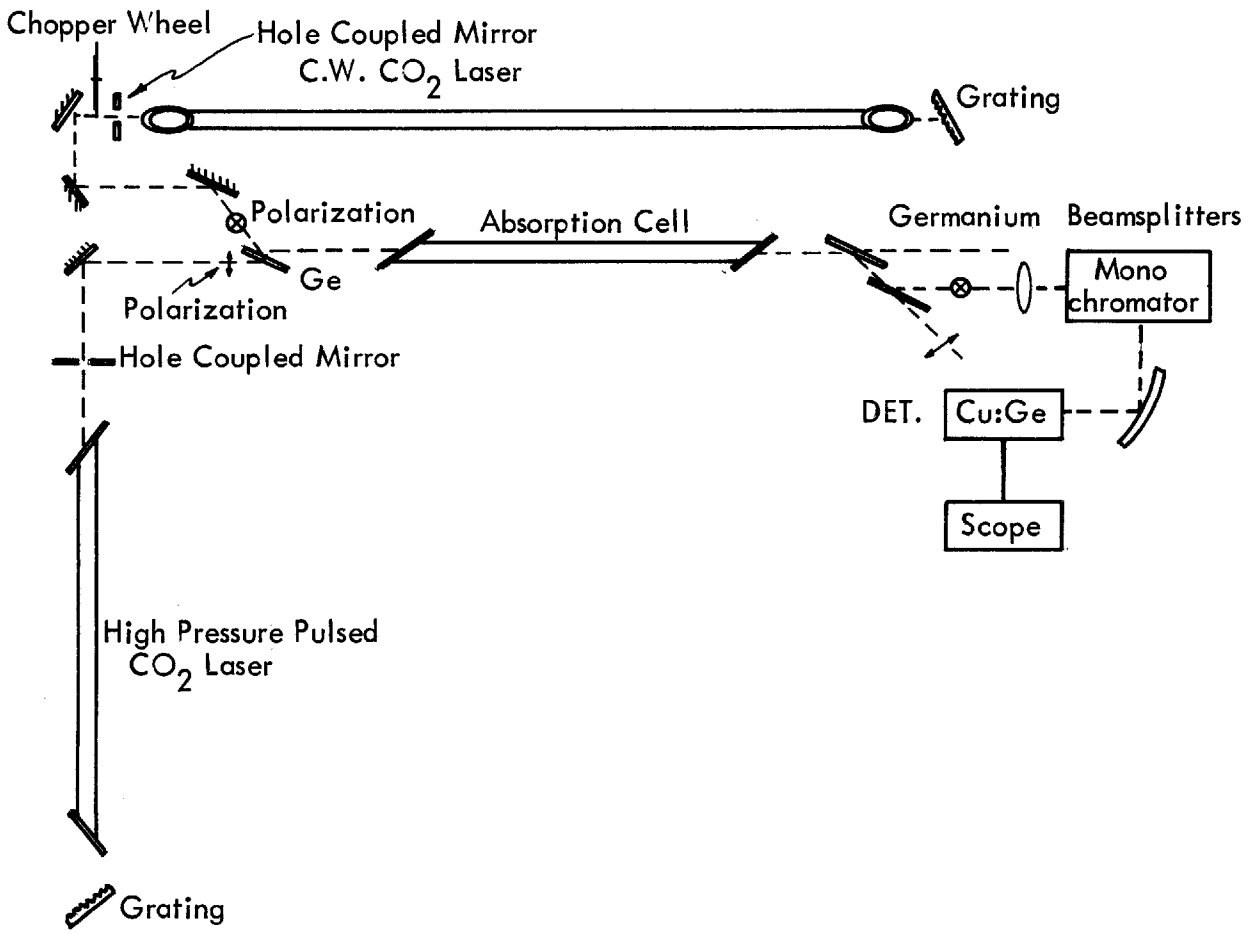

Fig.20. Infrared-infrared double resonance apparatus.

The pump laser was the CO_2 TEA laser described in Chapter (V) operating on the P(20) line with $\sim$ 3μsec duration. The grating coupled output was reflected off of polished copper mirrors and focused with a 4.0m radius canogen coated copper mirror from Laser Optics, Inc. The beam was then incident through several irises on to the opposite polarized ZnSe window. Approximately 70% of the CO_2 laser 400 millijoules of energy could be coupled into the absorption cell using this technique. Both the probe and pump beams were carefully aligned such that the beams transversed the tube perfectly collinearly. Both beams excited the cell through a NaCl end window, then, through an axis defining iris. The beams were focused through a BaF_2 lens and into a monochromator with a 20μm grating calibrated on the 3rd order. The monochromator was tuned to transmit the P(32) probe beam at 9.65μm. This signal output was transmitted through the slits onto a 3.0cm focal length elliptical mirror and into a Cu:Ge detector loaded to 6KΩ. The detector response time was about 3.0μsec. Signals were viewed on a 545 Textronic oscilloscope.

The cell diagram is shown in Figure (21). This cell was designed to serve as a future laser cavity following heating measurements. It was designed to make temperature measurements as close as possible to lasing conditions. The ZnSe window oriented at Brewster's angle for vertical polarization was mounted on a carefully machined aluminum

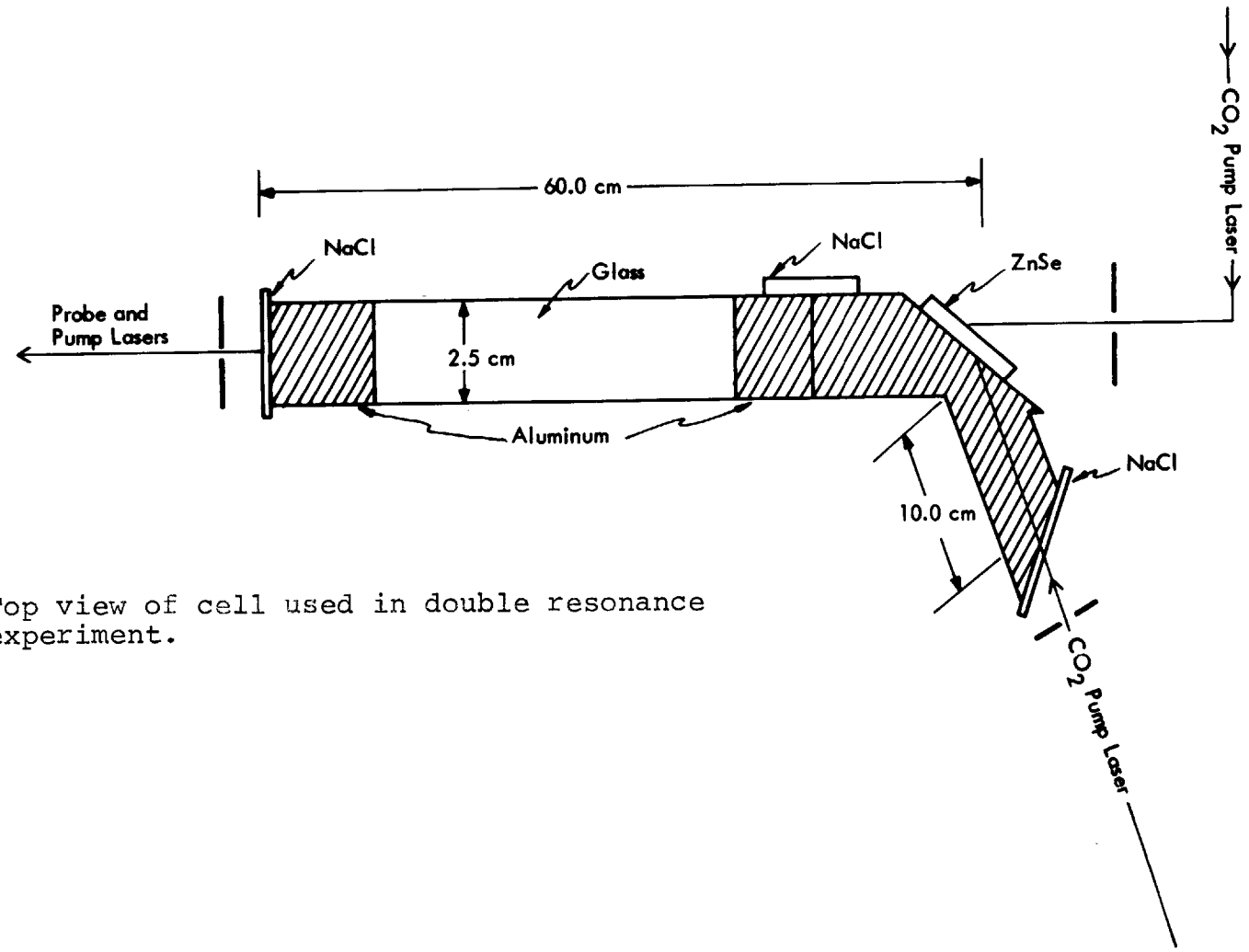

Fig.21. Top view of cell used in double resonance experiment.

block and sealed with red wax. The entrance window was a NaCl flat as well as the exit window. Both flats were mounted on aluminum blocks. At the top of the entrance aluminum block was mounted a sapphire window for viewing 3.3μm and 5.0μm fluorescence, while the double resonance experiment was in progress, if desirable. The glass tube was connected to the aluminum blocks with torr seal. The end of one block also contained a slot for a 1" mirror, if desired, for lasing. The optical path within the cell was 60.0cm for the probe laser and (70.0cm) for the pump laser.

The pump laser (P(20), 9.55μm) interacted with the P(12,2) transition of $^{12}CH_3F$ [43] in a 90% - 10% mixture of $^{12}CH_3F$-$^{13}CH_3F$. The probe laser interacted with the R(4,3) transition of the ^{13}C isotope. [46] CH_3F was introduced into the cell at various pressures and the amplitude of the reduced probe intensity was observed when the laser pulse occurred.

The relaxation of the 3.3μm fluorescence was simultaneously monitored using an InSb detector looking through the cell's sapphire window. Figure (22) shows oscilloscope traces of the probe laser intensity (top) and the fluorescence decay (bottom). The rate of change of the probe intensity does not occur on the time scale of a collision event. Rather, the change seems to be concurrent with the V-T decay process. The fact that V-T is depositing thermal energy into the translational degrees of freedom along with the time behavior of the probe intensity indicate that we're

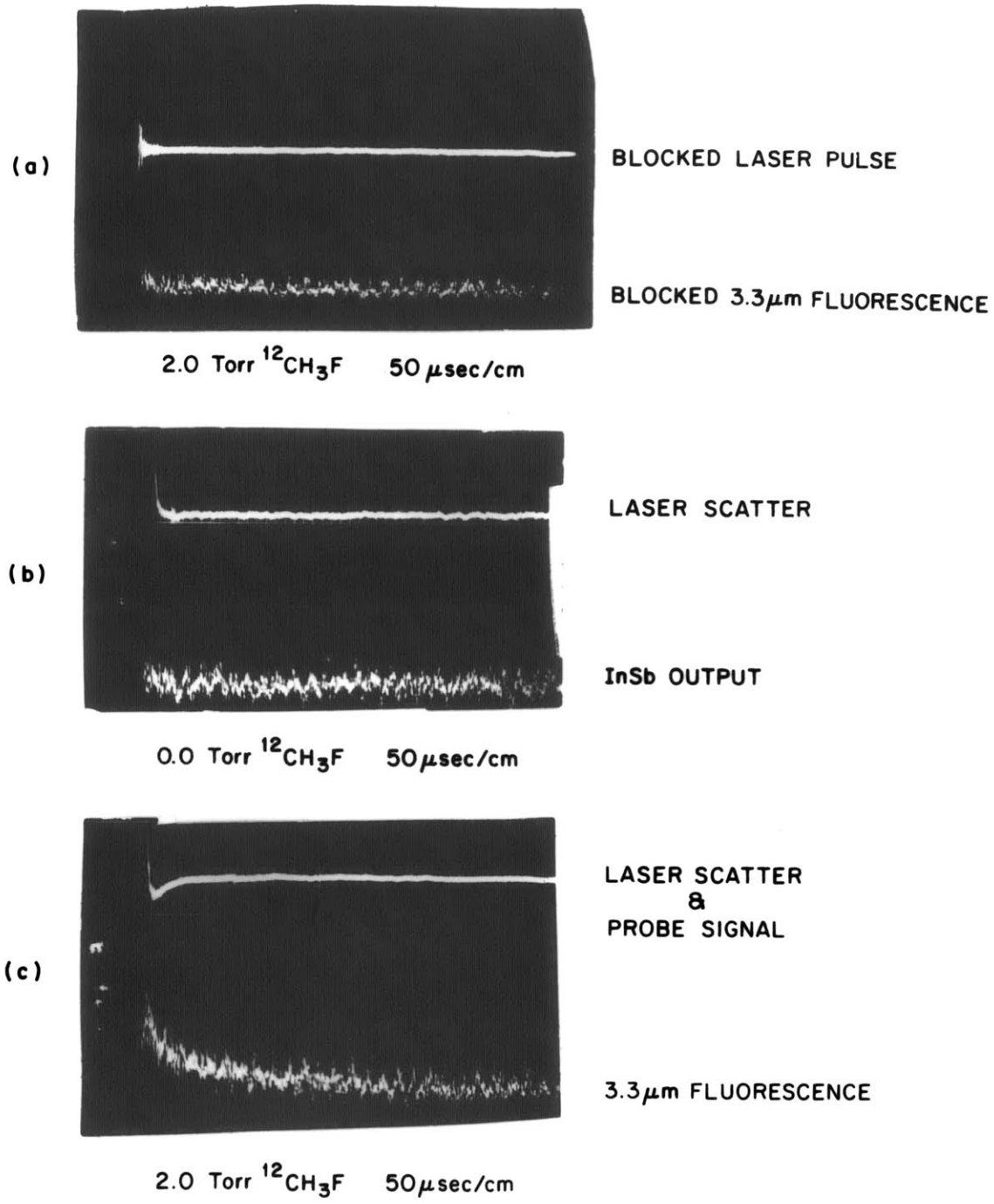

Fig.22. Simultaneous monitoring the c.w. probe signal (top trace) and the 3.3μm V-T relaxation (bottom trace) in CH_3F for increasing pressure.

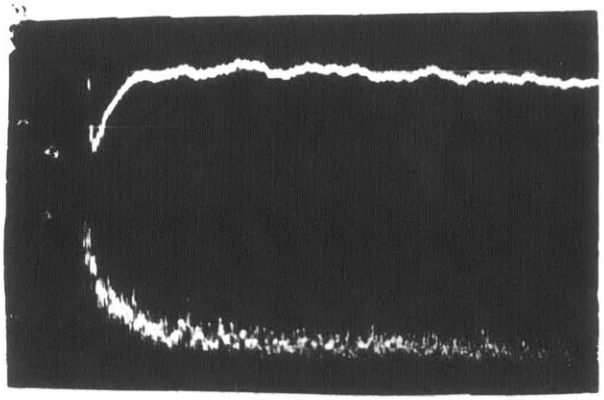

(d)

SCATTER & PROBE SIGNAL

3.3 μm FLUORESCENCE

3.0 Torr $^{12}CH_3F$ 50 μsec/cm

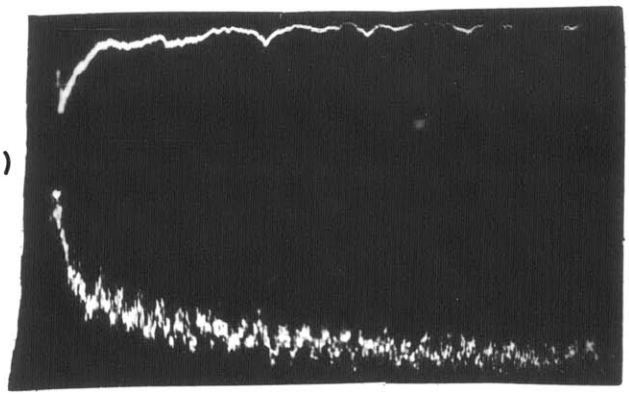

(e)

SCATTER & PROBE SIGNAL

3.3 μm FLUORESCENCE

5.0 Torr $^{13}CH_3F$ 50 μsec/cm

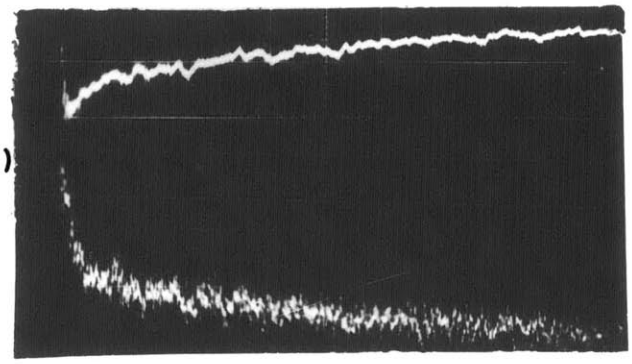

(f)

SCATTER & PROBE SIGNAL

3.3 μm FLUORESCENCE

9.0 Torr $^{12}CH_3F$ 50 μsec/cm

Fig.22 (Continued)

observing some transport phenomena instead of a V-V collisional event.[34]

It appears that by probing the population of two rotational transitions, the affect of kinetic heating causes a large change in the population of low J states. When a small quantity of energy is deposited through V-T into translation, the fast T-R equilibration causes a marked enhancement of the low J states. Since the probe intensity depends on, first, the populations of the two interacting rotational states, the probe will be very sensitive to thermally induced changes in the rotational distribution.

Thus, for high power excitation, and subsequent large energy deposition into translation, the double resonance technique seems to give erroneous results for vibrational temperature analysis. For low powers[15], the energy into translation does not appreciably disturb the room temperature rotational distribution, thus, the probe intensity change due to increased population of the upper vibrational manifold is not masked by the negligible shift in rotational distribution.[36]

It was decided that a technique that was less sensitive to rotational shifts and one that monitors simultaneously the entire vibrational band was needed. Because of the extremely fast rotational collisional thermalization, the double resonance technique, in principle, monitors the entire vibrational band. However, different rotational levels on

different points of the Boltzmann distribution are affected by small temperature changes in different ways.

At this point, the direction was changed to that of laser induced fluorescence to supply the information about energy storage.

IX. MEASUREMENT OF VIBRATIONAL TEMPERATURE BY COLD GAS FILTER

INTRODUCTION

Vibrational temperature measurements have been accurately made with a new and very successful method - the cold gas filter technique [absorption by a room temperature gas]. The theory and analysis of this very novel technique for temperature measurement shall be given here.

THEORY

Since it was discovered that several absorbed laser quanta reside somewhere within the vibrational degrees of freedom of CH_3F, the questions still remain -- how much energy is stored in the pumped vibrational mode, ν_3(9.6μm)? How much has been transferred to the other vibrational modes? This quantity has been measured with good accuracy using a newly developed technique for vibrational temperature analysis -- absorption by a cold gas filter.

This technique involves a measurement of the total fluorescence intensity assuming Boltzmann vibrational equilibrium,[16] then, removing the lowest component of vibrational fluorescence with a room temperature gas and comparing the amplitudes of the two transmitted intensities.

The assumption of a Boltzmann distribution is satisfied by the fast V-V collisions during and after the laser pulse. The V-V up the ladder rate has been measured by Earl and Ronn[24] to be $1.2 \pm .3$ $sec^{-1}torr^{-1}$ and by the absorption technique of Chapter VII to be $0.8 \pm .2$ $sec^{-1}torr^{-1}$. Thus, at 1.0 torr with 3.0μsec pulse, the V-V up-the-ladder process is complete. (There is a rapid V-V cross-over process occuring on similar time scales which will be investigated in the next chapter). These rapid V-V collisions carry laser energy up the vibrational ladder in the manner described in Chapter II. It should also be pointed out that all V-V exchanges are energy conserving processes where energy defects are compensated for by removing from or depositing energy into the translational degrees of freedom.[18, 35, 36]

Observation of fluorescence decay from the (ν_1, ν_4) the (ν_2, ν_5), and the ν_3 modes ((Fig. 23)) indicated that once the rapid V-V equilibrium was established the energy remained in the vibration until the V-T process relaxed it (which occurred on a much longer time scale). See also Fig. 28 for energy level diagram.

SPONTANEOUS EMISSION FROM VIBRATIONAL STATES

For a perfect harmonic oscillator of frequency ω the population in level v is defined by the vibrational temperature such that the number of molecules is given by[20]

$$n_v = n_o e^{-v\hbar\omega/kT_v} \qquad (IX-1)$$

where n_o is the ground state population and the vibrational partition function is given by

$$\sum_{v=0}^{\infty} e^{-v\hbar\omega/kT_v} = (1 - e^{-\hbar\omega/kT_v})^{-1}$$

After each level has been populated, each v→v-1 transition will begin to emit spontaneously with intensity given by

$$I_{v,v-1} = K\mu^2_{v,v-1} n_v \qquad (IX-2)$$

where $\mu_{v,v-1}$ is the transition dipole matrix element. Then, summing over all states, the total spontaneous emission intensity is found to be

$$I^{sp}_{tot} = \sum_{v=1}^{\infty} I_{v,v-1} = K \sum_{v=1}^{\infty} n_v \mu^2_{v,v-1} \qquad (IX-3)$$

The dipole matrix element is proportional to v, then, eq. (IX-3) can be written as

$$I^{sp}_{tot} = K' \sum_{v=1}^{\infty} v e^{-v\hbar\omega/kT_v} = \frac{K' e^{-\beta v}}{(1-e^{-\beta})^2} \qquad (IX-4)$$

where k is a constant geometric parameter and $\beta \equiv \hbar\omega/kT_v$.

I^{sp}_{tot} is an easily measurable quantity and it is a simple function of the vibrational temperature. In all of the high power fluorescence measurements discussed earlier, I^{sp}_{tot} is the quantity being observed.

In real molecules where the levels are not perfectly harmonic, a gas of the same type of molecules as those of the emitting molecules can be used to absorb out the v=1→0

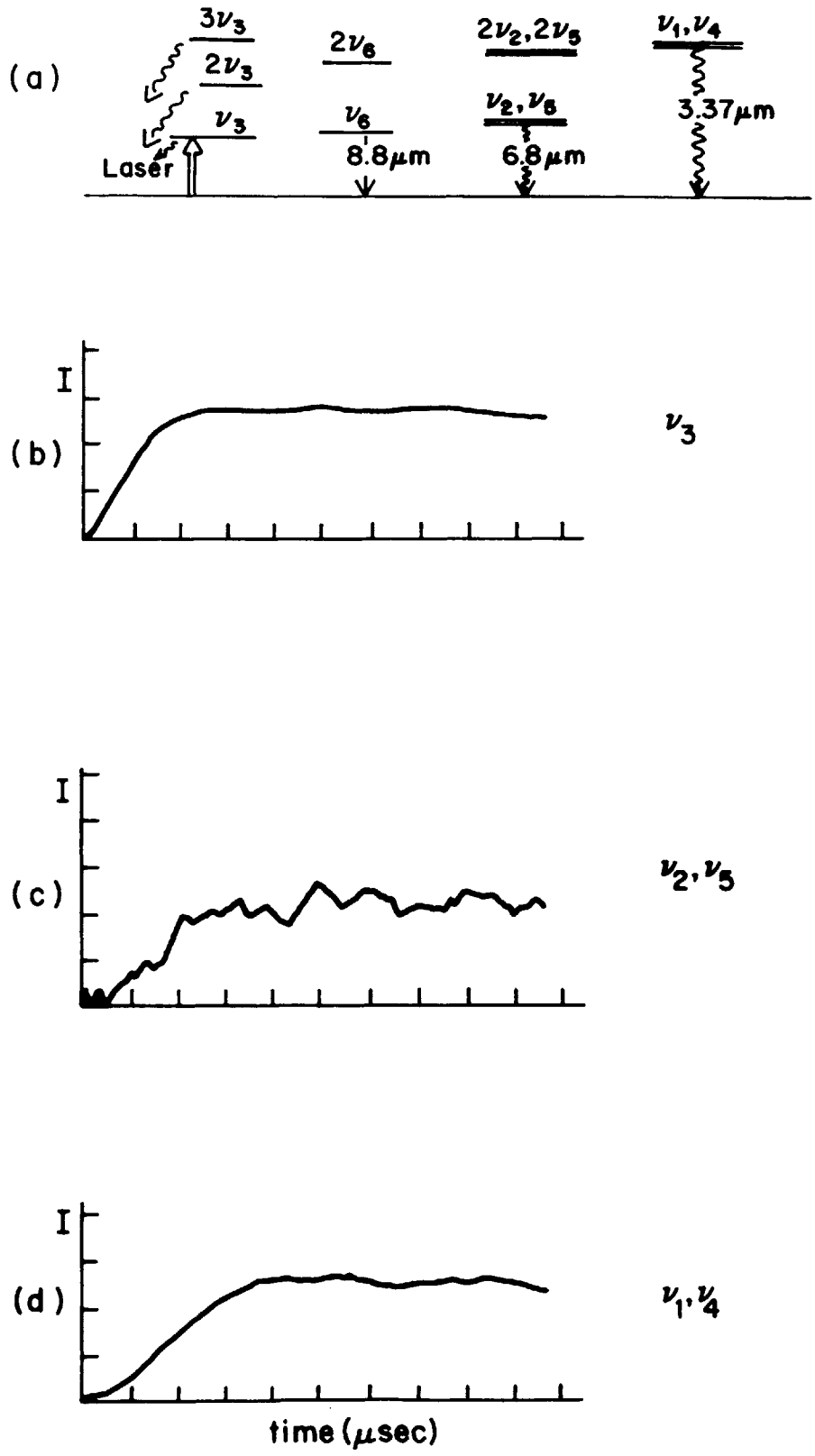

Fig. 23. Risetime of fluorescence from the vibrational modes of CH_3F . (a) ν_3(9.6μm), (b) ν_2,ν_5(6.8μm), (c) ν_1,ν_4(3.3μm)

component of fluorescence. The transmitted intensity is now given by $I_{tot}^{sp} - I_{10}^{sp}$, which can be expressed as

$$I_{tot}^{sp} - I_{10}^{sp} = K' e^{-\beta v} \left[\frac{1}{(1-e^{-\beta v})^2} - 1 \right] \qquad (IX-5)$$

Again, this is an easily measurable quantity. Either I_{tot}^{sp} or $I_{tot}^{sp} - I_{10}^{sp}$ could be used to evaluate T_v, but an evaluation of k is needed to perform an absolute intensity measurement. This would necessitate computing the detector solid angle, the detectivity of the detector, and the number of fluorescing molecules. All of these parameters would introduce large error on the final temperatures obtained which could distort the energy stored calculation at the lower pressures.

The problem of evaluating k' was circumvented by taking the ratio of I_{tot}^{sp} and $I_{tot}^{sp} - I_{10}^{sp}$ which gave another simple function from which the vibrational temperature could be evaluated, namely,

$$\frac{I_{tot}^{sp} - I_{10}^{sp}}{I_{tot}^{sp}} = 1 - (1-e^{-\beta})^2 \equiv R \qquad (IX-6)$$

EXPERIMENTAL ARRANGEMENT

The CO_2 laser used is described in Chapter V. The grating coupled output of the P(32) 9.65μm line was reflected off polished copper mirrors and focused by a 4.0 meter radius gold coated copper mirror. The experimental apparatus is shown in Fig. 24. The 0.25 Joule beam was focused to a 0.6 cm beam to give an average energy per square centimeter of

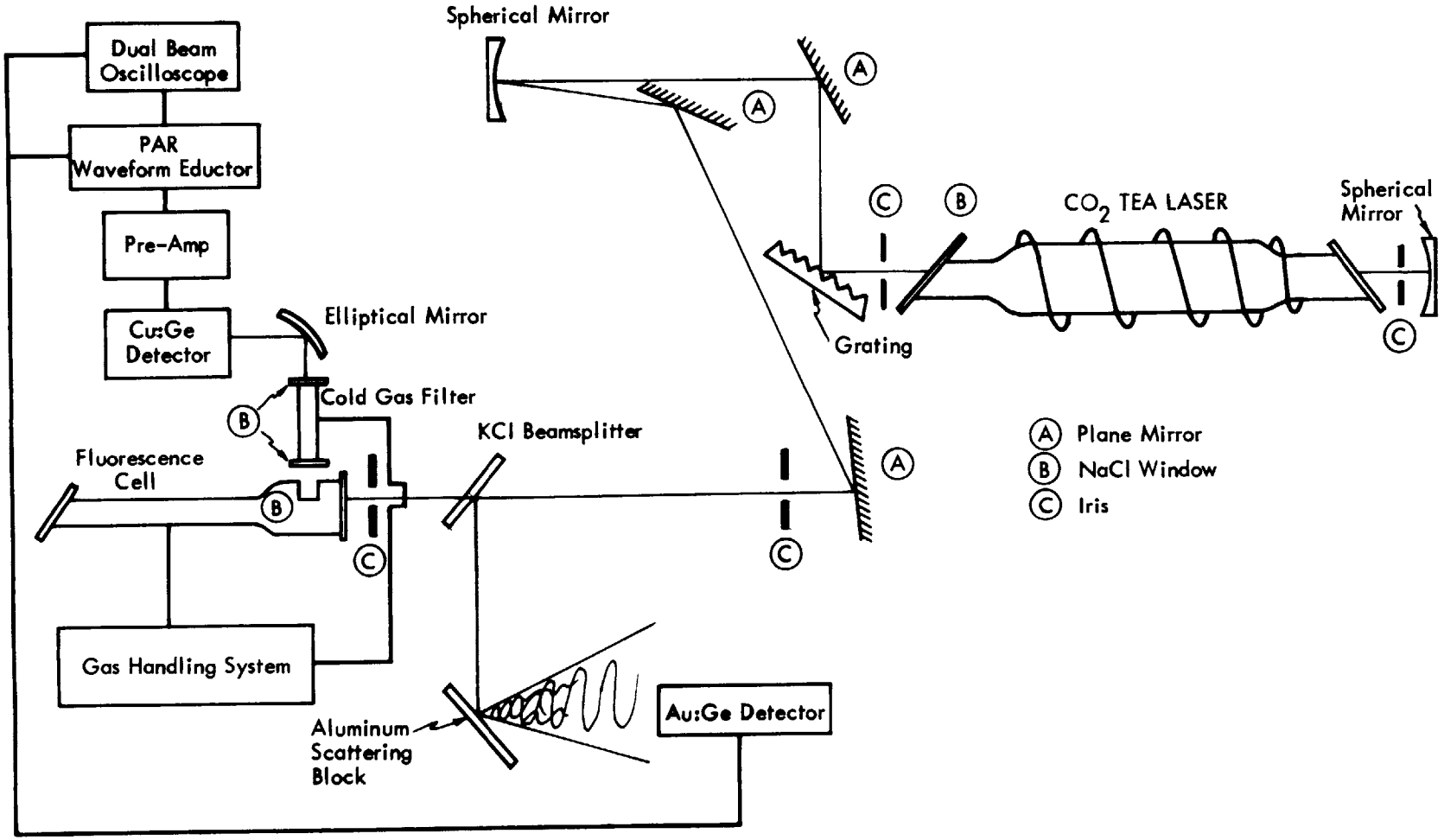

Fig. 24. Diagram of cold gas filter experiment.

0.88 J/cm^2. Laser pulses were typically 2-3.μsec duration to satisfy the theoretically imposed condition of $\tau_{vt} >> \tau_p >> \tau_{vv}$. Thus, the average peak laser power was approximately 295 kilowatts/cm^2. This peak power guarantees full saturation of the Doppler profile ($\sim$67 MHz) of either the ^{12}C or ^{13}C species of CH_3F. The focused laser beam was then passed through a fluorescence cell for viewing right angle emission of radiation. Before entering the cell a KCl beam splitter was placed at the Brewster's angle for the laser polarization to sample the laser beam for comparison of its time behavior with the fluorescence signals. The sample signal was reflected off of an aluminum scattering block and into a nitrogen cooled Au:Ge detector. With the detector loaded to 100Ω and using a type H plug-in amplifier and a Textronic 555 Dual Beam Oscilloscope, the risetime of the system was approximately 300 nanoseconds.

The fluorescence emission from the cell escaped through a NaCl window at 90° to the pump beam axis. The fluorescence then entered a 7.825 cm cell which served as a "cold gas filter" for absorbing out the lower component of fluorescence. The cold gas filter (c.g.f.) contained NaCl windows on both ends oriented parallel to the NaCl escape window on the cell. (See Figure 25) Both the c.g.f. and the fluorescence cell were connected to the all glass vacuum system where the gas flow paths and isolation of the cells were obtained by a battery of 2.0 mm hi-vacuum stopcocks as discussed in

Chapter V. After passing through the cold gas filter, the signal was focused by a 3.0 cm elliptical mirror into a liquid helium cooled copper doped germanium detector (Cu:Ge). The Cu:Ge was loaded to 1.0KΩ and the output was passed through a 1A7A plug-in amplifier and displayed on an oscilloscope. The risetime of the detection system was about 2.0μsec.

The gas samples used were re-cycled using the system described in Chapter V.

The problem of observing fluorescence at the same wavelength as that of the pump was solved by using the fluorescence cell design shown in Fig. 25. Most of the scattered radiation comes from reflections off the end windows. By making the end window far away from the side exit window, the absorption path of the scattered radiation is increased. If the absorption by the gas is strong enough (as it is in the case of $^{13}CH_3F$), then, the gas can reduce the intensity of the scatter before it reaches the detector. Another features of the cell (as can be seen from the cross-section view) is the recessed NaCl exit window. The NaCl was glued with red wax to a piece of aluminum which was machined to house a 2.0 cm NaCl window. The window was situated such that a 0.6 cm beam passing through the center of the cell would miss the window by 0.2 cm. This feature made it possible to bring the beam very close to the window, thus, permitting minimum absorption of the fluorescence as it

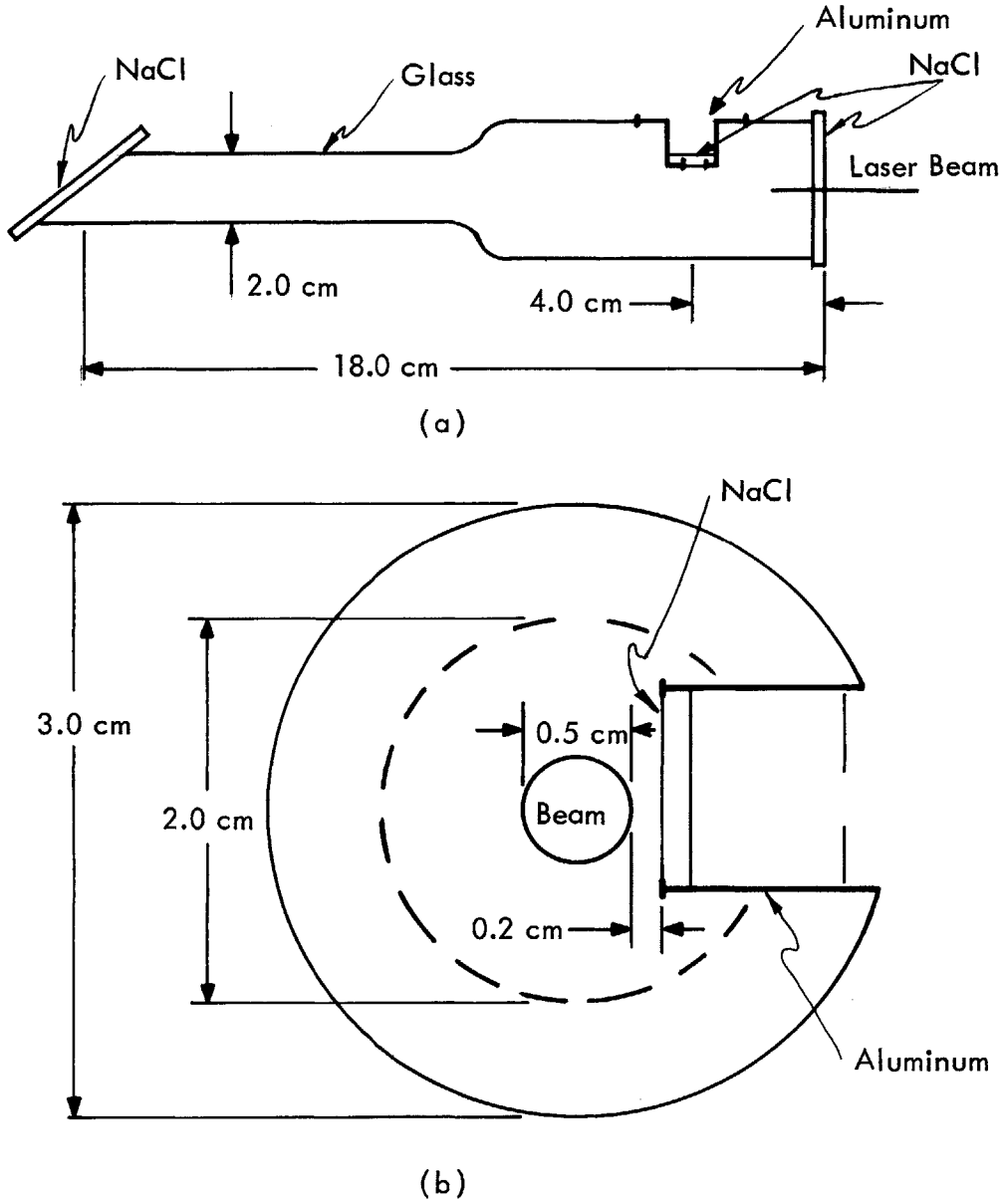

Fig.25. Cell used in fluorescence ecperiments with design to minimize laser scatter. (a) side view (b) view of cross section

leaves the excited volume to the exit window. Also, scattering from the edge of the front window was minimized with this design.

DATA ANALYSIS

Equation (IX-6) is valid in a cold gas filter experiment if all of the I_{10} signal has been removed. In practice, however, several problems are incurred in removing this component. The spontaneous emission from all the levels are composed of many rotational-vibrational lines. These lines originate from throughout the entire band -- P, Q, and R branches. Each rotational-vibrational transition has a Doppler broadened absorption coefficient $\alpha(J,K,J',K')$ given by

$$\alpha(JK,J'K') = \frac{4\pi^{3/2}}{h\nu_{10}} \frac{\mu_{10}^2(JK\rightarrow J'K')}{3} N_{tot} \left[\frac{f_{JK}f_{v}}{2J+1} - \frac{f_{J'K'}f_{v'}}{2J'+1}\right](2J+1)\frac{S(I,K)}{4} \qquad (IX-7)$$

where f_{JK} and $f_{J'K'}$, the fraction of molecules in states f_{JK} and $f_{J'K'}$, are given in Appendix D [eq. (D-7)]. $\mu_{10}^2(JK\rightarrow J'K')$ is the square of the dipole matrix element whose P, Q, and R branch values are given in Appendix D. $S(I,K)$ is the nuclear spin degeneracy factor arising from the presence of the three identical hydrogen atoms of the CH_3 group and the corresponding symmetry constraints imposed on the total wave function. ($I=1/2$ is the nuclear spin). Assuming inversion levels are degenerate, (eq. (D-6)) of Appendix D gives

$$S(I,K) = \begin{cases} 12 & K=3,6,9,\ldots \\ 6 & K \text{ not a multiple of } 3 \end{cases}$$

Since the matrix element μ_{JK} differs for each line across the vibrational band, the spontaneous emission will consist of strong and weak lines for the high and low $|J,K\rangle$ states. Consequently, these lines will be absorbed differently due to $|J,K\rangle$ with the intensity of the strong lines diminishing first, then, the weaker ones at higher pressure.

The entire I_{10} component can be filtered out by increasing the absorption length P'L'. If L', the length of the cold gas filter cell, is made longer, the signal viewed by the detector becomes very weak. If the pressure, P', is increased to the necessary amount, the pressure broadening regime is entered and the overtone transitions may be broadened into resonance. However, the data can be analyzed by simulating the intensity fall-off vs. pressure by computer. Therefore, an absorption factor must be included in I_{10}^{sp} given by

$$\mathcal{Q}_{10}(P') = I_{10}^{SP} e^{-\alpha(\xi)P'L'} = C \sum_{P,Q,R} \sum_{J,K} \mu_{10}^2(\xi) n_{JK} e^{-\alpha(\xi)P'L'} \qquad \text{(IX-9)}$$

, c is a constant

where $\xi =$ (J,K→J'K'), $\alpha(\xi)$ is given by eq. (IX-7), and each component of the P, Q, and R branches is included. The total intensity from all $|v\rangle$ can now be obtained (including partial absorption of I_{10}^{sp} component) by summing over all v to get

$$I_{tot}^{SP}(P') = \left[\mathcal{Q}_{10}^{SP}(P') + \sum_{v=2}^{\infty} I_{v,v-1}\right]$$

$$= \left[\sum_{P,Q,R} \sum_{J,K} \mu_{10}^2(\xi) n_{JK} e^{-\alpha(\xi)P'L'} + \left((1-e^{-\beta_V})^{-2} - 1\right) e^{-\beta_V} \right] C$$

$$= \left[\sum_{P,Q,R} \sum_{J,K} \mu_{10}^2(\xi) n_{JK} e^{-\alpha(\xi)P'L'} + H(T_V) \right] C \qquad \text{(IX-10)}$$

where Hc is the intensity from the $v \geq 2$ levels. Now, $I_{10}^{sp}(P')$ can be evaluated and fitted to three pressure dependent exponentials (See Appendix C) given by

$$\mathcal{I}_{10}(P') = 0.567 e^{-0.614 P'L'} + 0.331 e^{-0.145 P'L'} + 0.102 e^{-0.019 P'L'} \qquad \text{(IX-11)}$$

Using this in equation (IX-10), we can solve for

$$\frac{I_{tot}^{sp}(P')}{I_{tot}^{sp}(0)} = \frac{\mathcal{I}_{10}^{sp}(P') + H(T_V) + H(T_V)}{1 + H(T_V)} \qquad \text{(IX-12)}$$

$H(T_V)$ is a function of the vibrational temperature which can be adjusted until the computer generated curve for $I_{tot}^{sp}(P')/I_{tot}^{sp}(0)$ fits the corresponding experimental curve. Thus, a value for T_V and consequently the energy stored in the mode can be evaluated from this fit to the experimental data.

The observed fluorescence signal transversed several cells in which different absorption lengths were encountered before reaching the detector. That is, before leaving the fluorescence cell, the radiation passed through a 2.0 mm path from the beam pheriphery to the exit window, then, the radiation passed through the 7.825 cm cold gas filter. The cells contained different total pressures of the 90% $^{13}CH_3F$ gas. The absorption through each cell was evaluated by

eq. (IX-11) where corrections were made for each cell length and $^{13}CH_3F$ partial pressure. If PL is the absorption length in the fluorescence cell and P'L' is the absorption length in the cold gas filter, the exponential factor in eq. (IX-9) becomes $e^{-\alpha(\xi)(P'L'+PL)}$

Figure 26 shows the computer generated curves fitted to the experimental cold gas filter data. The cold gas filter pressure, P', was varied typically between 0.1 and 5.0 torr of $^{13}CH_3F$. For all signals, a fast decrease in intensity followed by a long slowly varying tail could be observed corresponding to the strong and weak lines being absorbed, respectively. The fluorescence cell pressure, P, ranged from 2.75 torr to 11.4 torr with temperatures from 1500-3200°K, or using eq. (V), the number of quanta, ε, stored in mode ranged from 0.58-1.68 (Fig. 26). Further evidence of energy absorption and storage by V-V pumping is shown by observing the following: For the higher fluorescence cell pressures, P, the changes in intensity from P'=0.1-5.0 torr is less than the change for lower cell pressures. This is true because the increased V-V rate at higher P causes the upper v states of the mode to become more heavily populated, thus, leaving fewer molecules in the v=1 state. Thus, most of the fluorescence comes from the upper v states and is unaffected by the cold gas filter

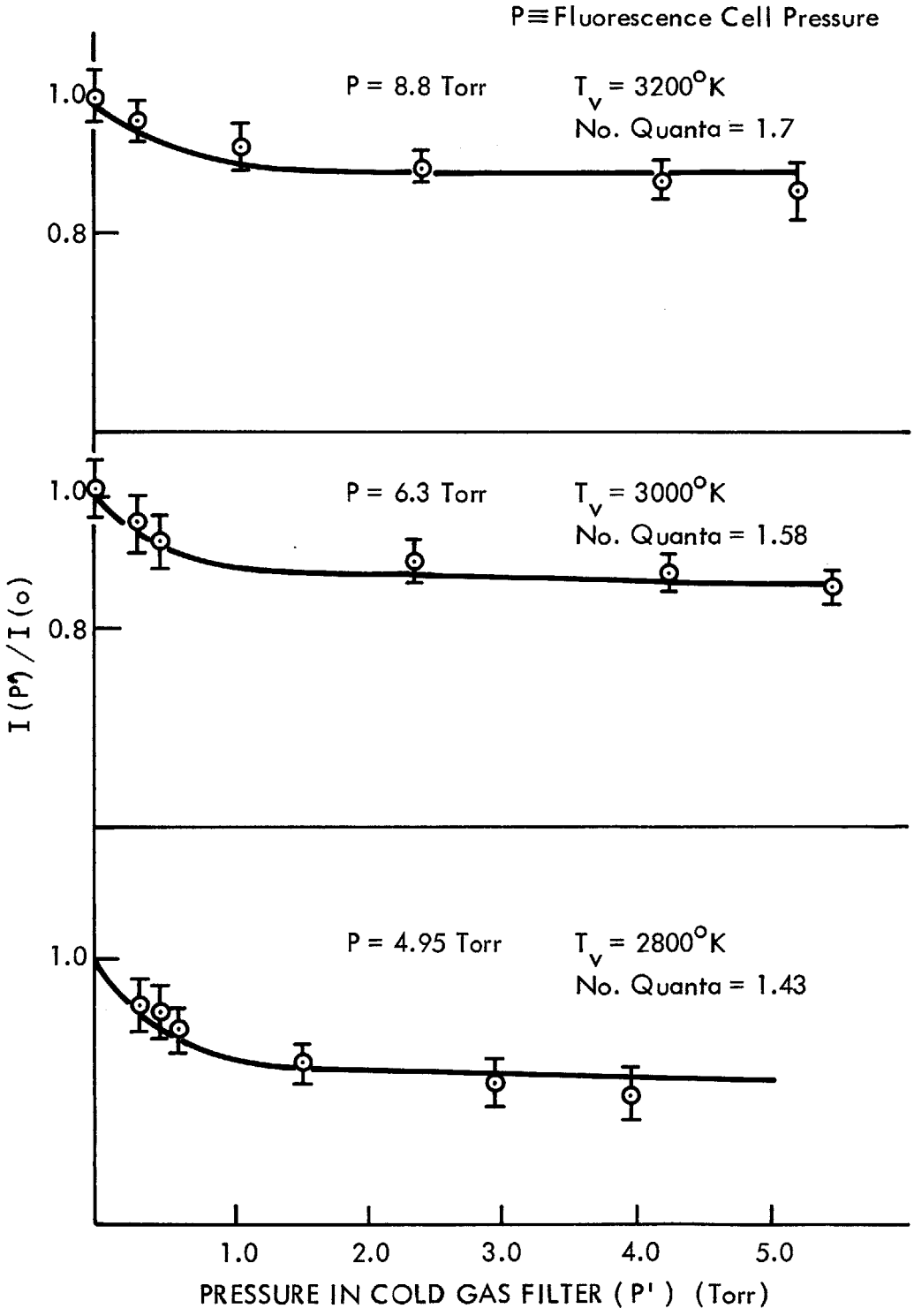

Fig. 26. Experimental cold gas filter data (circles) and computer fits (solid lines) for obtaining the vibrational temperatures.

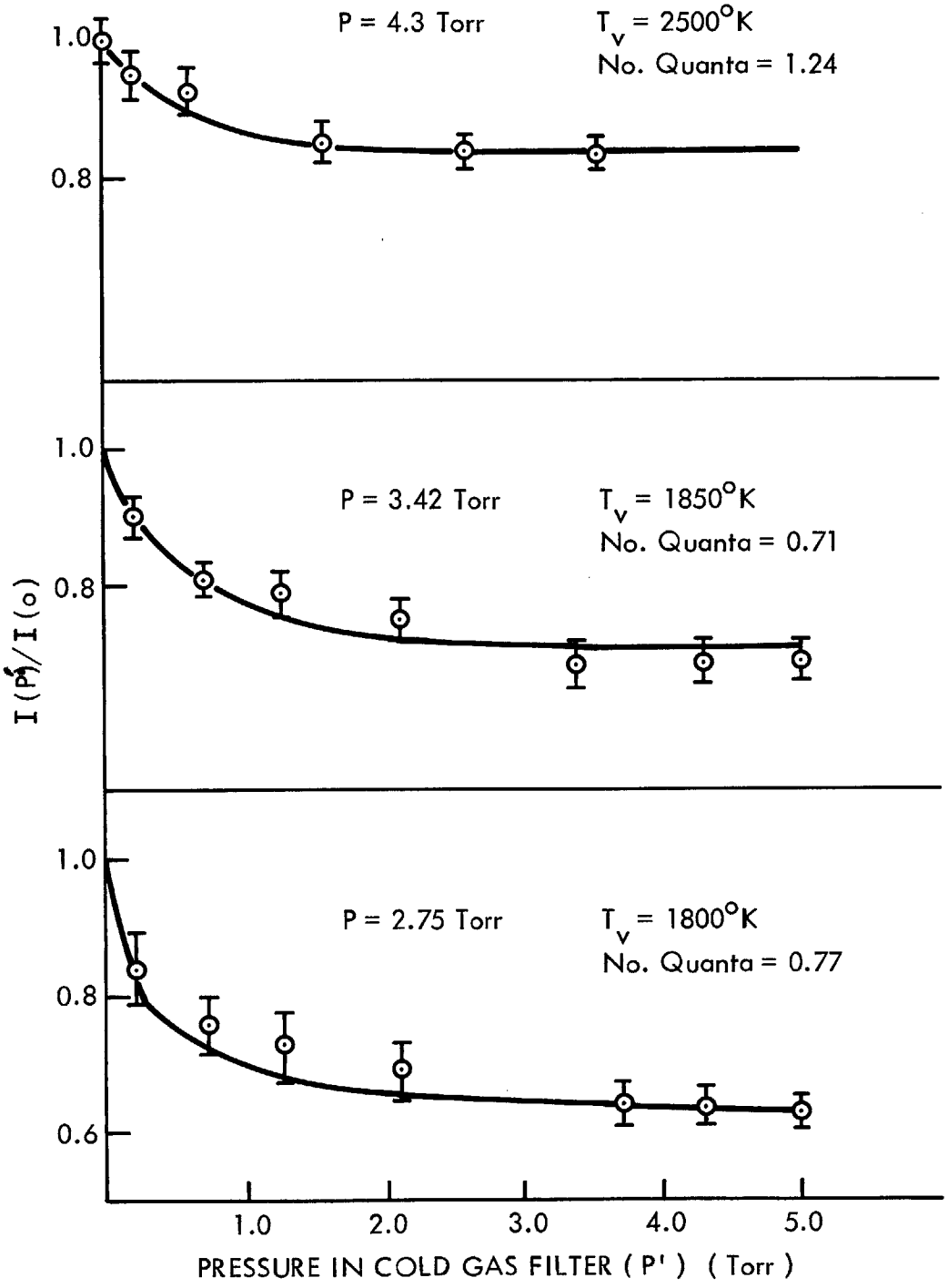

Fig. 26. (Continued)

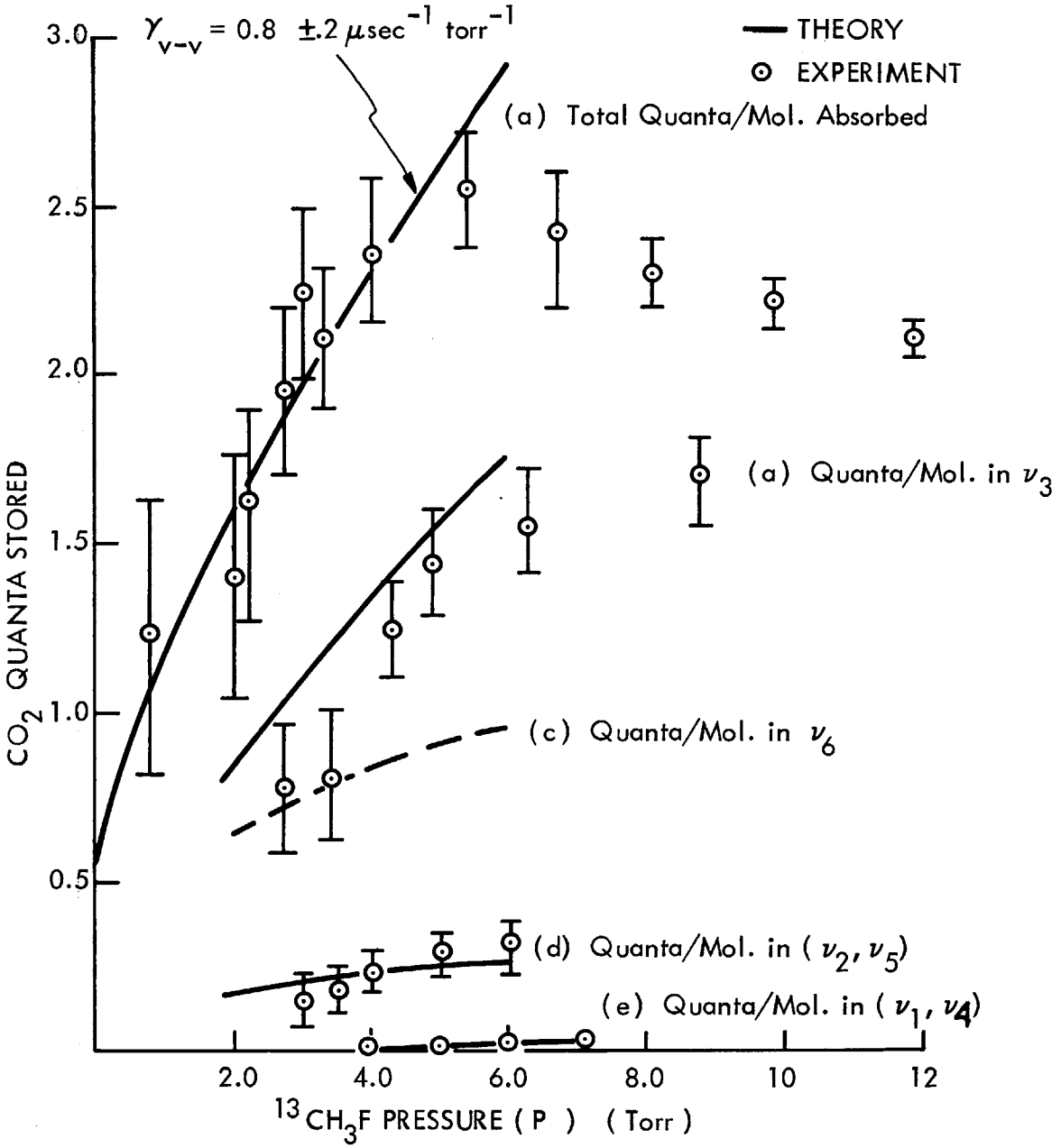

Fig. 27. CO_2 quanta stored (a) in molecule by absorption experiment (b) in ν_3 by cold gas filter experiment (c) in ν_6 by steady state theory (d) and (e) in (ν_2,ν_5) and (ν_1,ν_4) by intensity calibration. Energy in ν_6 was not measured.

X. MEASUREMENT OF THE ENERGY STORED IN THE $(\nu_1, \nu_4, \nu_2, \nu_5)$ MODES OF CH_3F

OBSERVATION OF RAPID INTRA-MODE V-V COUPLING

Cold gas filter measurements and relaxation data have together indicated that approximately 40-50% of the CO_2 energy absorbed by $^{13}CH_3F$ resides somewhere within the molecule. The energy level diagram (Figure 28) shows the close spacing of the energy levels in the modes of CH_3F which gives rise to close collisional coupling. Immediately following the pumping of the C-F stretch, ν_3 (9.6μm), fluorescence can be observed at 9.6μm, 6.8μm and 3.37μm indicating excitation and relaxation of the ν_3, (ν_2, ν_5) and (ν_1, ν_4) modes[25]. Without attempting to determine precisely the energy flow path by which the modes are excited, the rise time of the signals can be measured and compared to examine the time lag between equilibration of the pumped mode and the collisionally coupled modes.

The 3.3μm radiation from (ν_1, ν_4) and the 6.8μm from (ν_2, ν_5) were isolated with a quartz filter and a wide bandpass filter from Optical Coating Laboratories, respectively. All wavelengths were detected with the same geometry and detection apparati for comparison. Figure 23 shows the rise of the ν_3, (ν_2, ν_5), and (ν_1, ν_4) fluorescence intensities as a function of time. The rise time is seen to increase with pressure up to a point where the fluorescence amplitude

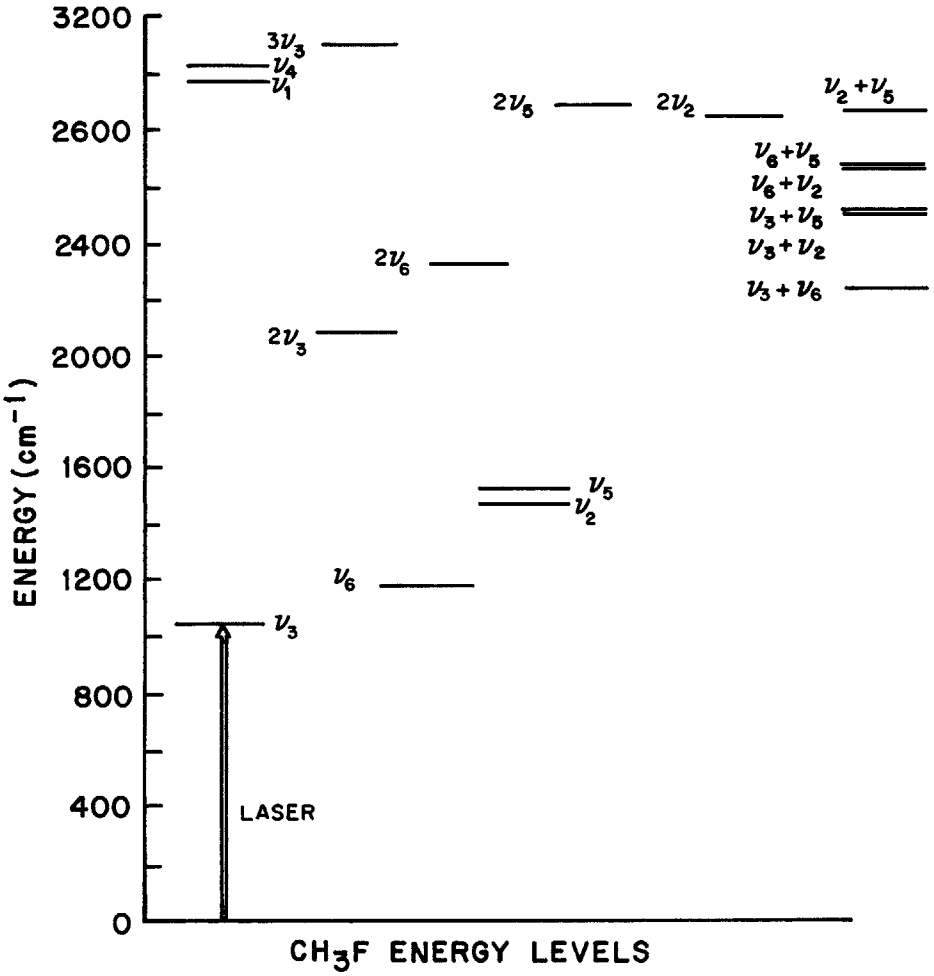

Fig.28. Methyl fluoride (CH_3F) energy level diagram up to $3000cm^{-1}$.(25)

remains a constant. For pressures ($P \geq 3$ torr) the fluorescence rise time is approximately the same as the laser pulse time and the ν_3 fluorescence rise time[27]. For lower pressures a slight time lag is observed between the peak of the ν_3 and the (ν_2,ν_5) and (ν_1,ν_4) signals. The constant rise at higher pressures show that rapid V-V cross-over processes are occurring, and that the equilibration of the other modes occur during the laser pulse. Thus, energy will continue to flow among the modes until the laser pulse is shut off. We, therefore, see a rise equal to the duration of the laser pulse. The low pressure time lag between the peaking of ν_3 and (ν_1,ν_4) yielded a rough V-V cross-over time of approximately 9.0 ± 3 μmsec-torr, in good agreement with previously measured V-V cross-over times in CH_3F[25].

Now that observation of the time scale of energy flow has given direct proof of fast intra-mode V-V coupling, the questions that now arises are -- how is the energy partitioned among the modes? What are the temperatures of the modes? What determines the partitioning of the energy? Can 50% of the total energy be accounted for?

Attempts at performing cold gas filter measurements were hampered by the very weak absorption by the other modes $(\nu_1,\nu_2,\nu_4,\nu_5,\nu_6)$. Cold gas filter data on the (ν_1,ν_4) mode yielded vibrational temperatures of $1200^{\circ}K$. This measurement was performed by using (as a cold gas filter) a 11.0 meter path length multiple reflection cell from

Wikes Co. Large error was incurred in this measurement due to the weak intensity after passing through the cold gas filter. In addition, very high pressures (>30.00 torr) were required to see appreciable absorption, thus, the interpretation of data became less certain because of pressure broadening effects[33]. Nevertheless, this approximate measurement indicated that the (ν_1,ν_4) states were "cold" relative to the ν_3 states. The even less absorbing[47] (ν_2,ν_5) states made cold gas filter data less obtainable.

A more precise method for measuring the temperatures of the weakly absorbing modes of CH_3F is desired. Thus far, the ν_3 temperature (T_3) and the relative intensities of all the modes (I_n/I_3) are well known where I_n and I_3 are the intensities of the n^{th} mode and ν_3, respectively. Perhaps these quantities can yield information about the temperature, T_n. Indeed, the relative intensities do yield the vibrational temperature if the content of the spontaneous emission is carefully analyzed.

SPONTANEOUS EMISSION INTENSITY RATIOS

The spontaneous emission intensity of any vibrational transition is given by[35,33]

$$I^{SP}_{v,v-1} = \tfrac{2}{3}\,\omega^4/c^3 \sum_{J,K} \left[\mu^2_{v-1,v}(JK \rightarrow J'K')\, n_{JK}\right] \qquad (X\text{-}1)$$

where n_{JK} is the population in the (J,K) rotational and $\mu^2_{v,v-1}(JK \rightarrow J'K')$ is the matrix element squared connecting states (J,K) and J',K'). The symmetric top matrix elements from Appendix D are as follows:

$$\mu^2_{v,v-1} = \begin{cases} (\mu^0_{v,v-1})^2 \dfrac{(J+1)^2 - K^2}{(J+1)(2J+1)} & \text{R-Branch } J+1 \leftarrow J \\ (\mu^0_{v,v-1})^2 \dfrac{K^2}{J(J+1)} & \text{Q-Branch } J \leftarrow J \\ (\mu^0_{v,v-1})^2 \dfrac{J^2 - K^2}{J(2J+1)} & \text{P-Branch } J-1 \leftarrow J \end{cases} \quad (X-2)$$

These matrix elements, as given by Townes and Schawlow[20], are for absorption, averaged over M-states where the number of M-states absorbing is determed by the J of the lower state of the transition. The above matrix elements can be converted to emission matrix elements by dividing by the number of M-states for the upper J and then multiplying by the number of lower (J,M) states. For the R-Branch, (J+1→J), the matrix element is multiplied by the factor (2J+1)/(2J+3) and for the P-Branch, (J-1→J), the factor is (2J+1)/(2J-1). The J's for the upper and lower of the Q-Branch are the same. Then,

$$\mu^2_{v,v-1} \begin{cases} \dfrac{(J+1)^2 - K^2}{(2J+3)(J+1)} (\mu^0_{v,v-1})^2 & \text{P-Branch } (J+1) \leftarrow J \\ \dfrac{J^2 - K}{J(2J-1)} (\mu^0_{v,v-1})^2 & \text{R-Branch } (J-1) \leftarrow J \\ \dfrac{K^2}{J(J+1)} (\mu^0_{v,v-1})^2 & \text{Q-Branch } J \leftarrow J \end{cases} \quad (X-3)$$

Let us now make the substitution $J=J'-1$ for the R-Branch and $J=J'+1$ for the P-Branch. This substitution makes J the initial level for emission. Then,

$$\mu^2_{v,v-1} = \begin{cases} (\mu^0_{v,v-1})^2 \dfrac{(J+1)^2-K^2}{(J+1)(2J+1)} & \text{P-Branch } (J-1 \rightarrow J) \\ (\mu^0_{v,v-1})^2 \dfrac{K^2}{J(J+1)} & \text{Q-Branch } (J \longrightarrow J) \\ (\mu^0_{v,v-1})^2 \dfrac{J^2-K^2}{(2J+1)J} & \text{R-Branch } (J+1 \rightarrow J) \end{cases}$$

In evaluating the spontaneous emission intensity, the sum $\sum_{\substack{P,Q,R \\ J,K}} \mu^2 n_{JK}$ is to be evaluated. Summing over (J,K) in P,Q, and R Branch matrix elements, we obtain

$$\sum_{J,K} \sum_{P,Q,R} [n_{JK} \mu^2_{v,v-1}(JK \rightarrow J'K')] = \sum_{J,K} \left[\frac{J^2-K^2}{J(2J+1)} + \frac{(J+1)^2-K^2}{(J+1)(2J+1)}\right.$$

$$\left. + \frac{K^2}{J(J+1)}\right] n_{JK} (\mu^0_{v,v-1})^2 = \sum_{JK} (1) n_{JK} = n_v (\mu^0_{v,v-1})^2 \qquad (X-4)$$

Thus, $I^{SP}_{v,v-1} = K\omega^4 n_v (\mu^0_{v,v-1})^2$ where $\mu^0_{v,v-1}$ is the $v \longrightarrow v-1$ transition dipole moment. We see that the spontaneous emission intensity is (to within a constant) a function of the oscillation frequency, the dipole moment, and the population, n_v.

To obtain the total intensity from the mode's vibrational levels, we must sum over all v, which gives

$$I^{tot}_{v,v-1} = \sum_{v=1}^{\infty} K\omega^4 n_v (\mu^0_{v,v-1})^2 \qquad (X-5)$$

using $(\mu^0_{v,v-1})^2 \propto v(\mu^0_{10})^2$ and $n_v = n_0 e^{-v\hbar\omega/kT_v}$ we get,

$$I^{tot}_{v,v-1} = K(\mu^0_{10})^2\omega^4 \sum_{v=1}^{\infty} v e^{-v\hbar\omega/kT_v}$$

$$= K(\mu^0_{10})^2\omega^4 e^{-\beta}(1-e^{-\beta})^{-2} \qquad (X-6)$$

where $\beta = \hbar\omega/kT_v$. The μ^0_{10} dipole moment may be obtained from absorption spectra by noting that the absorption coefficient $\alpha(J)$ is given by

$$\alpha(J) = \frac{4\pi^2\chi}{\hbar\Delta_w}(\mu^2_{10})_z (2J+1)e^{-BJ(J+1)/kT} \qquad \chi = \omega/c \qquad (X-7)$$

Δ_ω is the width of the spectrometer used which replaces the Doppler width and $(\mu^0_{10})_z$ is the z component of the dipole moment used in absorption. For the P and R-Branch we find, using $(\mu^0_{10})^2_z = (\mu^0_{10})^2/3$

$$\alpha_R(J) = (4\pi\chi/3\Delta_w)(\mu^0_{10})^2 f(J)$$

$$\alpha_P(J) = (4\pi\chi/3\Delta_w)(\mu^0_{10})^2 g(J) \qquad (X-8)$$

or

$$(\mu^0_{10})^2 = (\text{Const.})\alpha_P(J) f(J)/\omega$$

$$(\mu^0_{10})^2 = (\text{Const.})\alpha_R(J) g(J)/\omega \qquad (X-9)$$

Thus, by choosing the appropriate J in the P or R branch, the dipole moment μ^0_{10} of any mode can be obtained from absorption data. Substituting $(\mu^0_{10})^2$ into eq. (X-7) , we find

$$I^{tot}_{v,v-1} = (\text{Const.})\alpha\omega^3 e^{-\beta}(1-e^{-\beta})^{-2} \qquad (X-10)$$

For measuring vibrational temperatures from relative in- (I_n/I_3), the α chosen for both modes must be for the same J value. The details of the J-dependence of the absorption is, then, eliminated. For two modes ω_1 and ω_2 emitting spontaneous emission, their vibrational temperatures are related to their emission intensities by[27]

$$e^{-\beta_2}(1-e^{-\beta_2})^{-2} = \frac{I^{tot}_{(\omega_1)}}{I^{tot}_{(\omega_2)}}\left(\frac{\omega_1}{\omega_2}\right)^3 \frac{\alpha_1}{\alpha_2}(1-e^{-\beta_1})^{-2}e^{-\beta_1} \qquad \text{(X-11)}$$

The relative absorption in CH_3F, I/I_0, was taken from absorption spectra by Bennett & Meyer[36] Smith and Mills[37], and Yates and Nielson[38]. The absorption value was taken at the peak of the P-Branch for each mode. Using the change in transmitted intensity, a cell length of ~6.0cm and the linear absorption formula

$$I = I_0 e^{-\alpha PL}$$

the ratios α_1/α_2 for all modes (where $\alpha_1=\alpha_{\nu_3}$) was calculated and are shown in Table (II).

ν_2,ν_5 was treated as a triply degenerate mode because of the doubly degenerate ν_5[19]. Likewise, ν_1,ν_4 was treated as being triply degenerate because of doubly degenerate ν_4[19]. The contribution from the $2(\nu_2,\nu_5)$ state was neglected and its absorption was excluded from the $3_{\mu m}$ spectra. Thus, all the parameters of eq. (IX-11) are known

TABLE II

Mode (ν_n)	Degeneracy	α_3/α_n
ν_1, ν_4	3	2.90
ν_2, ν_5	3	23.20
ν_6	2	63.04
ν_3	1	1.00

The ratio of the absorption coefficient of the n^{th} mode to ν_3 is shown with the total degeneracy of each mode(s).

and only an intensity measurement of each mode is needed to determine the vibrational temperatures.

All fluorescence intensities were focused with a lens into a Cu:Ge detector with a 0.5μsec response time. Correction factors were included in the intensity measurements for the error introduced by differing detectivity at the three wavelengths -- 9.6μm, 6.8μm, and 3.37μm. For 6.8μm and 3.37μm the correction factors were 1.31 and 3.15, respectively, taken from the Santa Barbara Infrared Detection Chart. In addition, correction factors were added for the various filters used for separating the emission. A 20% correction was made for the quart filter in the 3.3μm experiment; a 20% correction was made for the wide bandpass filter in the 6.8μm measurement; and the background of 3.3μm and 6.8μm were subtracted from the total intensity to give the 9.6μm signal.

Figures (29) and (30) show the absolute measured intensities of the 9.6μm and 3.3μm mode versus pressure. The magnitude of the fluorescence intensities are found to be compatible with the strengths of the emissions[47] (if degeneracies are included). The absolute intensities shown do not give explicitly the vibrational temperatures, but they exhibit the pressure variation of the temperatures and their relation to each other.

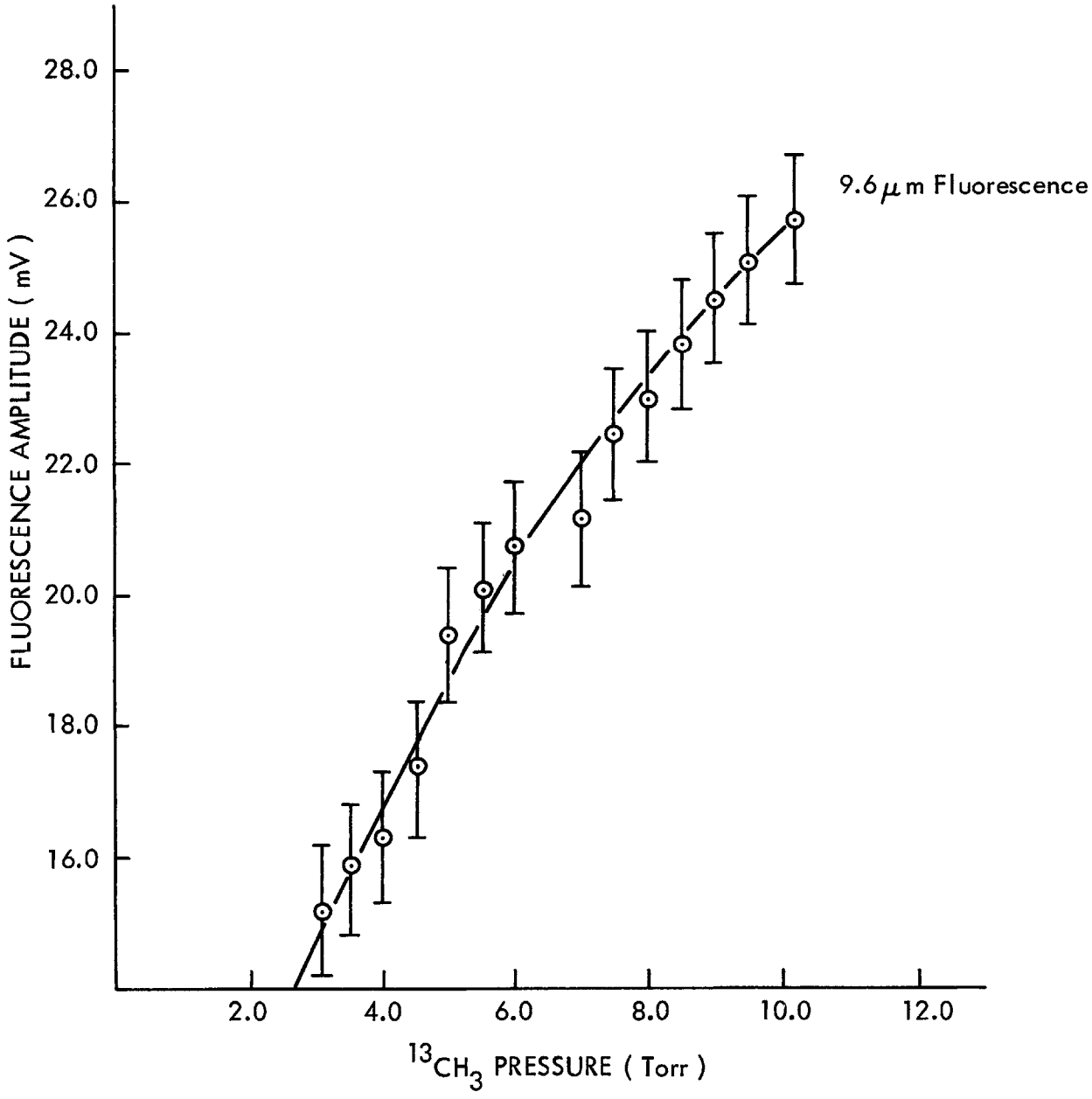

Fig. 29. Measurement of 9.6μm fluorescence intensity vs. vs. pressure.

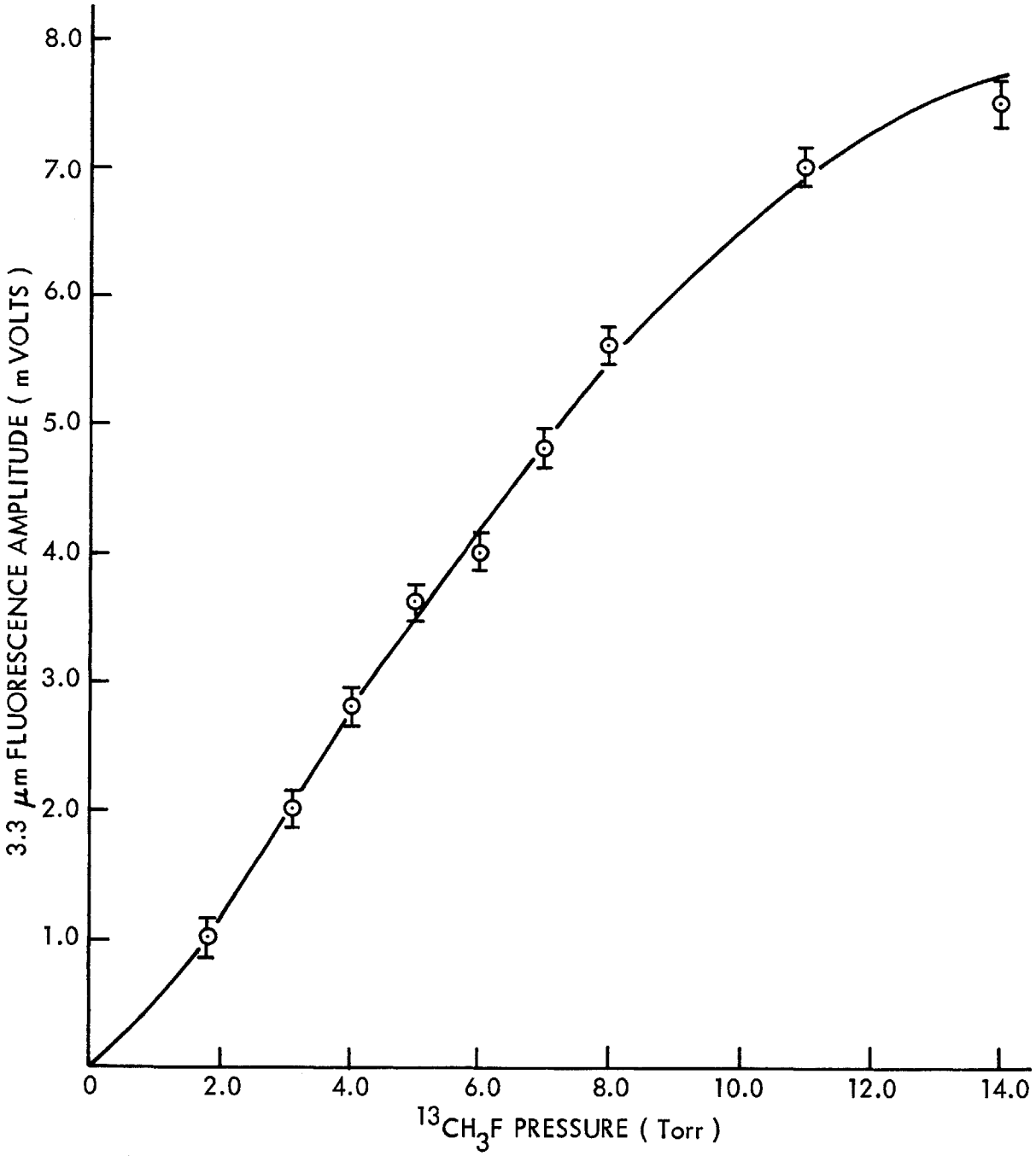

Fig.30. Measurement of 3.3μm fluorescence intensity vs. pressure.

Using the intensities of figures (29) and (30), the vibrational temperature, and the appropriate correction factors, equation (IX -11) was solved for the vibrational temperature. The equation was solved using Newton's Numerical Method on the Hewlett Packard 25 calculator. The temperatures were evaluated and converted into CO_2 quanta by treating the modes of the polyatomic as separate harmonic oscillators[26]. The results of this analysis are shown in Figure (27). The energy stored (ε) in the CH_3F vibrational modes -- $\varepsilon_{\nu_3}, \varepsilon_{\nu_2,\nu_5}$, and $\varepsilon_{\nu_1,\nu_4}$ -- are plotted as a function of CH_3F pressure in figures 27b, 27d, and 27e, respectively. $\varepsilon_{\nu_2,\nu_5}$ and $\varepsilon_{\nu_1,\nu_4}$ are the sums of all the constituent degenerate modes energies. As the energy spacing of the fundamentals became higher, the energy stored within the modes bec me smaller (i.e., $\varepsilon_{\nu_1,\nu_4} > \varepsilon_{\nu_2,\nu_5} > \varepsilon_{\nu_3}$).

Therefore, it has been found that during steady state equilibrium among the vibrational modes of a polyatomic, the energy stored within the modes is partitioned in a well defined manner -- the lowest energy mode having the largest energy storage.

Based on the proof of a vibrational equilibrium among the modes, a model for calculating the steady state energy partitioning among modes assuming a constant kinetic temperature has been developed. This model is discussed in Chap.XI.

Thus, the absolute energy in the modes of CH_3F has been measured, and a distribution of energy rendering each

mode at a different vibrational temperature has been found. Differing vibrational temperature among the modes of a polyatomic along with a constant translational temperature make possible many new laser schemes among polyatomic intra-mode transitions.

XI. MODEL FOR VIBRATIONAL STEADY STATE ENERGY DISTRIBUTION

CONDITIONS FOR VIBRATIONAL STEADY STATE

Since a long lived steady state equilibrium among modes has been observed in methyl flouride, it is possible to solve the rate equations (II-10) for each coupled set of oscillators in the steady state limit. In this chapter, such an analysis will be used to predict the steady state partitioning of energy among the modes of CH_3F. Comparison of the model predicted energy distribution shows good agreement with measurements of Chapter X and the energy flow path used is found to be correct at high and low excitation.

The steady state energy distribution among the modes of polyatomic can be found by considering pairs of coupled modes in vibrational equilibrium.[36] In Chapter III, the energy flow in two coupled modes with one underlaser irradiation was found to be eq. (III-10),

$$\dot{\epsilon}_A = \gamma_{AB}(\alpha\epsilon_A - \epsilon_B) - (1-\alpha)\epsilon_A\epsilon_B\gamma_{AB} + \dot{\epsilon}_L$$

$$\dot{\epsilon}_B = \gamma_{AB}(\alpha\epsilon_A - \epsilon_B) + (1-\alpha)\epsilon_A\epsilon_B\gamma_{AB}$$

(See also eq. (III-7).

The laser is shut off by setting $\dot{\epsilon}_L = 0$ and the steady state is treated by setting $\dot{\epsilon}_A = \dot{\epsilon}_B = 0$. Using the relations for the energy stored in an oscillator,

$$\epsilon_A = (e^{\Theta_A} - 1)^{-1} \quad \text{and} \quad \epsilon_B = (e^{\Theta_B} - 1)^{-1}$$

along with the conditions imposed by detailed balancing[22]

$$\alpha = exp[(E_B - E_A)/K T_R]$$

where T_R is room temperature, either of the equations for ϵ_A or ϵ_B can be solved to yield

$$\frac{E_B}{T_B} - \frac{E_A}{T_A} = \frac{\Delta E}{T_R}$$

where $\Delta E = E_B - E_A$ and $E_B > E_A$. (XI-1)

Thus, the steady state solution to the rate equations yield the above simple relationship between two coupled normal modes in a vibrational equilibrium.

THE APPLICATION OF THE STEADY STATE EQUATION TO THE MODES OF CH_3F

For many modes in equilibrium, the steady state relation can be applied to each mode pair that is directly collisionally coupled. By using the proper endothermic or exothermic energy defect,[29] the steady state partitioning of energy can be calculated. The energy storage was calculated for the two different paths in CH_3F. These paths are as follow:[25]

PATH 1

(a) $CH_3F(\nu_3) + CH_3F(0) \underset{\gamma_b}{\overset{\gamma_f}{\rightleftharpoons}} CH_3F(\nu_6) + CH_3F(0) - \Delta E(147 cm^{-1})$

(b) $CH_3F(\nu_6) + CH_3F(0) \underset{\gamma_b'}{\overset{\gamma_f'}{\rightleftharpoons}} CH_3F(\nu_1, \nu_5) + CH_3F(0) - \Delta E(275 cm^{-1})$

$$(c)\ 2CH_3F(\nu_2,\nu_5) \underset{\gamma_b''}{\overset{\gamma_f''}{\rightleftarrows}} CH_3F(2\nu_2,2\nu_5) + CH_3F(0) - \Delta E(68cm^{-1})$$

$$(d)\ CH_3F(2\nu_2,2\nu_5) + CH_3F(0) \underset{\gamma_b'''}{\overset{\gamma_f'''}{\rightleftarrows}} CH_3F(\nu_1,\nu_4) + CH_3F(0) + \Delta E(103cm^{-1})$$

PATH 2

$$(e)\ CH_3F(\nu_3) + CH_3F(\nu_3) \underset{\gamma_b}{\overset{\gamma_f}{\rightleftarrows}} CH_3F(2\nu_3) + CH_3F(0) - \Delta E$$

$$(f)\ CH_3F(2\nu_3) + CH_3F(\nu_3) \underset{\gamma_b'}{\overset{\gamma_f'}{\rightleftarrows}} CH_3F(3\nu_3) + CH_3F(0) - \Delta E$$

$$(g)\ CH_3F(3\nu_3) + CH_3F(0) \underset{\gamma_b''}{\overset{\gamma_f''}{\rightleftarrows}} CH_3F(\nu_1,\nu_4) + CH_3F(0) + \Delta E$$

Applying equation (XI-1) first to step (a) in Path 1, we find, $\frac{E_6}{T_6} - \frac{E_3}{T_3} = \frac{\Delta E^{(1)}}{T_R}$

, where $\Delta E^{(1)} = 147cm^{-1}$, and

$$T_6 = \left(\frac{\Delta E^{(1)}}{T_R} + \frac{E_3}{T_3}\right)^{-1} E_6 \qquad (XI-2)$$

Applying eq.(XI-1) to step (b), we get

$$\frac{E_5}{T_{5,2}} - \frac{E_6}{T_6} = \frac{\Delta E^{(2)}}{T_R}$$

, where $E = 275cm^{-1}$, and

$$T_{5,2} = \left(\frac{\Delta E^{(2)}}{T_R} + \frac{E_6}{T_6}\right)^{-1} E_{5,2} = T_{2,5} \qquad (XI-3)$$

Applying eq.(XI-1), again, to step (d) gives

$$\frac{E_{1,4}}{T_{1,4}} - \frac{2E_{2,5}}{T_{2,5}} = \frac{\Delta E^{(3)}}{T_R}$$

, where $E = 103cm^{-1}$, and

$$T_{1,4} = \left(\frac{\Delta E^{(3)}}{T_R} + \frac{2E_{2,5}}{T_5}\right)^{-1} E_{1,4} \qquad (XI-4)$$

By combining equations (XI-2) and (XI-3), we obtain

$$T_{2,5} = \left[\frac{\Delta E^{(2)} + \Delta E^{(1)}}{T} + \frac{E_3}{T_3}\right]^{-1} E_3 \qquad \text{(XI-5)}$$

Combining equations (XI-3) and (XI-4) gives

$$T_{1,4} = \left[\frac{\Delta E^{(3)}}{T_R} + 2\left(\frac{\Delta E^{(2)} + \Delta E^{(1)}}{T_R} + \frac{E_3}{T_3}\right)\right]^{-1} E_3 \qquad \text{(XI-6)}$$

Equations (XI-2), (XI-5), and (XI-6) express the temperatures of all the modes as a function of T_3, the temperature of ν_3, assuming that the kinetic temperature (T_R), remains constant. Given the temperature of each mode, the number of quanta stored was calculated by (using the expression for energy stored in an oscillator),

$$\mathcal{E}_3 = \left(e^{\Theta_3} - 1\right)^{-1}$$

$$\mathcal{E}_{2,5} = 3\left(e^{\Theta_{2,5}} - 1\right)^{-1}$$

$$\mathcal{E}_{1,4} = 3\left(e^{\Theta_{1,4}} - 1\right)^{-1} \qquad \text{(XI-7)}$$

$$\mathcal{E}_6 = 2\left(e^{\Theta_6} - 1\right)^{-1}$$

or in general

$$\mathcal{E}_n = d_n\left(e^{\Theta_n} - 1\right)^{-1}$$

where d_n is the degeneracy factor for the n^{th} mode and $\mathcal{E}_n$ is the quanta stored in oscillator at temperature Θ_n. The

energy stored in each mode was evaluated as function of the ν_3 temperature, T_3. Figure 31 shows a plot of total energy stored ($\mathcal{E}_{tot}$), $\mathcal{E}_3$, $\mathcal{E}_{2,5}$, and $\mathcal{E}_{1,4}$ vs. T_3 where

$$\mathcal{E}_{tot} = \mathcal{E}_3 + \mathcal{E}_6 + \mathcal{E}_{2,5} + \mathcal{E}_{1,4} \qquad \text{(XI-8)}$$

and $Q = \mathcal{E}$ in figure 31. Note that approximately half of the total energy resides in ν_3 and smaller fractions in ν_6, $\nu_{2,5}$, and $\nu_{1,4}$, respectively.

A comparison of the experimental results with the steady state theory was made by plotting the calculated $\mathcal{E}_n$ as a function of pressure. This was acheived by using the measured total energy absorbed vs pressure and finding the corresponding energies in the other modes. A comparison of the theoretically and experimentally determined quanta per molecule vs. pressure is given in Fig. 27. Note that the curves predicted by the steady state theory for Path I follows close to the experimental quanta vs. pressure curves. The energies observed do not exactly add up to the total energy measured in absorption experiment, however, within the limits of experimental error, agreement is obtained within 20%.

An examination of Path II shows that for $T_3 = 2000^\circ K$. the temperature of $\nu_{1,4}$ would be (from eq. (XI-1) and using Path II-(g),

$$T_{1,4} = \left(\frac{3E_3}{T_3} - \frac{\Delta E}{T_R}\right)^{-1} E_{1,4} = \left(\frac{3090\,cm^{-1}}{2000^\circ K} - \frac{16\,cm^{-1}}{300^\circ K}\right)^{-1} 2984\,cm^{-1}$$

$$T_{1,4} = 2000.45^\circ K \quad \text{or} \quad \mathcal{E}_{1,4} = .13 \text{ Quanta.}$$

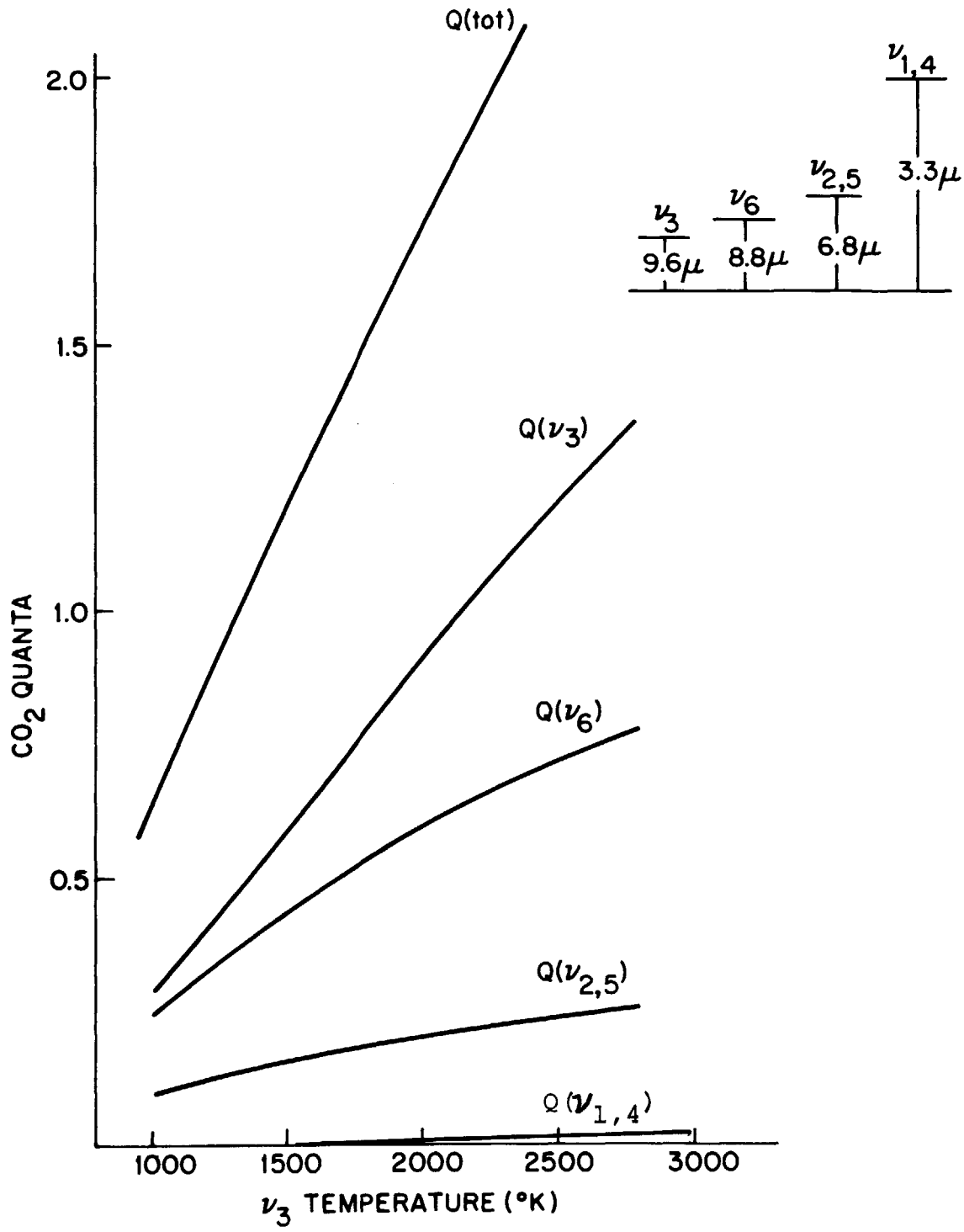

Fig.31. Steady state distribution of energy for varying ν_3 temperature.

This value is approximately four times greater than the value measured for $\varepsilon_{1,4}$, therefore, indicating an erroneously high temperature and a poorly chosen path. Hence, the energy flow path as determined by Flynn and co-workers at low excitation is shown to be valid even at strong excitation, and the steady state model accurately predicts the distribution of energy among collisionally coupled modes of a polyatomic molecule

APPENDIX A

INCLUSION OF ROTATIONAL STATES IN LASER INDUCED VIBRATIONAL HEATING

The rate equation analysis with the inclusion of rotational levels takes the form

$$\frac{1}{c}\frac{\partial I}{\partial t} + \frac{\partial I}{\partial z} = \left(n_j^u - n_{j'}^L\right)\sigma_{jj'} I \qquad \text{(A-1)}$$

$$\frac{\partial n_j^u}{\partial t} + \left(\frac{n_j^u - z_j N_v^u}{T_r}\right) = -\left(n_j^u - n_{j'}^L\right)\sigma_{jj'} I + z_j\left(\frac{\partial N_v^u}{\partial t}\right)_{coll} \qquad \text{(A-2)}$$

$$\frac{\partial n_{j'}^L}{\partial t} + \left(\frac{n_{j'}^L - z_{j'} N_v^L}{T_r}\right) = \left(n_j^u - n_{j'}^L\right)\sigma_{jj'} I + z_{j'}\left(\frac{\partial N_v^L}{\partial t}\right)_{coll} \qquad \text{(A-3)}$$

$$\frac{\partial N_v^u}{\partial t} = -\left(n_j^u - n_{j'}^L\right)\sigma_{jj'} I + \left(\frac{\partial N_v^u}{\partial t}\right)_{coll} \qquad \text{(A-4)}$$

$$\frac{\partial N_v^L}{\partial t} = \left(n_j^u - n_{j'}^L\right)\sigma_{jj'} I + \left(\frac{\partial N_v^L}{\partial t}\right)_{coll} \qquad \text{(A-5)}$$

$$\frac{\partial N_v^i}{\partial t} = \left(\frac{\partial N_v^i}{\partial t}\right)_{coll} \qquad \text{(A-6)}$$

where n_j^u and $n_{j'}^L$ are the population densities of the upper and

lower rotational states which interact with the laser directly. N_v^u and N_v^L are the vibrational population densities of the v=0 and v=1 vibrational states, respectively. N_v^i is the population density of the remaining vibrational states ($j \geq 2$). τ_r and $\tau_{r'}$ are the rotational thermalization times of the v=1 and v=0 vibrational levels, and z_j and $z_{j'}$ are the equilibrium values

$$z_j = \left(n_j^{ou}/N_v^{ou}\right) \qquad \text{(A-1)}$$

$$z_{j'} = \left(n_{j'}^{oL}\right)/N_v^{Lo}\Big) \qquad \text{(A-8)}$$

The $\left(\frac{\partial N_v}{\partial t}\right)_{coll}$ terms are identical with those terms occurring in the model neglecting rotational levels. Rotational selection rules governing (R-R) and (V-R) relaxation processes have been ignored.

In our usual manner we assume that the incoming laser pulse is of sufficient intensity to saturate the $j \rightarrow j'$ vibration-rotation transition so that

$$\frac{\partial n_j^u}{\partial t} \approx \frac{\partial n_{j'}^L}{\partial t} \qquad \text{(A-9)}$$

We further assume $\tau_r = \tau_{r'}$ and $z_j = z_{j'}$ to simplify matters. Thus, from (A-9), (A-2), and (A-3), we obtain

$$\left(n_j^u - n_{j'}^L\right) = \frac{z_j}{\left[2\sigma_{jj'} I + 1/\tau_r\right]}\left[\frac{N_v^L - N_v^u}{\tau_r} + \left(\frac{\partial N_v^L}{\partial t}\right)_{coll} - \left(\frac{\partial N_v^u}{\partial t}\right)_{coll}\right] \qquad \text{(A-10)}$$

substituting (A-10) into (A-2), (A-3), (A-4) and (A-5) we obtain the following set of equations.

$$\frac{\partial n_j^u}{\partial t} + \frac{n_j^u - z N_v^u}{\tau_r} =$$

$$\frac{z_j \sigma_{jj'} I}{[2\sigma_{jj'} I + 1/\tau_r]} \left[\frac{(N_v^L - N_v^u)}{\tau_r} + \left(\frac{\partial N_v^L}{\partial t}\right)_{coll.} - \left(\frac{\partial N_v^u}{\partial t}\right)_{coll} \right] + z_j \left(\frac{\partial N_v^u}{\partial t}\right)_{coll} \qquad (A\text{-}11)$$

$$\frac{\partial n_j^L}{\partial t} + \frac{n_j^L - z_j N_v^L}{\tau_r} =$$

$$\frac{-z_j \sigma_{jj'} I}{[2\sigma_{jj'} I + 1/\tau_r]} \left[\frac{N_v^L - N_v^u}{\tau_r} + \left(\frac{\partial N_v^L}{\partial t}\right)_{coll} - \left(\frac{\partial N_v^u}{\partial t}\right)_{coll} \right] +$$

$$z_j \left(\frac{\partial N_v^L}{\partial t}\right)_{coll} \qquad (A\text{-}12)$$

$$\frac{\partial N_v^u}{\partial t} = \frac{z_j \sigma_{jj'} I}{(2\sigma_{jj'} I + 1/\tau_r} \left[\frac{N_v^L - N_v^u}{\tau_r} + \left(\frac{\partial N_v^L}{\partial t}\right)_{coll} - \left(\frac{\partial N_v^u}{\partial t}\right)_{coll} \right]$$

$$+ \left(\frac{\partial N_v^u}{\partial t}\right)_{coll} \qquad (A\text{-}13)$$

$$\frac{\partial N_v^L}{\partial t} = -\frac{z_i \sigma_{ij} I}{(2\sigma_{jj} I + 1/\tau_r)}\left[\frac{N_v^L - N_v^u}{\tau_r} + \left(\frac{\partial N_v^L}{\partial t}\right)_{coll} - \left(\frac{\partial N_v^u}{\partial t}\right)_{coll}\right]$$

$$+\left(\frac{\partial N_v^L}{\partial t}\right)_{coll}$$

(A-14)

Combining (A-13) and (A-14) we then find

$$\frac{\partial}{\partial t}\left(N_v^u - N_v^L\right) =$$

$$\frac{2 z_i \sigma_{ij} I}{(2\sigma_{jj} I + 1/\tau_r)}\left[-\frac{(N_v^u - N_v^L}{\tau_r} + \left(\frac{\partial N_v^L}{\partial t}\right)_{coll} - \left(\frac{\partial N_v^u}{\partial t}\right)_{coll}\right] +$$

$$\left(\frac{\partial N^u}{\partial t}\right)_{Coll} - \left(\frac{\partial N_v^L}{\partial t}\right)_{coll}$$

(A-15)

or

$$\frac{\partial}{\partial t}\left(N_v^u - N_v^L\right) =$$

$$\frac{-2 Z_j \sigma_{jj} I}{2\sigma_{jj} I + 1/\tau_r}\left[\frac{N_v^u - N_v^L}{\tau_r}\right] +$$

$$\left[\left(\frac{\partial N_v^u}{\partial t}\right)_{Coll} - \left(\frac{\partial N_v^L}{\partial t}\right)_{Coll}\right]\left\{\frac{2\sigma_{jj} I(1-Z_j) + 1/\tau_r}{2\sigma_{jj} I + 1/\tau_r}\right\}$$

(A-16)

Assuming I is independent of time (flat pulse assumption) we can integrate (A-16) to obtain

$$\left(N_v^u - N_v^L\right) = \left(N_v^{ou} - N_v^{oL}\right) e^{-\alpha t} +$$

$$e^{-\alpha t}\int_0^t e^{\alpha t'} \beta \, dt'$$

(A-17)

where

$$\alpha = \left\{ \frac{2 z_j \sigma_{jj'} I}{2 \sigma_{jj'} I \tau_r + 1} \right\} \qquad \text{(A-18)}$$

and

$$\beta = \left[\left(\frac{\partial N_v^u}{\partial t} \right)_{coll} - \left(\frac{\partial N_v^L}{\partial t} \right)_{coll} \right] \times \left[\frac{2 \sigma_{jj'} I \tau_r (1 - z_j) + 1}{1 + 2 \sigma_{jj'} I \tau_r} \right] \qquad \text{(A-19)}$$

Let us now assume that β is a slowly varying function of time, with respect to $(1/\alpha)$ and perform the integration in (A-17) over a time short compared to the the time for significant variation of β . We then have

$$N_v^u - N_v^L = \left(N_v^{ou} - N_v^{oL} \right) e^{-\alpha t} + \frac{\beta}{\alpha} \left[1 - e^{-\alpha t} \right] \qquad \text{(A-19)}$$

which for $t >> 1/\alpha$ reduces to

$$N_v^u - N_v^L \approx (\beta/\alpha) = \left[\left(\frac{\partial N_v^u}{\partial t} \right)_{coll} - \left(\frac{\partial N_v^L}{\partial t} \right)_{coll} \right] \times \left[\frac{1 + 2 \sigma_{jj'} I \tau_r (1 - z)}{2 z_j \sigma_{jj'} I} \right] \qquad \text{(A-20)}$$

Note that if $z \approx 1$ this is identical to the result obtained when rotational distribution effects were neglected

If we now substitute (A-20) into (A-10), we find

$$\left(n_j^u - n_j^L \right) = \frac{- z_j \tau_r}{2 \sigma_{jj'} I \tau_r + 1} \left[- \frac{\beta}{\alpha \tau_r} + \left(\frac{\partial N_v^L}{\partial t} \right)_{coll} - \left(\frac{\partial N_v^u}{\partial t} \right)_{coll} \right] = \qquad \text{(A-21)}$$

$$\frac{-z_j \tau_r}{1+2\sigma_{jj'} I \tau_r}\left[\left(\frac{\partial N_v^L}{\partial t}\right)_{coll}-\left(\frac{\partial N_v^u}{\partial t}\right)_{coll}\right]\left[1-\frac{1+2\sigma_{jj'} I \tau_r(1-z)}{2z_j \sigma_{jj} I \tau_r}\right]=$$

$$\left(\frac{-z_j \tau_r}{1+2\sigma_{jj'} I \tau_r}\right)\left[\left(\frac{\partial N_v^L}{\partial t}\right)_{coll}-\left(\frac{\partial N_v^u}{\partial t}\right)_{coll}\right]\left[\frac{1+2\sigma_{jj'} I \tau_r}{2z_j \sigma_{jj'} I \tau_r}\right]=$$

$$-\left[\left(\frac{\partial N_v^L}{\partial t}\right)_{coll}-\left(\frac{\partial N_v^u}{\partial t}\right)_{coll}\right]\frac{1}{2\sigma_{jj'} I} \qquad \text{(A-22)}$$

which is consistent with our initial assumption for saturation if $2\sigma I > \frac{1}{\tau_v}$ and leads us back to the problem where we can ignore rotational relaxation effects. Therefore, we can ignore rotational relaxation processes entirely if the change of β with time is less than $1/\alpha$. Examining (A-18) we have

$$2\sigma_{jj'} I \tau_r << 1$$

$$\alpha = 2z_j \sigma_{jj'} I \qquad \text{(A-21)}$$

and

$$\beta \cong \left\{\left[\frac{\partial N_v^u}{\partial t}\right]_{coll}-\left[\frac{\partial N_v^u}{\partial t}\right]_{coll}\right\}$$

Consequently β changes significantly in a characteristic V-V collision time, hence, if

$$2z_j \sigma_{jj'} I > \frac{1}{\tau_{vv}}. \qquad \text{(A-23)}$$

then, $N_v^u \; N_v$ (eq.A-20) is satisfied and we can ignore rotational effects. Since we require in the limit

$$2\sigma_{jj'} I \tau_r << 1 \qquad \text{(A-24)}$$

that $$2 Z_j \sigma_{jj'} I \tau_{vv'} > 1 \qquad (A-25)$$

we then must have

$$\tau_{vv'} >> (\tau_r / Z_j) \qquad (A-26)$$

for our assumption to be statisfied. Similiar results follow in the limit

$$2 \sigma_{jj'} I \tau_r >> 1 \qquad (A-27)$$

Here a similar analysis shows that all we need is that

$$\boxed{\tau_{vv'} >> \tau_r / Z_j} \qquad (A-28)$$

Hence, as long this condition is satisfied and

$$\boxed{2 \sigma_{jj'} I \tau_{vv'} >> 1} \qquad (A-29)$$

we can ignore the rotational distribution. If (A-28) does not hold we are in the rotational bottleneck regime and the energy will flow into the system less rapidly than what was computed based solely on V-V processes. Simililarly, if (A-29) does not hold we are not saturating the transition and once again the energy will flow less rapidly into the system. If (A-28) does not hold, we are free to decrease τ_r by the addition of an appropriate buffer gas (He), with the restriction that in doing so we do not decrease σ to the point where (A-29) no longer holds.

APPENDIX B

Consider two colliding particles A and B,each having two states of internal energy (A,A*) and (B,B*) with * representing the excited states. We assume that these particles are collisionally coupled through their lowest order transition moments (M_A and M_B), and that each collision is energy conserving an exchange of a single quantum. For the process

$$A^* + B \longrightarrow A + B^*$$

Landau and Teller showed that under the above assumptions and when the interaction Hamiltonian is linear in the transition moments R, the probability per collision, is (23)

$$R(A^*B \quad AB^*) = kM_A^2M_B^2$$

where k is a constant.

For two indentical harmonic oscillators with levels v and v', we find using dipole selection (60)

$$R(v,v' \longrightarrow v+1,v-1) = P_{10}(v+1)v'$$

$$R(v,v' \longrightarrow v-1,v'+1) = P_{10}v(v'+1)$$

where P_{10} is the transition probability per collision for the $1 \longrightarrow 0$ transition, $R(v,v' \longrightarrow v+1,v'-1)$ is the probability per collision for the enerby transfer $v \rightarrow v+1$ as $v' \rightarrow v'-1$, and similiarly for $R(v,v' \rightarrow v-1,v'+1)$

The rate of change of probability of occupying level v, P_v, is then

$$\frac{dP_v}{dt} = \left(\frac{\gamma_{v-v}}{2}\right) \sum_{v'} \left[R(v,v' \rightarrow v+1, v'-1) P_v P_{v'} - R(v,v' \rightarrow v-1, v'+1) P_v P_{v'} \right.$$

$$\left. R(v+1,v' \rightarrow v, v'-1) P_{v+1} P_{v'} + R(v-1, v'; v, v'-1) P_{v-1} P_{v'} \right]$$

where $P_{10} = \gamma_{v-v}/2$ is defined such that for an isolated three level system γ_{v-v} is rate of populating the v=1 state. Using

$$R(v,v' \rightarrow v+1, v'-1) = (v+1) v' P_{10}$$

$$R(v,v' \rightarrow v-1, v'+1) = (v'+1) v P_{10}$$

$$R(v+1,v' \rightarrow v, v'+1) = (v+1)(v'+1) P_{10}$$

$$R(v-1,v' \rightarrow v, v'-1) = v v' P_{10}$$

we have (60)

$$\frac{dP_v}{dt} = \frac{\gamma_{v-v}}{2} \sum_{v'} - \left[(v+1) v' + v(v'+1) \right] P_v P_{v'} + v v' P_{v-1} P_{v'}$$

$$+ (v+1)(v'+1) P_{v+1} P_{v'}$$

APPENDIX C

The transmission of resonant radiation through a gas of symmetric top molecules was caculated on a PDP-12 computer. The absorption coefficient from eqs. (VIII-4), VIII-5, and (D-8) is given by

$$\alpha(J,K)=\frac{4\pi^{3/2}}{hu}e^{-(\Delta/ku)}\frac{\mu_{JK}^2}{3}\frac{S(I,K)\sqrt{B^2C}}{4\sqrt{\pi}\sqrt{(kT)^3}}e^{-[BJ(J+1)+(C-B)K^2]/kT_R}$$

$$=(CN)\,S(I,K)\mu_{JK}^2\,e^{-[BJ(J+1)+(C-B)K^2]/(kT_R)}$$

where CN is a constant factor for all (J,K) states. The absorption coefficient for the R(4,3) transition of CH_3F was caculated to be α =0.5633cm^{-1}torr^{-1}. This α is in good agreement with measured values if the detuning parameter (Δ =25.7MHz) is included.(61) Using this α, CN was calculated for all transitions to be CN=2.85x10^{-2}. The transition dipole moment used in this calculation was 0.19 Debye.(53) The intensity of radiation transmitted normalized to unity is given by

$$\mathcal{I}_{10}^{SP}(P')=\sum_{P,Q,R}\sum_{J,K}e^{-\alpha(J,K)P'L'}$$

where the sum is over (J,K) and the P,Q, and R Branches. Program 1 computes these intensities for various P'L'. $\mathcal{I}_{10}^{SP}(P')$ could be fitted to three decaying exponentials of the form

$$\mathcal{I}_{10}^{SP}(P')=Ee^{-\epsilon P'L'}+Fe^{-\eta P'L'}+Ge^{-\theta P'L'}$$

where E+F+G=1 at P'L'=o. Then, from eq.(1x-10)

$$I_{tot}^{sp}(P') = \mathcal{L}_{10}^{P}(P') + H(T_v).$$

Program 2 computes, $I_{tot}(P')/I_{tot}(0)$ for a given vibrational temperature, T_v. The partial pressure of the isotopic mixture (90% $^{13}CH_3F$ and 10% $^{12}CH_3F$) in the flourescence cell (P) and the cold gas filter (P') is included. T_v is varied until $I_{tot}(P')/I_{tot}(0)$ fits the experimentally obtained $I_{tot}(P')/I_{tot}(0)$. These curve fittings are shown in Fig. 26.

The intensities at which these curves level off are insensitive to the size of the absorption coefficient, α, since for sufficiently large P'L', $I_{tot}(P')$ must approach $I_{tot}(0)-I_{10}$. When the calculated value of α is used, the experimental data could easily be fitted.

```
?01.00 @ 05.40
*L L 11
*1.02 S CN=2.85E-2
*W 1.02
01.02 S CN=2.85E-2
*W A
C LASER FOCAL

01.02 S CN=2.85E-2
01.03 S L=.44; S M=-1.05; S N=.49; S P=-.49; S Q=.07
01.04 S R=-.0822; S U=-.012; S V=.57; S W=-.16
01.06 S IR=0; S IP=0; S IQ=0
01.08 S T=300; D 2.0
01.10 S T=500; D 2.0
01.20 Q

02.02 S BF=1.22/T
02.03 S AF=6.05/T
02.05 T !!!!,"TEMP",T,!!!
02.10 F PL=0,2,10; D 3.0
02.15 F PL=15,5,30; D 3.0
02.16 F PL=40,20,80; D 3.0
02.20 R

03.10 F K=0,1,15; D 4.0
03.15 S IT=IQ+IP+IR
03.20 T !!,"PL",%3.00,PL,"     IT",%,IT
03.25 S IR=0; S IP=0; S IQ=0
03.30 R

04.10 F J=K,1,45; D 5.0
04.15 R

05.10 S TEST=K
05.15 IF (FITR(TEST-3+.01))5.25,5.30,5.20
05.20 S TEST=TEST-3; G 5.15
05.21
05.25 S A=4; G 5.35
05.30 S A=8
```

PROGRAM 1

```
05.34 C COMPUTE R BRANCH INTENSITY
05.35 S MR=((J+1)*(J+1)-K*K)/((J+1)*(2*J+1))
05.37 S D=FEXP(-BF*(J+1)*(J+2)-AF*K*K)
05.39 S I=A*(2*J+3)*MR*D
05.41 S E=FEXP(-4.1E-3*J*(J+1)-.02*K*K)
05.43 S B=CN*A*(2*J+1)*MR*E*PL
05.45 IF (B-100)5.49,5.62,5.62
05.49 S S=L*FEXP(M*B)+N*FEXP(P*B)+Q*FEXP(R*B)+U*FSIN(V*B)*FEXP(W*B)
05.50 S IR=IR+I*S
05.60 C COMPUTE P BRANCH INTENSITY
05.62 S MP=((J+1)*(J+1)-K*K)/((J+1)*(2*J+3))
05.64 S G=FEXP(-BF*J*(J+1)-AF*K*K)
05.66 S I=A*(2*J+1)*MP*G
05.68 S H=FEXP(-4.1E-3*(J+1)*(J+2)-.02*K*K)
05.70 S B=CN*A*(2*J+3)*MP*H*PL
05.72 IF (B-100)5.76,5.81,5.81
05.76 D 5.49
05.78 S IP=IP+I*S
05.80 C COMPUTE Q BRANCH INTENSITY
05.81 IF (J)1.20,5.98,5.84
05.84 S MQ=(K*K)/(J*(J+1))
05.86 S I=A*(2*J+1)*MQ*G
05.88 S B=CN*A*(2*J+1)*MQ*E*PL
05.90 IF (B-100)5.92,5.98,5.98
05.92 D 5.49
05.94 S IQ=IQ+I*S
05.98 R
*
```

PROGRAM 1 (Continued)

```
C LASER FOCAL

01.10 A "PRESSURE FLOURESCENCE CELL",PF
01.15 A "EFF ABS LENGTH F CELL", L1
01.20 A "LENGTH ABS CELL",LA

02.05 T !!!!
02.10 A "TEMP",T
02.12 A "NORM PRESS",NP
02.15 D 3.0
02.20 G 2.05

03.10 S B=1-FEXP(-1508/T)
03.15 S H=(1/(B*B))-1
03.16 S P=NP; D 4.10; D 4.15; D 4.20; D 4.25; D 4.30; S NC=P
03.20 F P=0,2,10; S P=P/10; D 4.0
03.25 F P=15,5,60; S P=P/10; D 4.0
03.35 R

04.10 S C=.9*PF*L1; D 6.10; S K1=K
04.15 S C=.1*PF*L1; D 6.10; S K2=K
04.20 S C=.9*P*LA; D 6.10; S K3=K
04.25 S C=.1*P*LA; D 6.10; S K4=K
04.30 S P=(H+.9*K1*K3+.1*K2*K4)/(H+.9*K1+.1*K2)
04.35 T "TORR",%2.1,P,"     R",%4.4,R/NC,!
04.40 S P=P*10

06.10 S K=.364*FEXP(-.414*C)+.494*FEXP(-.108*C)+.142*FEXP(-.0136*C)
*
```

PROGRAM 2

APPENDIX D. PROPERTIES OF SYMMETRIC TOP MOLECULES

ROTATIONAL SPECTRA

The moment of inertia of a molecule or any system of masses may be represented by an ellipsoid whose orientation is fixed in the molecule and whose center coincides with the center of mass. The shape of the ellipsoid is such that the molecular moment of inertia about any axis through the center of mass is just equal to half the distance between intersections of this axis and the ellipsoid. Every ellipsoid has three perpendicular principal axes, and if the coordinate system is oriented so that x,y, and z are along the principal axes of the elipsoid of inertia, then, the equation of the ellipsoid of inertia may be written simply

$$\frac{x^2}{I_x^2}+\frac{y^2}{I_y^2}+\frac{z^2}{I_z^2}=1$$

where I_x, I_y, and I_z are the moments of inertia along the directions of the principal axes, and are called the principal moments of inertia.

A molecular rotation can usually most simply be described in terms of motions about the principal axes. The special case of a linear molecule has an ellipsoid of inertia which is a flat disk, since the moment of inertia along the molecular axis, which will be taken as the z direction, is very small;

The general rotating body where all three principal moments of inertia are different is called an asymmetric rotor or asymmetric top, and usually the principal moments of inertia are represented by I_A, I_B, and I_C in order of increasing size. For some molecules, two moments of inertia such as I_A and I_B or I_B and I_C may be equal, in which case the molecule is called a symmetric rotor or symmetric top.

The energy levels of a symmetric top can be deduced from classical arguments and the Correspondence Principle.[20] In Fig. 32 the axis of the molecule precesses around the total angular momentum P with a frequency given by $P/2\pi I_B$. At the same time it may spin about its axis. The energy of rotation would be given by

$$E = \frac{1}{2} I_x \omega_x^2 + I_y \omega_y^2 + \frac{1}{2} I_z \omega_z^2$$

$$= \frac{P_x^2}{2I_x} + \frac{P_y^2}{2I_y} + \frac{P_z^2}{2I_z} \qquad \text{(IV-1)}$$

where x,y, and z are directions along the principal axes of inertia, z being the symmetry axis of the molecule. Now, since the molecule is symmetric top, I_x and I_y are equal and will both be called I_B, which is the normal symbol for the moment of inertia of intermediate size. I_z will be designated as I_A

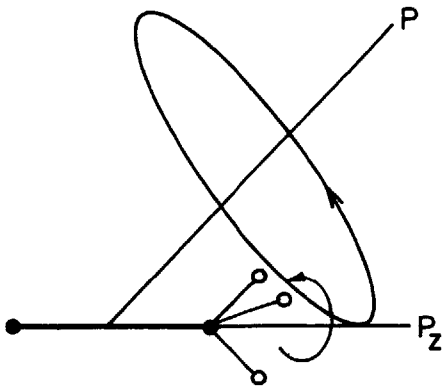

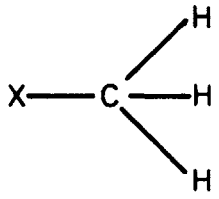

Fig. 3.2. Classical motion of a symmetric top.[20] This is a combined rotation around the molecular axis associated with P_z and a precession of this axis around the total angular momentum **P**.

or I_C according to whether it is smaller or larger than I_B. Using $I_x=I_y=I_B$ and $P^2=P_x^2 + P_y^2 + P_z^2$, equation (IV-1) becomes

$$E=\frac{P^2}{2I_B}+P_z^2\left(\frac{1}{2I_C}-\frac{1}{2I_B}\right) \qquad \text{(IV-2)}$$

The square of the total angular momentum is quantized and must be equal $J(J+1)\hbar^2$, where J is an integer. Similiarly, the component of the angular momentum along the molecular symmetry axis (the z axis), is quantized, so that $P_z^2=K^2\hbar^2$, where K is an integer, Then, equation (IV-2) becomes

$$E=\frac{J(J+1)\hbar^2}{2I_B}+\left(\frac{\hbar^2}{2I_C}-\frac{\hbar^2}{2I_B}\right)K^2$$

or defining rotational constants

$$A=\frac{\hbar}{2I_A}\ ,\ B=\frac{\hbar}{2I_B} \quad \text{and} \quad C=\frac{\hbar}{2I_C}\ ,$$

we have

$$\frac{E}{\hbar}=BJ(J+1)+(C-B)K^2. \qquad \text{(IV-3)}$$

Equation (3) gives the correct allowed energy levels for a symmetric top. If K=0, the energy becomes that of a linear molecule. For a given value of J, K can assume integer values over the range

$$K = J, J-1, \ldots. -J+1, -J,$$

therefore, having 2J+1 different values.

If the moment of inertia about the symmetry axes I_z is smaller than the moment of inertia about the other principal axes, the molecule is called prolate symmetric top. If I_z is larger than the other two principal moments of inertia, the molecule is oblate, symmetric top. Figure 33 shows the energy levels of a prolate and oblate symmetric top. If all principal moments of inertia are equal, we have a spherical top molecule.

INTENSITIES OF SYMMETRIC TOP TRANSITIONS

Selection rules for a symmetric top dipole radiation, dipole moment taken along the molecular axis, are

$$\Delta J = 0, \pm 1 \qquad \Delta K = 0 \qquad \text{and} \quad + \longrightarrow -$$

where + and - are the parities of the inversion doublets. The non-zero absorption dipole matrix elements are given by[20]

$$J+1 \leftarrow J, \; K \leftarrow K \quad \text{(R-Branch)}$$

$$|\mu_{ij}|^2 = \frac{\mu^2[(J+1)^2 - K^2]}{(J+1)(2J+1)}$$

$$J \leftarrow J, \; K \leftarrow K \quad \text{(Q-Branch)} \qquad \text{(IV-4)}$$

$$\mu_{ij} = \frac{\mu^2 K^2}{J(J+1)}$$

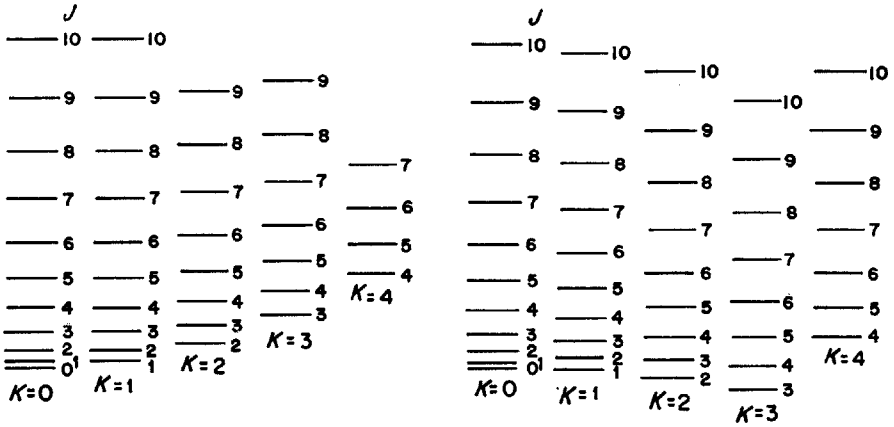

Fig. 33. Energy levels of typical symmetric top molecules[20]
(a) prolate (b) oblate

$J-1 \leftarrow\!\!- J \;,\; K \leftarrow\!\!- K$ (P-Branch)

$$|\mu_{ij}|^2 = \mu^2 \frac{J^2 - K^2}{J(2J+1)}$$

These matrix elements represent the sum of the components of $|\mu_x|^2, |\mu_y|^2$, and $|\mu_z|^2$ for a particular orientation specified by M, the projection of J on the space fixed **z** axis, to all final M states. For K=0, these matrix elements reduce to those of a diatomic, given by

$$|\mu_{ij}|^2 = \begin{cases} \mu^2 \frac{J+1}{2J+1} & \text{R-Branch} \\ \mu^2 \frac{J}{2J+1} & \text{P-Branch} \end{cases} .$$

The fraction of molecules in a particular rotational state, f_{JK}, is given by

$$f_{JK} = \frac{(2J+1)e^{-[BJ(J+1)+(C-B)K^2]\hbar/\,T}}{\sum_{J=0}^{\infty}\sum_{K=-J}^{J}(2J+1)e^{-[BJ(J+1)+(C-B)K^2]\hbar/kT}} . \qquad (\text{IV-5})$$

Due to the presence of three identical Fermions located symmetrically about the z axis of the methyl halides, the total wave function of the molecule is constrained to posess specific symmetry properties. For certain values of K the total wavefunction posesses the proper symmetry. However, for other values of K, where the symmetry is not suitable,

the spin wave function must be considered. This results in differing populations for various K states, where the weighting factor for a given I is expressed as

$$S(I,K)=\begin{cases}2(4I^2+4I+3)\\(4I^2+4I+3)\\2(4I^2+4I)\end{cases}$$

where I is the nuclear spin. Allowing for this degeneracy due to nuclear spin statistics, eq.(IV-5) becomes

$$f_{JK}=\frac{S(I,K)(2J+1)e^{-[BJ(J+1)+(C-B)K^2]\hbar/kT}}{\sum_{J=0}^{\infty}\sum_{K=0}^{J}S(I,K)(2J+1)e^{-[BJ(J+1)+(C-B)K^2]\hbar/kT}} \qquad (IV-7)$$

Assuming that B and C are small compared to KT, the sums may be changed to integrals and one obtains

$$f_{JK}=\frac{S(I,K)(2J+1)}{4I^2+4I+1}\sqrt{\frac{B^2C}{(KT)^3\pi}}\;e^{-[BJ(J+1)+(C-B)K^2]\hbar/kT}$$

For small J and K, eq. (IV-7) reduces to

$$f_{JK}=\frac{S(I,K)(2J+1)}{4I^2+4I+1}\sqrt{\frac{B^2C}{\pi(kT)^3}} \qquad (IV-8)$$

VIBRATIONAL SPECTRA

The fraction of molecules residing in any vibrational

state of an oscillator is given by

$$f_v = \frac{e}{\sum_{v=0}^{\infty} e^{-v\hbar\omega/kT_{vib.}}} = e^{-v\hbar\omega/kT_{vib.}}\left(1 - e^{-\hbar\omega/kT_{vib.}}\right) \qquad \text{(IV-9)}$$

where is the frequency of oscillation and $T_{vib.}$ is the vibrational temperature. For n normal modes of a polyatomic, the fraction f_v is given by

$$f_v = e^{-v\hbar\omega/kT_{vib.}}\left(1 - e^{-\hbar\omega_1/kT_1}\right)^{d_1}\left(1 - e^{-\hbar\omega_2/kT_2}\right)^{d_2}\cdots\left(1 - e^{-\hbar\omega_n/kT_n}\right)^{d_n}$$

$$= e^{-v\hbar\omega/kT_{vib.}} \prod_n \left(1 - e^{-\hbar\omega_n/kT_n}\right)^{d_n} \qquad \text{(IV-10)}$$

where d_n represent the degeneracy of the n^{th} mode and

$$\prod_n \left(1 - e^{-\hbar\omega_n/kT_n}\right)^{d_n}$$

is the total vibrational partition function.

Figure 34 gives a pictorial diagram of the six normal modes of oscillation of the methyl halide group of symmetric tops (CH_3X).[19] The totally symmetric vibration ν_1, ν_2, ν_3 give rise to parallel bands in the infrared while the doubly degenerate vibration ν_4, ν_5, ν_6 give rise to perpendicular bands. The highest energy modes ν_1 and ν_4 are essentially C-H stretching vibrations, while that of the lowest frequency mode, ν_3, is a C-F stretch. The lowest frequency perpendicular vibration, ν_6, is essentially a bending (C≡H) vibration while the two intermediate frequencies are essentially methyl (CH_3) deformation vibrations.

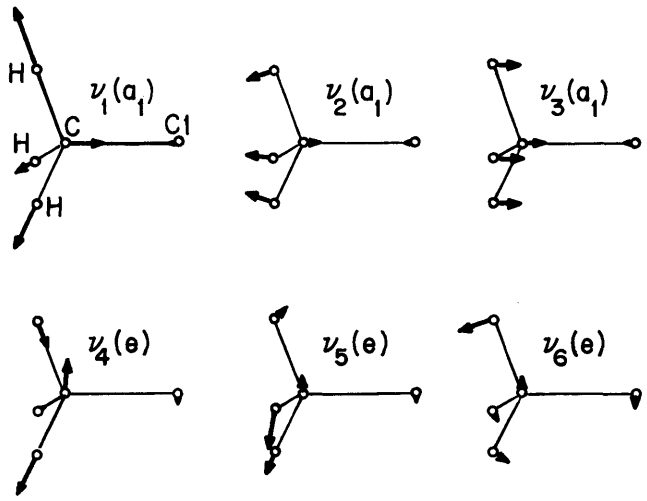

Fig. 34. Normal vibrations of CH_3X (schematic)[19]. Side views and only one component of each degenerate vibration is given.

Table III lists the fundamental frequencies of the methyl halides (CH_3F, CH_3Cl, CH_3Br, CH_3I, CD_3Cl and CD_3Br. Note that the ν_1 and ν_4 fundamentals and the ν_2 and ν_5 fundamentals are nearly degenerate. It should also be pointed out that the $2\nu_5$ and $2\nu_2$ states are in Fermi resonance[19] with the ν_1 and ν_4 states. That is, because of the mixing of the eigenfunctions of the states, the normally weak $|2\nu_5, 2\nu_2\rangle \rightarrow |0\rangle$ radiative intensity will "borrow" intensity from the ν_1 and ν_4 states[19].

If the transition moment of the vibrational transition is parallel to the top axis (|| band) we have for the selection rules

$$\Delta V = \pm 1 \quad \Delta K = 0 \quad \Delta J = 0, \pm 1 \quad \text{if } K \neq 0$$

$$\Delta V = \pm 1 \quad \Delta K = 0 \quad \Delta J = \pm 1 \quad \text{if } K = 0$$

If the transition is perpendicular to the top axis (band), we have

$$\Delta V = \pm 1 \quad \Delta K = \pm 1 \quad \Delta J = 0, \pm 1$$

In this work, the rotational-vibrational transitions of a specific symmetric top, methyl fluoride (CH_3F), will be considered in detail. Some general properties of CH_3F are listed in Table III. In Figure 28 the fundamentals and combination states are shown up to 3000cm^{-1}.

TABLE III. SOME CONSTANTS OF CH_3F

$B=0.85\ cm^{-1}$

$C=5.1\ cm^{-1}$

$\alpha_{12}=0.018 cm^{-1} torr^{-1}$	$\Delta= \omega-\omega_0= 47MHz$	
$\alpha_{12}=0.04\ cm^{-1} torr^{-1}$	$\Delta= 0$	P(20) CO_2
$\alpha_{13}=0.3\ cm^{-1} torr^{-1}$	$\Delta= 25$ MHz	
$\alpha_{13}=0.563 cm^{-1} torr^{-1}$	$\Delta=0$	P(32) CO_2

Dipole Moment = 1.9 Debye

Transition Moment (v=0→1) = .19 Debye

Doppler Width (FWHM)= 67 MHz

Self Broadening Coefficient= 40.0 MHz/torr

CH_3F Fundamentals:

Mode	Frequency (cm^{-1})
ν_1	2964.5
ν_2	1475.3
ν_3	1048.2
ν_4	2982.2
ν_5	1471.1
ν_6	1195.5

REFERENCES

1. R.E. McNair, "Lasers in Chemical Physics", Laser Focus, (29) Nov. 1975.
2. E. Weitz and G. Flynn, Ann. Rev. of Phys. Chem. 25 (275) 1975.
3. J.T. Yardley and C.B. Moore, J. Chem. Phys. 49(1111)1968.
4. C.B. Moore, R.E. Wood, Bei-Luk Hu, and J.T.Yardley, J. Chem. Phys. 46 (4222) 1967.
5. H.L. Chen, J. Chem. Phys. 55 (5551) 1971.
6. H.L. Chen, J. Chem. Phys. 55 (5557) 1971.
7. H. Babrov, J. Chem. Phys. 40 (831)1964.
8. R.M. Osgood, A. Javan, and P. B. Sackett, Appl. Phys. Lett. 20 (469) 1972.
9. R.M. Osgood, Ph.D. thesis, M.I.T., Cambridge.
10. S.D. Rockwood, J.E. Brau, W.A. Proctor, and G.H. Canavan IEEE Journal of Quant. Elect. Vol. QE-9 (120) 1973.
11. R.V. Ambartzumian, V.S. Letokhov, E.A. Ryabov, and N.V. Chekalin, JETP Lett. 20 (275) 1975.
12. J.L. Lyman, R.J. Jensen, J. Rink, C.P. Robinson, and S.D. Rockwood, Appl. Phys. Lett. 27 (87) 1975.
13. S. Mukamel and J. Jortner, Chem. Phys. Lett. 40 (150)1976.
14. A.M. Ronn, "Mechanisms of Infrared-Laser Photochemistry", Laser Focus, p. 53, Aug. 1976.

15. E. Weitz, G. Fynn, and A.M. Ronn, J. Chem. Phys. 56 (6060) 1972.

16. F.R. Grabiner, G.W. Flynn, A.M. Ronn, J. Chem. Phys. 59 (2330) 1973.

17. K. Shuler, J. Chem. Phys. 32 (1692) 1960.

18. C.E. Treanor, J.W. Rich, and R.G. Rehm, J. Chem. Phys. 48 (1798) 1968.

19. G. Hertzberg, "Infrared and Raman Spectra", V.N. Reinhold Co. 1945.

20. C.H. Townes and A.L. Schawlow, "Microwave Spectroscopy", McGraw-Hill Co. 1955.

21. D.T. Hodges and J.R. Tucker, Appl. Phys. Lett. 27 (667)1975.

22. B.J. Feldman, IEEE J. Quan Elec., Vol. QE-9 (1070) 1973.

23. L. Landau and E. Teller, Physik Z. Sovjetunion 10 (34)1936).

24. B.L. Earl, P.C. Isolani, and A.M. Ronn, Chem. Phys. Lett., 39 (95) 1976.

25. E. Weitz and G.W. Flynn, J. Chem. Phys. 58 (2781) 1973.

26. R. Forber, M.S. Feld, and R.E. McNair, to be published.

27. R.E. McNair, M.S. Feld, S.F. Fulghum, G.W. Flynn, and B.J. Feldman, submitted to Phys. Rev. Lett.

28. L.O. Hocker, M.A. Kovacs, C.K. Rhodes, G.W. Flynn, and A. Javan, Phys Rev. Lett. 17 (233) 1966.

29. F.R.Grabiner, D.R. Siebert, and G.W. Flynn, Chem Phys. Lett. 17 (189) 1972.

30. T. Oka, J. Chem. Phys. 45 (754) 1966.

31. C.K. Rhodes, M.J. Kelly, and A. Javan, J. Chem Phys. 48 (5730) 1968.

32. J.I. Steinfeld, I. Burak, D.G. Sutton, and A.V. Movak, J. Chem. Phys. 52 (5421) 1970.

33. A. Yariv. " Quantum Electronics", Wiley & Sons, 1967.

34. V.S. Letokhov and A.S. Mararov, JETP 36 (1091) 1973. This discussion assumes a large rotational bottleneck effect.

35. W. Heitler, "The Quantum Theory of Radiation", 3rd Ed. Oxford Press, 1966.

36. I. Shamah and G.W. Flynn, J. Chem. Phys., to be published.

37. A.Siegman, "Introduction to Lasers and Masers" McGraw-Hill 1971.

38. K.P. Yates and H.H. Nielsen, Phys. Rev. 71 (349) 1947.

39. T.C.Cottrell and J.C. McCoubrey,"Molecular Energy Transfer in Gases (Butterworths, Londons, 1961).

40. E. Merzbacher, "Quantum Mechanics", 2nd Ed., Wiley & Sons, 1970.

41. F.Marion,"Electromagnetic Radiation",Wiley, 1967.

42. E. Weitz and G. Flynn, Ann. Rev. of Phys. Chem. 25 (275) 1975.

43. The pump and probe lasers are acting on two different rotational levels which are collisionally coupled through R-R transfer.

44. In this equation, Δ is the detuning parameter ($\Delta = \omega - \omega_o$), u is the average thermal velocity, T_R is room temperature, μ is the transition dipole moment, $K = \omega/c$, and E_v is the vibrational energy of the pumped mode.

45. The exponent has been multiplied by $(T_R/300^oK)$ for an α_H in terms of T_R/T_V.

46. Methly fluoride occurs in a natural abundance of 99% $^{12}CH_3F$ and 1% $^{13}CH_3F$. Although the $^{13}CH_3F$ occurs in such a small quantity, its absorption of the P(32) line of Co_2 is stronger by a factor of 10 than the $^{12}CH_3F$ absorption of the P(20) line. This is due partly because of the large population f_{JK} in the R(4,3) state and the proximity of the P(32) line to the absorption resonance [$\sim$25MH_z in $^{13}CH_3F$ and 44MH_z in $^{12}CH_3F$].

47. G.M. Barrow and D.C. McKean, Proc. Roy, Soc. (London) A213,27(1952).

48. S.M. Freund, G. Duncan, M. Romheld, J.T. Tiedje and T. Oka, Journ. Mol. Spect., 52(38) 1974.

49. T.Y. Chang and C. Lin.,J. Opt. Soc.Am. 66 (362) 1976

50. F.A. Liuima, A.V. Bushkovitch and A.G. Rouse, Phys. Rev. 96(434) 1954.

51. D.H. Rank, D.P. Eastman, B.S. Rao and T.A. Wiggins, Journ. Mol. Spect. 10(34) 1963.

52. H.A. Gebbie and N.W.B. Stone, Proc. Phys. Soc. (London) 82(309) 1963.

53. W.K. Bischel, P.J. Kelly and C.K. Rhodes, Phys. Rev. A, to be published.

54. The case of $E_B > E_A$ or $\Delta E = E_B - E_A = 150_{cm}^{-1}$ is being treated here for later comparison with CH_3F experiments where these conditions are true.

55. This approximation is valid when the energy defect between the modes is of order KT_R.

56. For high vibrational temperature ($\sim$2000 K), a large amount of the total population resides in the upper vibrational states, hence, leaving only a small amount in the V=1 state. At $t=0$ $P=1/2$ and goes to smaller values with time. It is, therefore, valid to make a small P approximation ($P \ll 1$) for times $t>0$ with the parameters used in this problem.

57. The energy stored in the individual modes add up to the total energy absorbed by the molecule to within experimental error. Although ν_6 was the not measured, steady state theory predicts its energy storage which has been included in the total. Note that (a), (c), (d) and (e) of Fig.27 were measured by different experiments.

58. R.G. Gordon, W.K. Klemperer and J.I. Steinfeld, "Vibrational and Rotational Relaxation," Ann. Rev. Phys. Chem. 19,(215) 1968.

59. T.Y. Chang and T.J. Bridges, Optics Comm. 1(423) 1970; T.Y. Chang, T.J. Bridges, and E.G. Burkhard, Appl. Phys. Lett. 17(357) 1970.

60. K. Shuler and G.H. Weiss, J. Chem. Phys. 45 (1105) 1966.